



Choosing The Right Animal Model for Renal Cancer Research [☆]



Paweł Sobczuk ^{1,2}, Anna Brodziak ^{1,2}, Mohammed Imran Khan ³, Stuti Chhabra ⁴, Michał Fiedorowicz ^{5,*},
 Marlena Weśniak-Kamińska ⁵, Kamil Synoradzki ⁵, Ewa Bartnik ⁶,
 Agnieszka Cudnoch-Jędrzejewska ¹, Anna M. Czarnecka ^{2,5}

¹ Department of Experimental and Clinical Physiology, Laboratory of Centre for Preclinical Research, Medical University of Warsaw, Warsaw, Poland

² Maria Skłodowska-Curie Memorial Cancer Center and Institute of Oncology, Warsaw, Poland

³ Department of Otolaryngology - Head & Neck Surgery, Western University, London, Ontario, Canada

⁴ Department of Biochemistry, CSIR-Central Drug Research Institute, Lucknow, India

⁵ Department of Experimental Pharmacology, Mossakowski Medical Research Centre Polish Academy of Sciences, 5 Pawinskiego Str., Warsaw, Poland

⁶ Institute of Genetics and Biotechnology, Faculty of Biology, University of Warsaw, Warsaw, Poland

ARTICLE INFO

Article history:

Received 19 November 2019

Received in revised form 4 January 2020

Accepted 6 January 2020

Available online xxx

ABSTRACT

The increase in the life expectancy of patients with renal cell carcinoma (RCC) in the last decade is due to changes that have occurred in the area of preclinical studies. Understanding cancer pathophysiology and the emergence of new therapeutic options, including immunotherapy, would not be possible without proper research. Before new approaches to disease treatment are developed and introduced into clinical practice they must be preceded by preclinical tests, in which animal studies play a significant role. This review describes the progress in animal model development in kidney cancer research starting from the oldest syngeneic or chemically-induced models, through genetically modified mice, finally to xenograft, especially patient-derived, avator and humanized mouse models. As there are a number of subtypes of RCC, our aim is to help to choose the right animal model for a particular kidney cancer subtype. The data on genetic backgrounds, biochemical parameters, histology, different stages of carcinogenesis and metastasis in various animal models of RCC as well as their translational relevance are summarized. Moreover, we shed some light on imaging methods, which can help define tumor microstructure, assist in the analysis of its metabolic changes and track metastasis development.

© 2020 The Authors. Published by Elsevier Inc. on behalf of Neoplasia Press, Inc. This is an open access article under the CC BY-NC-ND license (<http://creativecommons.org/licenses/by-nc-nd/4.0/>).

Introduction

According to the most recent, fourth edition of the World Health Organization (WHO) classification of urogenital tumors, kidney tumors can be classified into different subtypes on the basis of cell of origin. Over 85% of the malignant renal tumors are renal cell carcinomas (RCCs). The other 15% include nephroblastic, mesenchymal and metanephric tumors (Table 1).

As RCC is the most common kidney cancer subtype it will be the focus of this article. RCC constitutes approximately 3% of all malignancies in

humans with the lifetime risk of 1.3% and 1.8% [1]. Clear cell RCC (ccRCC) is the most common RCC subtype, accounting for approximately 75% of cases, followed by papillary (pRCC) and chromophobe (chRCC) types. Globally around 20-30% of patients are diagnosed in the metastatic stage, whereas the majority of the remaining patients develop distant metastases in the later course of the disease within next 5 to 10 years [2] resulting in unsatisfactory survival rates. In fact, median overall survival of patients with metastatic RCC treated with sunitinib is approximately 20 months [3]. However, patient survival has improved significantly in recent years due to development of new targeted therapies, including sunitinib, sorafenib, everolimus, cabozantinib, as well as immunotherapy with immune checkpoint inhibitors and sequence use of these agents. Nevertheless, treatment efficacy is still unsatisfactory and new therapeutic strategies are urgently needed. Before a new compound reaches the first phase of clinical trials it must be tested *in vitro* and validated in preclinical setting using cell lines and animal models.

Currently there are over 60 RCC cell lines established in various laboratories with over 20 deposited in commercial cell banks and used worldwide [4]. Moreover, it is relatively easy to establish primary cultures and new cell lines from fresh or frozen specimens obtained by nephrectomy or nephron sparing

[☆] Declarations of interest: none

* Address all correspondence to: Michał Fiedorowicz, PhD, Department of Experimental Pharmacology, Mossakowski Medical Research Centre Polish Academy of Sciences, Warsaw, Poland.

E-mail addresses: pawel.sobczuk@interia.pl, (P. Sobczuk), anbrodziak@gmail.com, (A. Brodziak), imrankhanbioinfo@gmail.com, (M.I. Khan), chhabrastuti@gmail.com, (S. Chhabra), mfiedorowicz@imdik.pan.pl, (M. Fiedorowicz), marlenak@imdik.pan.pl, (M. Weśniak-Kamińska), ksynoradzki@imdik.pan.pl, (K. Synoradzki), ewambartnik@gmail.com, (E. Bartnik), agnieszka.cudnoch@wum.edu.pl, (A. Cudnoch-Jędrzejewska), amczarnecka@imdik.pan.pl. (A.M. Czarnecka).

<http://dx.doi.org/10.1016/j.tranon.2020.100745>

1936-5233/© 2020 The Authors. Published by Elsevier Inc. on behalf of Neoplasia Press, Inc. This is an open access article under the CC BY-NC-ND license (<http://creativecommons.org/licenses/by-nc-nd/4.0/>).

Table 1
Types of available preclinical models resembling histology of human renal tumors according to WHO 2016 classification

Tumor type according to WHO 2016 Classification	Available preclinical models				
	Syngeneic	GEMs	Chemically-induced models	CDX	PDX ^a
Renal cell tumors					
Clear cell renal cell carcinoma	X	X		X	X
Multilocular cystic renal neoplasm of low malignant potential					
Papillary renal cell carcinoma		X		X	X
Hereditary leiomyomatosis and renal cell carcinoma associated renal cell carcinoma		X		X	X
Chromophobe renal cell carcinoma		X		X	X
Collecting duct carcinoma	X	X			
Renal medullary carcinoma					
MiT family translocation renal cell carcinomas		X			
Succinate dehydrogenase deficient renal cell carcinoma					
Mucinous tubular and spindle cell carcinoma					
Tubulocystic renal cell carcinoma					
Acquired cystic disease-associated renal cell carcinoma					
Clear cell papillary renal cell carcinoma					
Renal cell carcinoma, unclassified	X	X	X	X	X
Papillary adenoma			X		
Oncocytoma		X			
Metanephric tumors					
Metanephric adenoma		X			
Metanephric adenofibroma					
Metanephric stromal tumor					
Mesenchymal tumors					
			X		
Mixed epithelial and stromal tumor family					
Adult cystic nephroma					
Mixed epithelial and stroma tumor			X		
Nephroblastic tumors					
Nephroblastoma		X	X	X	
Nephrogenic rests and nephroblastomatosis					
Cystic nephroma and cystic partially differentiated nephroblastoma					
Mesoblastic nephroma					
			X		
Clear cell sarcoma					
			X		
Rhabdoid tumor of kidney					
		X		X	
Renal epithelial tumors of childhood					
Papillary renal cell carcinoma		X		X	X
Renal medullary carcinoma					
Translocation associated RCC (Xp11.2 / t(6;11)) translocations		X			
Rare tumors					
Ossifying renal tumor of infancy					

CDX, cell-derived xenograft; GEM, genetically engineered mice; PDX, patient-derived xenograft; RCC, renal cell carcinoma.

^a PDX models can be possible to obtain for every kind of tumor but in the table we summarize published and available results.

surgery [5]. The advantages of cell line usage in biomedical research are the large number of available cell lines, ease of manipulation, and the possibility to compare results obtained in different laboratories in experiments performed with the same cell line – cross-validation of results. On the other hand, cells in regular 2D culture are deprived of interaction with the tumor microenvironment and other cell types [6]. Cell culture based experiments do not allow to study successive stages of carcinogenesis or metastatic spread. Novel techniques, such as 3D cultures or organoids, have slightly reduced the disadvantages of cell line based research but for the moment even advanced culture techniques are unable to completely eliminate the need for animal research [7] needed for of tumorigenesis mechanism studies and drug discovery [8].

Four types of animal models are widely accepted in cancer research: syngeneic models, genetically engineered mouse models (GEM), chemically-induced models and xenograft models. Xenografts can be further divided based on the source of the tumor – xenografts with conventional cell lines (cell line-derived xenografts, CDX) or with use of specimens obtained from patients with RCC (patient derived xenografts, PDX). Despite many advantages, each model has several limitations its utility in different areas of cancer research (Figure 1). Most of the available models enable new drug testing, however, only some syngeneic, CDX and GEM are suitable for research on mechanisms involved in distant metastases development. Moreover, not all models are suitable for studies on tumor microenvironment or the role of the immune system.

To achieve significant progress in the treatment of cancer patients, comprehensive understanding of tumor pathology is essential, and it cannot be achieved without the use of appropriate animal models of the disease. As mentioned above, WHO classified human renal tumors into over 30 different types that differ by cells of origin, genetic alterations and prognosis. Such a large variety of subtypes is a great challenge that cancer researchers have to face every day. First of all despite large variety of available cell lines, GEM and syngeneic models, most of the kidney tumor subtypes are not represented in animals yet. Many syngeneic models in mice or rats are of poorly differentiated histotype and do not correspond directly to any human cancer or sarcoma. Some similarities to rare kidney tumors, such as mesenchymal tumors, mesenchymal nephroma or clear cell tumors, can be found in chemically-induced tumors, however, difficulties in inducing these tumors, its large heterogeneity and low reproducibility are significant problems. The greatest similarity between animal experiments and clinical situation is found in GEM or CDX models. Many of GEM and CDX tumors present with similar histology and genetic alterations to typical human renal cancers. Currently, validated and reproducible models are available for ccRCC, pRCC, chrRCC, hereditary leiomyomatosis and renal cell carcinoma associated renal cell carcinoma or nephroblastoma (Table 1).

In this review, we comprehensively describe each of the above-mentioned models providing their histological and genetic characteristics, its relation to human kidney tumor types and the rationale for their use in RCC research (Table 1, Figure 1).

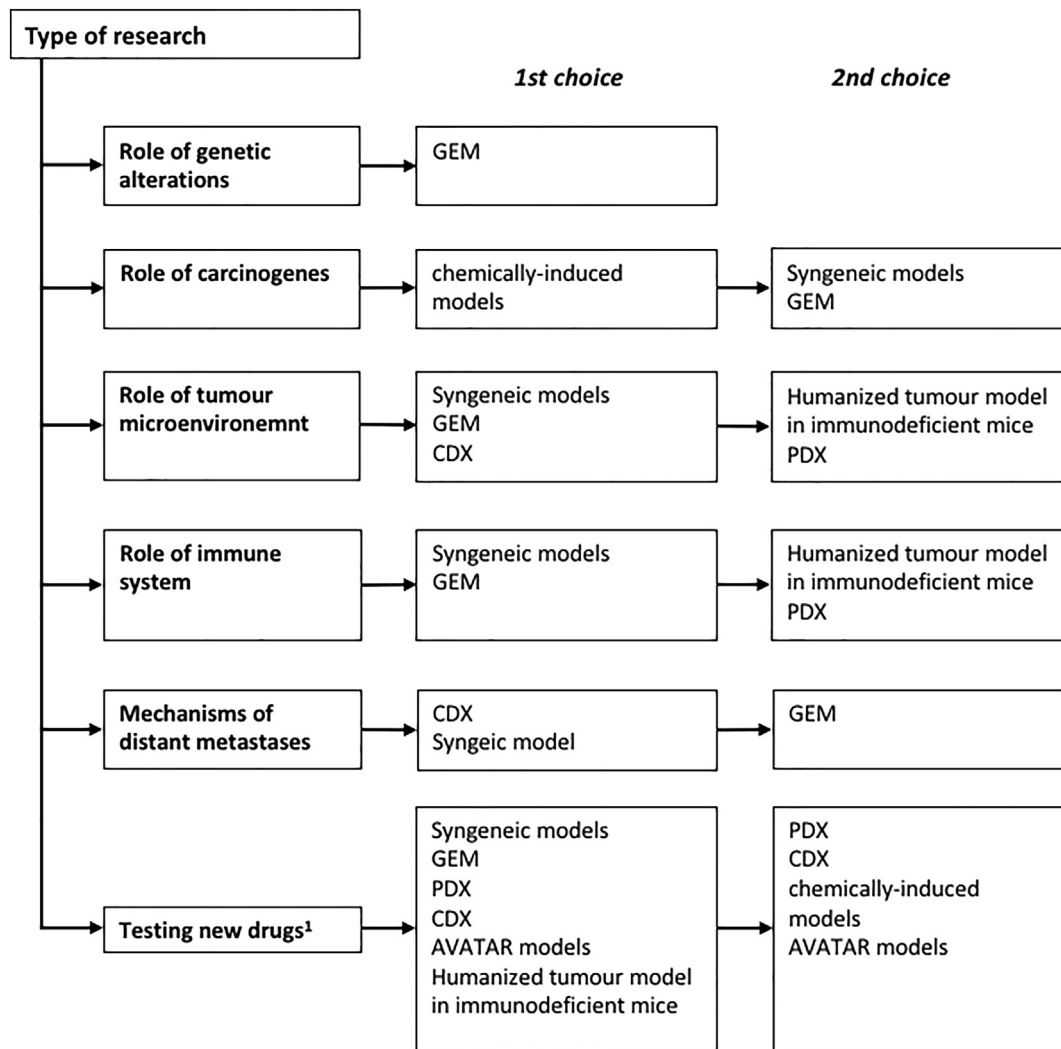


Figure 1. Diagram allowing selection of the most appropriate model depending on the type of research. Models have been divided into 1st choice models, that in the view of the authors are the most suitable, and 2nd choice models that can be considered but have more limitations or are supported by weaker evidence. ¹- more details in [Table 7](#) describing selection of animal models depending on type of studied drug.

Syngeneic Models

Syngeneic animal models developed over 50 years ago are one of the earliest oncogenic animal models. These models are based on animal-derived spontaneous tumor tissues transplanted into a genetically identical, immunocompetent host animal. Allografts (tumors) formed in syngeneic models avoid rejection due to the shared genetic background of the tissue donor and the transplant recipient. Despite the invention of new animal models, i.e. human xenografts or GEM, syngeneic models maintain the advantage of an intact immune system of the animal, which makes them a useful tool to study the tumor microenvironment. Other advantages of syngeneic animal models include their relatively low price and simplicity of animal housing. Due to that syngeneic models can be used in studies that require large animal groups, that can be difficult to obtain when using GEMs or PDXs. Syngeneic animals with RCC have, in fact, been proved useful in identifying therapeutically active drugs [9,10]. With the development of check-point inhibitors and the introduction of immunotherapy into medical oncology and RCC treatment, syngeneic models gained more interest in RCC research due to the intact immune system of the studied animals. In comparison with xenografts in immunocompromised animals, syngeneic models may be used to study the immune response, changes in

tumor microenvironment and effects of treatment with immunotherapy agents. However, syngeneic models also have some limitations. These models currently lack known cancer stem cells and other progenitor cell populations that are typically observed in tumor microenvironment. Tumors in syngeneic models arise as poorly differentiated malignancies and were not reported to undergo the natural steps of tumor evolution that can be observed in GEMs. This often results in rapid tumor growth, preventing immunotherapy agents from developing a full anticancer effect, which is achieved after a latency period in this groups of drugs (in contrast to cytotoxic agents). Therefore syngeneic models do not fully reflect human RCC or ccRCC biology, which prevents the direct translation of study results into clinical practice and diminishes their role in preclinical studies. Nevertheless with introduction of immunotherapy to cancer treatment, syngeneic models have been widely used in preclinical RCC research even despite the possible differences in animal and human cancer pathophysiology. In general benefits and limitations of syngeneic models should be taken into account when choosing the right animal model for RCC research ([Table 2](#)).

The most commonly used syngeneic animal models in RCC research include the murine syngeneic renal adenocarcinoma (RENCA), the kidney carcinoma in the Wistar-Lewis rat model and models of hereditary RCC the Eker rat and the Nihon rat.

Table 2
Advantages and disadvantages of various types of animal models of renal tumors

Model type	Advantages	Disadvantages
Syngeneic models	<ul style="list-style-type: none"> - intact immune system - possibility of studying immunotherapy - low price - simplicity 	<ul style="list-style-type: none"> - do not fully reflect human cancer biology - different genetic landscape - no direct translation to humans - lack of tumor heterogeneity - lack of native tumor microenvironment
Genetically engineered mouse (GEM) models	<ul style="list-style-type: none"> - intact immune system - possibility to study tumor microenvironment - possibility of studying immunotherapy - partial resemblance of genetic background to human tumors - possibility of testing the role of specific genetic alterations 	<ul style="list-style-type: none"> - high-risk of complications - results translate only for patients with specific genetic abnormalities - low metastatic rates - high costs - difficult to obtain
Chemically induced models	<ul style="list-style-type: none"> - allow to study sequential stages of carcinogenesis - high heterogeneity - intact immune system - possibility of studying tumor microenvironment - possibility of studying immunotherapy - low induction success rates 	<ul style="list-style-type: none"> - do not reflect the natural course of the disease - high variability between animals - induction of lesions in various organs and tissues - do not fully reflect human cancer biology - different genetic landscape
Cell-derived xenografts	<ul style="list-style-type: none"> - use of human cancer cells - easy to compare between studies when commercial cell lines are used - possibility to achieve metastatic disease - high homogeneity between tumors - easy to obtain 	<ul style="list-style-type: none"> - no direct translation to humans - low intratumoral heterogeneity - lack of human microenvironment - immunodeficiency - no possibility of studying immunotherapy
Patient-derived xenografts	<ul style="list-style-type: none"> - use of human cancer samples - natural microenvironment of human tumor - direct translation of results for donor patient - allow personalization of therapy 	<ul style="list-style-type: none"> - limited amount of cancer tissue to generate model - low heterogeneity - immunodeficiency - no possibility to study immunotherapy
Humanized mouse models	<ul style="list-style-type: none"> - functional immune system - use of human cancer samples or cancer cell lines - possibility of studying tumor microenvironment - possibility of studying immunotherapy 	<ul style="list-style-type: none"> - limited evidence - high costs - high complexity

RENCA Model—Murine Renal Adenocarcinoma

The RENCA murine adenocarcinoma model is a syngeneic, standardized experimental model of metastatic RCC, developed in the 1970s by Murphy and Hrushesky [11]. The Renca tumor is a spontaneous malignancy that originates in the Balb/c mouse [11]. Histologically, RENCA cells were described as poorly differentiated renal cortical adenocarcinoma of the granular type, pleomorphic with large nuclei [12]. RENCA cells can be cultured *in vitro* or transplanted *in vivo* by intraperitoneal (i.p.), subcutaneous (s.c.) or subcapsular renal injection in syngeneic Balb/c mice. Metastatic progression patterns in the RENCA model depend on the route of administration. After s.c. injection cells form a solid localized tumor [13]. When injected under the renal capsule, RENCA cells induce formation of a primary tumor, as well as development of metastases, mainly in lymph nodes, lungs, liver and peritoneum, mimicking progression of human RCC and allowing staging and therapy evaluation analogically to human RCC [11,14,15]. The RENCA orthotopic model of RCC enables research of localized disease as well as early and late stage metastatic disease. Moreover, the RENCA model allows nephrectomy of the kidney where the primary tumor originates, therefore enabling research of advanced metastatic disease that mimics the clinical situation of post-nephrectomy metastatic RCC patients [16]. Therefore, the RENCA model has been used extensively as a preclinical model in development of various therapeutic strategies for metastatic RCC including chemotherapy, targeted therapy and immunotherapy [14, 15,17–21].

RENCA Subcutaneous Model

This model is created by s.c. (ectopic) inoculation of RENCA cells into the flank of 6- to 8-week-old Balb/c mice. 1×10^5 - 10^6 cells can be administered in 0.1 ml Hank's balanced salt solution (HBSS) or Phosphate-buffered saline (PBS). By day 14 small tumors may be detected, growing progressively with maximum weight of 2.4 grams on day 40 [11] or volume of 2000 to 3000 mm³ at 4 weeks [22]. Large tumors may become ulcerative and necrotic. In this model metastases are not formed and the disease remains localized at the site of inoculation. The subcutaneous RENCA

model is a simple, reproducible and well established model. It allows easy measurement of tumor size during treatment. Moreover, a bioluminescent imaging technique can be performed for more accurate evaluation of the tumor volume, when luciferase-transfected RENCA cells (RENCA-luc) are used [22]. This model is useful for conducting preliminary screening tests of potentially active substances, however, it fails to reflect the complexity of the RCC pathophysiology including differences in innervation of vasculature [23], tumor microenvironment [24] and metastases are not developed.

RENCA Orthotopic Model

The renal RENCA orthotopic model is induced when RENCA cells are implanted into the kidney of BALB/c mice either under the kidney capsule [25] or directly into the kidney [26]. In the first approach $1-2 \times 10^5$ RENCA cells in medium (PBS or HBSS) are injected under the renal capsule [16,27] with two possible implantation methods [28]. In the first method - called superficial implantation - the needle should be inserted under the kidney capsule, above the parenchyma in the lateral kidney border and inserted slightly forward through the renal cortex. RENCA cells should be placed under the renal capsule without puncturing it and white bubbles should appear on the surface of the capsule. In the second method, called the internal technique, needle insertion is performed starting from the side of the kidney opposite to the final implantation site and inserted through the kidney until the needle is visible in the sub-capsular space on the anteromedial surface of the kidney. Cells should be injected without puncturing the renal capsule until white bubbles form.

Recently another RENCA orthotopic model was established [26]. In this version of the model, tumor cells are injected directly into the kidney. When performing direct intrarenal injection, 2×10^6 RENCA cells in HBSS are injected into the kidney of the animal through the peritoneum. Compared to subcapsular implantation, this technique is fairly non-invasive and does not require suturing. Analogously to the subcutaneous RENCA model, bioluminescent RENCA-luc cells can be implanted under the renal capsule or directly into the kidney to develop an orthotopic RCC model, that enables non-invasive monitoring of tumor growth [26,29].

In both these orthotopic models, subcapsular and 'direct', the primary tumor mass grows progressively in the kidney followed by formation of

spontaneous metastases. In the subcapsular injection method, macroscopic primary tumors can be detected by days 7 to 10 and at day 25 to 35 can measure up to 8 cm³ but high variability can be observed [30]. In this model, the tumor first metastasizes to regional lymph nodes, then to the lungs and liver [31]. Pulmonary metastases can be detected by days 15 to 20 after subcapsular implantation and are present in most animals by day 21 [30]. Liver metastases, hemorrhagic ascites and carcinomatosis are observed after day 21 [30]. In this model metastases do not appear in the contralateral kidney and therefore renal failure does not contribute to the mortality [31]. Mice begin to die on day 21 with approx. 50% survival at day 37 and less than 10% after 45 days [31].

In the direct kidney implantation method the growth of the primary tumor is rapid, and results in histologically detectable tumor formation at day 7 [32]. By day 14 normal architecture is lost in nearly the entire kidney, and necrotic areas within renal tumors are observed by day 21. On day 24, primary tumors reach a weight of 1 to 3 g [26]. Metastases to the lungs are also observed at that time [26].

RENCA Intraperitoneal Injection

Intraperitoneal injection of 10⁵ RENCA cells into BALB/c mice can be used to induce a metastatic model of RCC [11]. In comparison to intrarenal/subcapsular injection of cancer cells, i.p. inoculation results in relatively low tumor mass in the peritoneum (approx. 50% less than in the intrarenal approach) [11]. Metastases are formed relatively early in the mesenteric lymph nodes and can be detected by day 16 [13]. As the tumor progresses, carcinomatosis and liver metastases appear [13]. Liver metastases can be detected in approx. 38% of the mice and lung metastases in up to 5% [13]. Although this model results in metastatic disease it fails to fully mimic the course of metastatic RCC, due to the lack of the primary tumor in the kidney.

RENCA Intravenous Injection

Similarly to i.p. injection, intravenous (i.v.) administration of RENCA cells results in metastatic disease with relatively low tumor mass [11]. Intravenous injection of 10⁵ RENCA cells into the tail vein results in formation of numerous lung metastases, while other organs seem to be uninvolved [33]. Microscopic tumor nodules scattered in the lung tissue can be observed around day 10 [19]. Macroscopic lung metastases appear from day 15 after cell injection and constantly grow. The number of lung metastases is reaching 100 to 200 by day 20 [34]. The median survival time of mice in this model is 38 days [12]. Similarly to the i.p. administration, the i.v. method is a predictable model of lung metastases that mimics the clinical situation of patients after nephrectomy with lung metastases. This model can be useful in evaluation of therapeutic approaches for the treatment of lung metastases in RCC.

CRISPR-Mediated VHL Knockout RENCA Model

The discovery and utilization of novel genetic tools, such as homologous recombination and small hairpin RNA (shRNA) gene knockdown, have led to a myriad of important discoveries in this field. In the last few years, the CRISPR-based technology has revolutionized genome editing. CRISPR is a technique that allows easy and accessible gene knockouts. Recently, the first syngeneic mouse model of metastatic RCC deficient in the von Hippel-Lindau (VHL) gene was established by CRISPR-mediated knockout of VHL with the use of lentiviral transduction [35]. Based on this approach it might be possible to create syngeneic mouse models of RCC which better recapitulate the genetic features of human RCC.

The Wistar-Lewis Rat Renal Adenocarcinoma

The Wistar-Lewis rat renal adenocarcinoma was first described in 1980 by White and Olsson [36]. It arose spontaneously in a Wistar-Lewis rat's kidney and originated from renal cortical tubules. In electron microscopy studies it was shown that rat RCC cells share various histopathological characteristics with human RCC cells, i.e. the presence of large nuclei, large vacuoles and abundant glycogen granules [37]. The model is induced by

transplantation of rat tumor cells in the flank of syngeneic rats. After s.c. transplantation, a tumor is formed after 3 weeks and does not possess metastatic potential [36]. When the tumor is placed under the renal capsule, metastatic dissemination can be observed, however, the time required for that process is highly unpredictable. Around 13 weeks after implantation, 85% of the animals develop macroscopic metastatic disease in the lungs [37]. Doubling time of the primary tumor in the subcapsular transplantation method is estimated to be only 2.6 days [37]. By 3 months following the implantation the rats are moribund with a massive tumor load. Alternatively, in order to induce metastases a splenectomy can be performed followed by i.p. injection of tumor cells after 24 hours. Formation of metastases can be observed throughout the abdominal cavity 9 weeks later [36]. The Wistar-Lewis rat renal adenocarcinoma model has been used as a pre-clinical model in development of chemotherapeutics used for treatment of RCC, however, it is considered to be less predictable and more time-consuming than the RENCA model [38].

Eker and Nihon Rats

In 1954 Reidar Eker described renal adenomas in Wistar rats. Lesions started to appear in 5 month rats and tumors developed up to one year. These tumors were varied in size, multiple and bilateral, without metastases. In 1961 Eker and Mossige noticed that a single dominant gene determined the development of tumors [39,40]. In later research Eker rats (Wistar strain) were bred on a Long Evans genetic background [41–43]. After several studies, a positional cloning approach allowed to identify a mutation in the rat *Tsc2* gene (so called the Eker mutation) that is the predisposing factor for tumors in Eker rats [41,44–47]. Homozygous rat embryos (with the Eker mutation in two alleles) died at approx. 12 days of gestation. They were characterized by atypical brain development (smaller, abnormal segmentation) [41]. Renal tumors appear in heterozygotes and in accordance with the Knudson “two-hit” hypothesis, a tumor occurs when a wild type allele is inactivated by loss of heterozygosity or somatic mutation [41,45,48–51].

Renal tumors in Eker rats (Long-Evans rats bearing the Eker mutation) are usually multicentric and bilateral with epithelial origin. They are mostly clear and cystic nodules up to 3 mm in diameter. Larger tumors (reaching up to 30 mm in diameter) are observed less frequently. Large tumors occur in young individuals and develop from renal proximal tubular epithelium. Cancer cells most often have abundant eosinophilic cytoplasm containing one or more vacuoles [52]. Tumor cells are basophilic or eosinophilic and are arranged in trabecular, solid, acinar and papillary histologic patterns [53]. Clear cell (cytoplasm) cytological variants such as found in humans ccRCC were not observed in these tumors [52]. Renal cancers from Eker rats are highly vascularized with large and irregular vesicular areas [54]. Primary neoplasms in these rats are also found in spleen, uterus and vagina, not only in kidney. Finally tumors in smooth muscles in older animals (14-month old) were also observed [52]. No evidence of metastases was reported by now.

Studies on cells derived from Eker rats compared to cells derived from human renal cancer cells show similarities, like overexpression of transforming growth factor α (TGF α), stable and high expression of hypoxia inducible factor 2 α (HIF2 α), and up-regulated vascular endothelial growth factor (VEGF) [54,55]. Although the frequency of mutations in p53 is not fully determined, many studies in human renal cancer derived tissues indicate that mutations in p53 occur rarely, as in Eker rats [56–59].

RCC in humans is mostly related to mutations in the *VHL* gene [60] while in Eker rats they are observed in *Tsc2* gene [45,48,61]. In humans, alterations in TSC genes (humans possess two *TSC1* or *TSC2* genes) are connected with tuberous sclerosis [60]. The presence of this mutation in the Eker model has an additional impact on the obtained results. Eker rats that have elevated glucose level and abnormal insulin secretion or utilization, also exhibit hyperketonemia. In the skeletal muscle, metabolic abnormalities with mitochondrial dysfunction and reduction of their number are observed [62,63]. Additionally, most studies were done on the Long-Evans strain that carried the Eker mutation, but crossing with other rat strains was

also used [47, 64]. Different genetic background (strain) was found to affect size and number of tumors in heterozygous animals as well type of the abnormalities found in homozygous embryo brains [64].

The Eker rat model is useful in cancer biology research, especially for studies on inherited types of cancer. It is a good tool for genetic studies on the role of various tumor genes and oncogenes. It is also useful for studying the possible role of exposure to chemical or physical factors in modifying the incidence of tumors. However, in the case of renal tumors, the lack of close similarity to a particular type of human kidney tumor, as well as the lack of distant metastases, limits the utility of this model in research into potential therapeutics. The Eker rat is also a model of tuberous sclerosis, and in this case trials with rapamycin with Eker rats have been conducted [65,66].

Another hereditary renal cancer model is called the Nihon rat (Sprague-Dawley strain) and it was described by Okimoto et al. in 2000 [67]. The predisposition for developing renal cancer in Nihon rats is dominantly inherited and results from the mutation in the *Bhd* gene [68]. In these animals, multiple types of adenomas and carcinomas are characterized including tubular, solid, cystic, or cystic-papillary histologic subtypes. Lesions began to appear very early in 3 to 4 week-old animals. Nihon rats also develop clear cell type renal cancer carcinoma. The majority of the found atypical tubules and tumors are of the clear or mixed cell type. Heterotopic ossification was also observed. Tumors were locally aggressive adhering to surrounding organs, but metastases were not observed. Additionally, other neoplastic lesions were found in endometrium, salivary glands and heart [67,69]. Nihon rats may be used to investigate human BHD-induced renal tumors or to study in general the genetic mechanisms of renal cancer development.

Genetically Engineered Mouse (GEM) models

Great progress that has been observed in recent years in the area of genetic engineering has opened new opportunities for generation of new animal models of RCC. Genetically engineered mouse (GEM) models are developed by the introduction of constitutively or conditionally expressed genetic alterations, associated with a particular disease/cancer. In GEM models one or several genes believed to be involved in transformation or malignancy are mutated, deleted or overexpressed. Conditional expression is dependent on the presence of additional stimuli, e.g. tamoxifen, that “switch on” or “switch off” the expression of the genes. In the constitutive

model, genes are altered from the embryonic period through the whole life. Some genetic modifications induced in the embryo may affect normal development and cause early lethality or significant functional impairment what significantly limits cancer research. For that reason it is recommended that mutated genes should be silent during embryogenesis and early post-natal development and preferentially mutated in selected tissues [70].

Depending on the modification system, genetic lesions can be initiated in specific tissues or in all tissues simultaneously. The first approach is considerably better because alteration occurs in the tissue and microenvironment that is relevant to the type of tumor being modeled. If the specific type of cells of tumor origin is known, the best approach would be to target genes in those cells only. There is a variety of site-specific promoters to model kidney diseases [71]. For example, for ccRCC that originates from proximal tubule cells, promoters such as Pax8 [72,73], Ksp-cadherin [74–78] and GGT [79,80] are the most commonly used and result in tissue-specific generation of RCC tumors that resemble human ccRCC.

Moreover, GEM models have an intact immune system and a well-developed tumor stromal compartment thus can be used to study the effect of immune-directed therapies and allow testing therapies acting on the tumor microenvironment. Additionally, distant metastases are more frequently observed in GEM models than in xenografts. Therefore, they are an optimal tool for studies of metastatic disease [81].

One of the major drawbacks of GEM models is the rather slow kinetics of tumor development that usually requires even over a year to develop a cancer. On the other hand, this allows testing multiple events that affect carcinogenesis or testing therapeutic strategies at different stages of tumor development. Slow growth results in generation of various additional mutations and finally higher heterogeneity that is often lacking in xenografts.

GEM models give the best opportunity to study the role of specific genetic or molecular abnormalities in carcinogenesis but data concerning the efficacy of therapeutic strategies should be interpreted with caution. Tumors in such models are mouse, not human tumors, and the results cannot be easily translated to predict the therapeutic response in humans. There is no direct correlation between response in the mouse and response in the clinical setting in patients [70].

Recent years have brought a breakthrough in the understanding of the genetic background of RCC and a few new GEM models of this disease (Table 3). The first trials were focused on the *Vhl* gene, which is the most

Table 3
Tested approaches to generate autochthonous genetically engineered mouse models of renal cancer

Genetic modification	Renal tumors (frequency if available)	Subtype	Metastases	Additional information	Ref
<i>Vhl</i> ^{Δ/Δ}	No	NA	NA	NA	[72, 84–90]
<i>Vhl</i> ^{Δ/Δ} + Notch1 activation	No	NA	NA	Only nests of dysplastic cells	[95]
HIF1α activation	No	NA	NA	“carcinoma in situ”-like changes	[79]
<i>Vhl</i> ^{Δ/Δ} <i>Pbrm1</i> ^{Δ/Δ}	Yes, 100%	ccRCC	no		[72]
<i>Vhl</i> ^{Δ/Δ} <i>Pbrm1</i> ^{Δ/Δ}	Yes, 100%	Low-grade ccRCC	no	Impaired renal function	[73]
<i>Vhl</i> ^{Δ/Δ} <i>Pbrm1</i> ^{Δ/Δ} <i>Tsc1</i> ^{Δ/-}	Yes, 100%	high-grade ccRCC	no	Faster development of tumors than in <i>Vhl</i> ^{Δ/Δ} <i>Pbrm1</i> ^{Δ/Δ} animals	[73]
<i>Vhl</i> ^{Δ/Δ} <i>Pbrm1</i> ^{Δ/Δ}	Yes, 33.3%	ccRCC	No	Impaired renal function and high mortality	[74]
<i>Vhl</i> ^{Δ/Δ} <i>Bap1</i> ^{Δ/-}	Yes	unknown	no	Very small lesions	[93]
<i>Vhl</i> ^{Δ/Δ} <i>Bap1</i> ^{Δ/-}	Yes	ccRCC	no	Impaired renal function and high mortality	[73]
<i>Vhl</i> ^{Δ/Δ} <i>Trp53</i> ^{Δ/Δ} <i>Rb1</i> ^{Δ/Δ}	Yes, 82%	high-grade ccRCC	no		[75]
<i>Flcn</i> ^{Δ/Δ}	Yes, 1–2%	unknown	no	Impaired renal function and early mortality	[77]
<i>Flcn</i> ^{Δ/-}	Yes	ccRCC, chRCC, oncoyoma	unknown		[76]
<i>Flcn</i> ^{Δ/-}	Yes, 3%	oncoyoma	no	Concomitant lung adenocarcinoma or diffuse lymphoproliferative disease	[111]
<i>Flcn</i> ^{Δ/Δ}	Yes, 53%	Various with dominant pRCC and sarcomatoid RCC	Yes, lymph nodes		[112]
Myc overexpression	Yes	collecting-duct carcinoma	unknown		[80]
Myc overexpression	Yes	type 2 pRCC	unknown		[78]
Myc overexpression + <i>Vhl</i> ^{Δ/Δ} <i>CDKN2A</i> ^{Δ/Δ}	Yes, 100%	ccRCC	Yes, liver		[78]
TFEB overexpression	Yes	ccRCC, pRCC	No	Impaired renal function	[94]
<i>Wt1</i> ^{-f1H19^{+/m}}	Yes, 64%	nephroblastoma	no		[120]

ccRCC, clear cell renal cell carcinoma; chRCC, chromophobe renal cell carcinoma; pRCC, papillary renal cell carcinoma; NA, not applicable.

frequently mutated in human ccRCC. *VHL* mutations occur at the earliest stage of tumor formation and are present in 82% to 92% of ccRCC [82,83]. Unfortunately, numerous mouse models with renal epithelial-specific *Vhl* knock out failed to develop RCC, suggesting that second-hit loss-of-function mutations are needed and that solitary *Vhl* mutations in the renal epithelium are insufficient for RCC development [72,84–90]. Thus, attempts with concomitant knockdown of *Vhl* gene together with other RCC-related genes, highly mutated in humans such as *PBRAM1*, *BAP1*, *Rb1*, *Trp53* were undertaken. For example, kidney epithelium specific co-deletion of *Vhl* and *Pten* [88] or *Kif3a* (Kinesin Family Member 3A) [91] in mice led to formation of simple, atypical cystic lesions that mimic precursor lesions observed in some ccRCC, however, no cancer cells were found. More promising are models with genetic modifications in *Vhl*, *Trp53* and *Rb1* [75], *Vhl* and *Pbrm1* [72,73,92], *Vhl* and *Bap1* [93], *Hif1a* [79], *Myc* [78,80], *Tfeb* [94], *Bhd* [77] or *NICD1* [95] that are described below in more detail.

It is necessary to underline that renal tumors, at the genetic and molecular level, are very complex diseases harboring multiple genetic alterations. Moreover, there is high genetic heterogeneity between each subtype of RCC what significantly complicates the possibility to generate a reliable GEM model fully resembling human disease. Analyses of data from The Cancer Genome Atlas (TCGA) has identified 16 significantly mutated genes including 9 associated with ccRCC, 11 associated with pRCC, and 2 associated with chrRCC with only two genes, *TP53* and *PTEN*, shared by all subtypes [96–99]. Each of these genes is an attractive target to generate a GEM model, however for the moment only several genes have been tested (Table 4). The majority of human RCC cells harbor multiple mutations whereas tumors in GEMs are induced by alterations in only a few genes. Even though secondary mutations, other than in targeted genes, are observed in GEMs, they do not fully resemble the broad spectrum of human RCC. Such genetic complexity opens wide perspectives for further research in this area by creating GEM models targeting other genes that have not been tested yet, preferably in combination with most common genes such as *VHL* or *PBRM1*.

Vhl^{Δ/Δ}*Pbrm1*^{Δ/Δ} Mice

In 2017 Espana-Augusti et al. [72] established a mouse model with the renal tubular specific deletion of *Vhl* and Polybromo-1 (*Pbrm1*) gene using Pax8CreER^{T2} transgenic mice. The *Pbrm1* gene that acts as the SWI/SNF

Table 4

Comparison of 16 significantly mutated genes across RCC subtypes (ccRCC, pRCC and chrRCC) based on TCGA data and their use on creating GEM models of RCC

Significantly mutated gene in TCGA analyses	RCC subtype	Successful GEM models of RCC targeting the gene
TP53	ccRCC, pRCC, chrRCC	<i>Vhl</i> ^{Δ/Δ} <i>Trp53</i> ^{Δ/Δ} <i>Rb1</i> ^{Δ/Δ} ,
PTEN	ccRCC, pRCC, chrRCC	NA
PBRM1	ccRCC, pRCC	<i>Vhl</i> ^{Δ/Δ} <i>Pbrm1</i> ^{Δ/Δ} , <i>Vhl</i> ^{Δ/Δ} <i>Pbrm1</i> ^{Δ/Δ} <i>Tsc1</i> ^{Δ/Δ}
SETD2	ccRCC, pRCC	NA
BAP1	ccRCC, pRCC	<i>Vhl</i> ^{Δ/Δ} <i>Bap1</i> ^{Δ/Δ} ,
VHL	ccRCC	<i>Vhl</i> ^{Δ/Δ} + Notch1 activation, <i>Vhl</i> ^{Δ/Δ} <i>Pbrm1</i> ^{Δ/Δ} , <i>Vhl</i> ^{Δ/Δ} <i>Pbrm1</i> ^{Δ/Δ} <i>Tsc1</i> ^{Δ/Δ} , <i>Vhl</i> ^{Δ/Δ} <i>Bap1</i> ^{Δ/Δ} , <i>Vhl</i> ^{Δ/Δ} <i>Trp53</i> ^{Δ/Δ} <i>Rb1</i> ^{Δ/Δ} , <i>Myc</i> overexpression + <i>Vhl</i> ^{Δ/Δ} <i>CDKN2A</i> ^{Δ/Δ} ,
KDM5C	ccRCC	NA
MTOR	ccRCC	NA
PI3KCA	ccRCC	NA
MET	pRCC	NA
NF2	pRCC	NA
KDM6A	pRCC	NA
SMARCB1	pRCC	NA
FAT1	pRCC	NA
STAG2	pRCC	NA
NFE2L2	pRCC	NA

chromatin remodeler, is the second most frequently mutated gene in human ccRCC, observed in roughly 50% of cases [100]. Concomitant loss of *Vhl* and *Pbrm1* is observed in up to 40% of cases in humans [100]. Espana-Augusti et al. established a model targeting both genes using the Pax8CreER^{T2} transgene that allows for spatial and temporal control of gene deletion and therefore specific targeting of fully developed renal tubular epithelium. All of *Vhl*^{Δ/Δ}*Pbrm1*^{Δ/Δ} mice by 20 months of age exhibited a spectrum of premalignant cysts and developed multifocal renal tumors arising within macroscopically normal parenchyma and they were confirmed to originate from proximal renal tubules. All malignant tumors presented with a typical histopathological picture of ccRCC - cells with clear or eosinophilic cytoplasm, increased proliferative index, prominent vasculature and positive staining for carbonic anhydrase 9 (CAIX). No macroscopic metastases were found in this model [72].

At the same time Gu et al. [73] published a report on a similar model of *Vhl/Pbrm1* knock-out mice. They used the same Pax8 promoter to drive constitutive expression of *Cre* recombinase from early kidney development. After 13 months 100% mice developed tumors resembling human low-grade (Fuhrman grade 1-2) ccRCC with sizes of 0.5 to 12 mm. Tumors were positive for CAIX, CD10, and vimentin. Moreover, they had increased expression of HIF target genes including *Vegf*, *Glut1*, or *Tgfa*. An additional knock-out of one copy of the mTORC1 negative regulator, *Tsc1* gene, in the kidneys along with *Vhl* and *Pbrm1* led to development of tumors with similar appearance to those observed in kidneys with intact *Tsc1*, but of higher grade and with increased mTORC1 activation. In *Vhl*^{Δ/Δ}*Pbrm1*^{Δ/Δ} *Tsc1*^{Δ/Δ} mice, tumor formation was accelerated by approximately 3 months [73]. *Vhl*^{Δ/Δ}*Pbrm1*^{Δ/Δ} mice that developed RCC had median survival of 15 months and impaired renal function, evaluated by blood urea nitrogen and creatinine levels [73], that may have been caused by tumors but also abnormal kidney development caused by the *Pbrm1* knock-out in the embryonic period.

A different approach was analyzed by Nargund et al. [74] who created a *Vhl* and *Pbrm1* deficient mouse model using a traditional Ksp-Cre driver which begins its expression at embryonic day 14.5. In this model mice developed renal hydronephrosis, polycystic kidney disease (67% of animals up to 14 months) and renal failure accompanied by markedly increased mortality. Serial MRI imaging revealed progressive changes from normal kidney through cysts to increased nodularity but histological examination revealed sheets of tumor cells only in one third of the kidneys. Tumors had high vasculature density, glycogen concentration and proliferation index but did not cause local tissue involvement nor distant metastases. Moreover, kidney lesions were positive for CAIX suggesting that they originate from proximal tubules. *Vhl*^{Δ/Δ}*Pbrm1*^{Δ/Δ} tumors had upregulation of HIF-1, STAT3 and mTORC1 pathways and downregulation of the OXPHOS pathway – molecular features of human ccRCC. Also the gene expression profile, compared with TCGA data from human ccRCC, confirmed that observation [74]. It is worth noting that *Vhl*^{Δ/Δ}*Pbrm1*^{Δ/Δ} tumors from this model were transplantable and formed visible tumors resembling histological and genetic features of parental cancers, when transplanted into the subrenal capsules of the kidney in NSG mice. Interestingly, tumor invasion into the liver was observed in two of the five transplanted cases, confirming their malignant and metastatic potential.

Three different approaches for concomitant *Vhl* and *Pbrm1* knock-out have been reported so far, varying in the use of different gene promoters and time of silencing. Deletion of *Vhl* and *Pbrm1* already during embryogenesis may affect normal development of the kidney [73] thus models with inducible deletion of targeted genes after completed organ development seem to be less biased and better resemble human ccRCC pathogenesis [72]. Use of the Ksp-Cre driver in the embryonic period seems to affect organ development to a lesser extent than Pax8 but tumors observed in this model are uniformly small and observed only in 30% of the animals, strongly limiting its potential use in studies on RCC pathogenesis and therapies [74].

Vhl^{Δ/Δ}*Bap1*^{Δ/Δ} Mice

In 2014 Wang et al. [93] described the role of *Vhl* and *Bracl* associated protein-1 (*Bap1*) deletion in mice. The *Bap1* gene encodes a deubiquitinase

of the ubiquitin carboxyl-terminal hydrolase. Complete Bap1 loss-of-function is observed in approximately 15% of human ccRCC, mostly in high-grade tumors [101]. Homozygous deletion of *Vhl* and *Bap1* in the mouse (Six2-Cre; *Vhl*^{Δ/Δ}*Bap1*^{Δ/Δ}) kidney resulted in early mortality before 1 month [93]. If Bap1 deletion was heterozygous (Six2-Cre; *Vhl*^{Δ/Δ}*Bap1*^{Δ/-}) some mice developed small tumor nodules (0.25-1.8 mm) with unknown molecular characteristics [102]. Use of the Pax8-Cre driver, instead of Six2-Cre, significantly improved the survival of animals and increased the frequency of RCC tumors. Pax8-Cre;*Vhl*^{Δ/Δ}*Bap1*^{Δ/Δ} died at around 3 months of age while animals with homozygous loss of function of Bap1 (Pax8-Cre; *Vhl*^{Δ/Δ}*Bap1*^{Δ/-}) survived 14.5 months and developed renal tumors observed at around 11 months of age. Tumors ranged from 0.7 to 2.4 mm in size, presented with pronounced cell pleomorphism, nucleolar prominence, atypia, mitosis, lymphovascular invasion, positive Ki-67, CAIX and CD10 staining and upregulation of HIF-1, HIF-2 and mTORC1. Such characteristics suggest similarity to high-grade (Fuhrman grade 3) human ccRCC. Similarly to Pax8-Cre;*Vhl*^{Δ/Δ}*Pbrm1*^{Δ/Δ} mice, animals in this model had impaired renal function, what can explain their early mortality [73].

It may seem interesting to evaluate the possibility of creation of a triple knock-out model for *Vhl*, *Pbrm1* and *Bap1* genes but such a combination rarely occurs in human ccRCC. For unknown reasons tumors tend to lose either *Pbrm1* or *Bap1*, but loss of both is rarely observed [101,103].

Vhl^{Δ/Δ}*Trp53*^{Δ/Δ}*Rb1*^{Δ/Δ} Mice

Harlander et al. [75] have recently (in 2017) characterized a new mouse model with simultaneous, inducible, renal epithelial cell-specific (Ksp1.3-^{CreERT2}) homozygous deletion of loxP-flanked alleles of *Vhl*, *Trp53* and *Rb1* genes. Expression of those genes was switched-off in pups by injecting nursing dams with tamoxifen or by feeding 5-week-old mice with tamoxifen-containing food. Within 25 to 61 weeks from tamoxifen treatment 32 of 38 (82%) mice developed a total of 159 tumors. Putative small precursor lesions were observed in mice that did not develop tumors suggesting that they may potentially develop them at later time points. Male mice developed tumors at earlier time points and presented with a higher number of tumors per animal, what correlates with higher frequency of RCC among men [2].

All tumors arose from proximal tubule epithelial cells and were classified as ccRCC grade 3 or 4, growing in acinar, solid and pseudopapillary patterns. 60% of tumors contained cells with either optically clear or weakly stained cytoplasm, while 28% exhibited more cytoplasmic eosin staining resembling the eosinophilic variant. The remaining tumors showed mixed phenotype or papillary-like features. All tumors displayed highly developed vascular network. No lung, liver, spleen, bone or brain metastases were observed in these mice [75].

Histologically and genetically *Vhl*^{Δ/Δ}*Trp53*^{Δ/Δ}*Rb1*^{Δ/Δ} tumors are highly similar to human ccRCC. All lesions displayed nuclear accumulation of HIF-2α, 75% displayed nuclear expression of HIF-1α, all had strong activation of mTORC1, while only a few were positive for markers of the RAS-MAPK pathway activation what is consistent with ccRCC tumors in man. Strong similarities were also observed for the expression of unique orthologous gene pairs between human and mouse ccRCC. Importantly, mutations in *Pbrm1*, *Bap1* and *Setd2* were not found in the examined animal tumors, providing evidence that this model may reflect approximately 50% of human ccRCC that do not harbor mutations in those tumor-suppressor genes [75].

Some therapeutic strategies have been tested by Harlander et al. in *Vhl*^{Δ/Δ}*Trp53*^{Δ/Δ}*Rb1*^{Δ/Δ} mice. These authors have proved that individual ccRCC tumors respond differently to first line therapy with sunitinib and second line everolimus suggesting the potential use of this model for evaluation of the mechanisms and biomarkers associated with therapeutic sensitivity and resistance. Moreover, they proved that acriflavine, inhibitor of the dimerization of HIF-1α and HIF-2α with HIF-2β, is effective in a small subset of tumors in the third line after sunitinib and everolimus [75].

Mice with deletion of *Trp53* and *Rb1* and normal wt *Vhl* could also develop RCC tumors but with a significantly lower frequency (24%). However, most of them exhibited a range of non-ccRCC phenotypes with

sarcomatoid or rhabdoid tumor cell morphology [75]. More detailed characterization of tumors obtained from this approach would help to elucidate the role of *Trp53* and *Rb1* genes in non-ccRCC pathogenesis.

Vhl Knock-Out and Notch1 (NICD1) Activation

In 2016 Johansson et al. [95] developed a conditional mouse model based on the ectopic expression of a constitutively active intracellular domain of *Notch 1* (NICD1) and the disruption of the *Vhl* gene in renal proximal tubular epithelial cells. The Notch signaling pathway plays an important role in embryonic and postnatal development but has also been established as oncogenic in a variety of tumors, like T-cell acute lymphoblastic leukemia [104], lung adenocarcinoma [105] or melanoma [106]. This has also been confirmed for ccRCC, where the Notch1 receptor is significantly overexpressed, and stimulates proliferation, migration and invasiveness of RCC cells [107,108]. Animals in this model were obtained by crossing the transgenic mouse strain CALSL-NICD, that conditionally confers ectopic expression of human NICD1, with mice carrying a floxed *Vhl* (*Vhl*^{fl/fl}) allele, and the Kap2-iCre mouse strain, in which improved Cre is driven by the androgen inducible and PTEC specific kidney androgen protein 2 (Kap2) promoter. Throughout 12 months, mice did not develop any detectable tumors but immunohistochemical staining of the kidneys revealed nests of dysplastic cells with a clear cytoplasm reproducing the key features of early human ccRCC. With no detectable tumors, this model only confirms the role of both genes in RCC carcinogenesis but has very low utility for further use in RCC research.

FLCN Gene Knock-Out

The *FLCN* gene that encodes FLCN protein is proposed as a candidate tumor-suppressor gene. Its loss of function is one of the causes of the Birt-Hogg-Dube (BHD) syndrome, that among others presents with RCC. This sheds some light on its potential role in RCC development and has led to testing of *FLCN* gene knock-out in the mouse model. *FLCN* homozygous deletion usually results in embryonic lethality [76,109,110].

In a model developed by Chen et al. [77] *Flcn* was deleted under a kidney-specific Ksp-Cre system in the distal tubules, collecting ducts, and the thick ascending limb of Henle's loop. Ksp-Cre;*FLCN*^{Δ/Δ} mice developed bilateral polycystic kidney but died by the age of 3 weeks due to kidney failure [77]. However, in the polycystic kidneys of mice older than 18 days tumors resembling cystic forms of RCC developed. This kind of RCC is extremely rare and accounts for 1% to 2% of all kidney tumors. Interestingly, rapamycin treatment extended mouse survival and delayed development of cysts and neoplasms, what was associated with increased mTOR activity in Ksp-Cre;*FLCN*^{Δ/Δ} mice. It is possible that if mice did not die early due to kidney failure, they could develop solid RCC tumors. Similar observations were also reported by Baba et al. [76] in a heterozygous model (Ksp-Cre;*FLCN*^{Δ/-}); they found that solid tumors displayed histological features similar to human kidney tumors that develop in BHD patients, including ccRCC, oncocytoma or oncocytic hybrid consisting of a mixture of chRCC and oncocytic cells. Molecular phenotypes, with activation of Akt and mTOR pathway, were similar between BHD patients and Ksp-Cre;*FLCN*^{Δ/-} mouse tumors [110].

Also, Hudon et al. [109] and Hartman et al. [111] created a model with a heterozygous *Flcn* loss-of-function mutation in a transgenic mouse strain carrying an in-frame β-galactosidase-neomycin-phosphotransferase II insertion between exons 8 and 9 of *Flcn* in all tissues. Approx. 50% of animals developed sporadic renal tubule hyperplasia, single cysts and multilocular polycystic kidneys before 24 months of age. Cystic lesions expressed markers typical for proximal tubules. Importantly, some mice showed lung adenocarcinoma or diffuse lymphoproliferative disease in several organs [111].

Later on, Chen et al. [112] generated a model with a homozygous knock out of the *Flcn* gene specifically in proximal tubules. To obtain it, *Flcn*^{lox/lox} mice were bred to Sglt2-Cre transgenic mice, with expression of *Cre* recombinase under the control of the kidney proximal tubule-specific

Sglt2 gene promoter (*Sglt2-Cre;Flcn^{Δ/Δ}*). The survival of animals was much longer than in *Ksp-Cre;FLCN^{Δ/Δ}* but none of the animals survived longer than 24 months. All animals at the time of death had significantly elevated levels of blood-urea nitrogen. 53% of animals developed kidney tumors, which is less than in the previous approach, possibly caused by a lower chance of second hit mutations. Histological appearance of tumors was changing with age – in mice younger than 6 months most of the kidney lesions were cysts and hyperplasia while older animals started developing multiple subtypes of solid kidney tumors with the majority of the high-grade RCCs observed in the oldest. Among RCCs different subtypes were present: pRCC (43.5%), high-grade sarcomatoid RCC (25.2%), chRCC (11.6%), oncocytoma (8.8%), ccRCC/oncocytoma hybrids (6.8%), ccRCC (3.4%) and metanephric adenoma (0.7%). Some tumors presented with lymph node metastasis, lymphovascular invasion, fat invasion, and tumor necrosis. Tumors showed activation of Akt and mTOR pathways as well as overexpression of TGF-β related genes, including MMP2, MMP14, and THBS2. Also in this model rapamycin significantly suppressed tumor growth.

Flcn knock-out models, especially *Sglt2-Cre;Flcn^{Δ/Δ}* with longer life span and relatively high penetrance, could be promising *in vivo* models for drug testing but their molecular background resembles only a small proportion of human RCC. The variety of histological subtypes of RCC observed after *Flcn* silencing is also a significant limiting factor. Further analyses, to answer the question what other factors determine the histological type of RCC in this model, are awaited.

Constitutively Active Mutant of HIF1α (TRANsgenic model of Cancer of the Kidney—TRACK model)

Fu et al. [79] attempted to generate a RCC mouse model resembling Von-Hippel Lindau kidney disease by constitutive HIF-1α activation. They created a triple mutant (P402A, P564A, N803A) human *HIF-1α* construct using the kidney proximal tubule specific type 1 γ-glutamyl transpeptidase (GGT) promoter to drive its expression in the proximal tubule cells. The DNA fragment with the mutations was injected into the pronuclei of one-cell embryos of C57BL/6 mice. This method of genetic modification had a rather low success rate – only 4 out of 51 founder mice harbored the integrated target gene. Transgenic mice developed normally and passed the transgene to offspring following a Mendelian inheritance pattern. Animals expressing this triple mutation have constitutively active *HIF-1α*, and exhibited kidney lesions that histologically resemble human VHL disease – cystic changes, distortion of tubular structure and presence of clear cells. The distorted tubule cells showed moderate to marked cellular swelling, cytoplasmic vacuolation, prominent cell membranes, large amounts of cytoplasmic glycogen, a feature of early human ccRCC. Moreover, clear cells had strong expression of CAIX, Glut-1, VEGF, Ki-67 and Proliferating Cell Nuclear Antigen (PCNA). However, no *bona fide* ccRCC has been observed in these mice, except one cystic ccRCC in twenty-two-month-old mice. Histopathological features suggest that clear cells observed in the TRACK model may represent early stage RCC, somewhere between carcinoma *in situ* and frank carcinoma. However, genome-wide profiling of the TRACK kidneys showed some similarities to the human ccRCC transcriptome [113]. When the transcriptome from the kidney cortex of TRACK animals was compared with Oncomide and TCGA database sets, similarities, such as increased expression of genes involved in glycolysis and the tricarboxylic acid cycle, were found. However, only 5 of the 20 genes most highly overexpressed in human ccRCC and none of 20 genes highly underexpressed in human ccRCC showed similar expression patterns in TRACK kidneys. Great caution is needed when evaluating these data since genetic similarity between TRACK model and human ccRCC is rather weak and visible only in the selected metabolic pathway implicating the role of HIF-1α in those pathways and not confirming the TRACK model as a reliable model of ccRCC.

These results indicate that *HIF-1α* functions as an oncogene in renal carcinogenesis and is an interesting target for research on reliable animal models. The insufficiency of inducing *bona fide* RCC in this model indicates

that further studies are required. The mouse model of Von-Hippel Lindau syndrome may be useful in sequential analysis of events leading to development of RCC but in the current state it cannot be used in evaluation of new treatment strategies for this cancer type.

Myc Overexpression

Shroff et al. [80] created a mouse model with conditional *Myc* overexpression using the Tet system. The MYC pathway is activated in most of human RCC [114] and thus was an interesting target for the development of RCC models in mice. *Myc* expression was driven by the kidney-specific GGT promoter coupled to the tetracycline transactivating gene (*tTA*). Induction of *Myc* resulted in fast development of RCC. Tumors were positive for PAX8, E-cadherin, CK5/6, CK7 and negative for CD20 – features of aggressive collecting-duct carcinoma. Additionally, tumors were completely dependent on *Myc* expression since MYC inactivation resulted in complete remission of RCC.

Later on, a similar attempt was undertaken by Bailey et al. [78] who generated mutant mice expressing a doxycycline-inducible *Myc* transgene, targeted to renal tubule cells under the control of the *Ksp* promoter (*Ksp-rtTA*; tet-O-*Myc* mice). Mice developed tumors with either papillary or more solid infiltrative appearance. Tumors were of high-grade and characterized by hyperchromatic cells with a high nuclear to cytoplasmic ratio, nuclei with large nucleoli and significant pleomorphism. *Myc*-tumors showed strong genetic correlation with human pRCC and co-clustered with type 2 pRCC [78].

Myc overexpression was combined further with *Vhl* and *Ink/Arf* (*Cdkn2a*) knock-out [78]. Renal tumor formation was found in 67% of animals with *Myc* activation and *Vhl* inactivation (VM mice) and 100% of mice with *Myc* activation, *Vhl* and *Ink/Arf* inactivation (VIM mice). Tumors in VM mice had tubulo-papillary or solid histology with occasional clear cell features. Similar features were found in VIM mouse tumors but some of them also harbored clear cell features strikingly similar to human ccRCC. Comparison of whole transcriptome centroids of mouse tumors with TCGA KIRC (ccRCC) and KIRP (pRCC) data revealed that they strongly correlate with human ccRCC. It is worth noting that the VIM model is the first autochthonous model of ccRCC that develops liver metastases. Cells from VIM tumors exhibit gene expression changes consistent with epithelial-to-mesenchymal transition and are associated with invasion and metastasis through remodeling of the extracellular matrix [78]. Studies on this model shed more light on the role of *Ink4a/Arf* loss as permissive event for the emergence of clones that are responsible for the metastatic potential of ccRCC. Thus, the VIM model may be used not only to study pathogenesis of ccRCC but also to test potential drugs aiming at reduction of cell invasion and metastases.

The difference in the histological subtypes of tumors induced by sole *Myc* overexpression in the above-mentioned models may be caused by the relative differences in expression patterns of the promoters used to overexpress *Myc* or different timing of this process. However, both models are of great value since they resemble more rare subtypes of RCC that are associated with worse prognosis. Use of *Myc*-overexpressing models may help to better understand the genetic and molecular bases of those types and to find better therapeutic options. The model with *Myc* overexpression under the GGT promoter is the only autochthonous transgenic mouse model of highly aggressive collecting-duct carcinoma that can be a useful tool to evaluate new therapeutic options for the treatment of this subtype of RCC. Additionally, concomitant mutations in other genes, besides *Myc*, significantly affect the histological appearance, confirming the complex genetic background of RCC and the underlying need for further research in those models.

TFEB Overexpression

Approximately 2% of ccRCC [115] and 12% of type II pRCC [97] present with chromosomal translocation of *TFEB* or *TFE3* genes, leading to their overexpression. The desire to understand the mechanism leading from *TFE* translocation to carcinogenesis has led to the creation of experimental

animal models with kidney-specific overexpression of the *Tfeb* gene [94]. The model ($Cdh16_{Cre}::Tfeb_{fs}$) was obtained by crossing the *Tfeb* conditional overexpressing mouse line carrying *Tfeb-3xFlag_{fs/fs}* under the control of the chicken beta-actin promoter with the *Cdh16_{Cre}* mouse strain, in which *Cre* recombinase is specifically expressed in renal tubular epithelial cells starting from the embryonic stage. To rule out effects of *Tfeb* overexpression during kidney development, Calcagni et al. [94] have also created a model ($Cdh16_{CreErt2}::Tfeb_{fs}$) with inducible *Tfeb* expression using the mouse line that carried a tamoxifen-inducible *CreErt2* element under the control of a *Cdh16* promoter for crossing. In both models, survival of animals was approx. 3 months. At autopsy, all animals had significantly enlarged kidneys with severe cystic disease. Histologically cysts from $Cdh16_{Cre}::Tfeb_{fs}$ animals presented markers that suggested that they originated from distal tubules and collecting ducts, while in $Cdh16_{CreErt2}::Tfeb_{fs}$ cysts arose from proximal and distal tubules. Moreover, analyses showed the presence of clear cells, fibrosis, multi-layered basement membranes and accumulation of collagen – features that resemble human *Tfeb*-fusion RCC tumors. Besides cysts, older animals presented neoplastic lesions, ranging in size from 0.1 to 2.93 mm. Moreover, 23% of $Cdh16_{Cre}::Tfeb_{fs}$ animals, older than 3 months, developed liver metastases. Studies in this model have revealed that TFEB overexpression leads to significant activation of the WNT pathway. Additionally, the WNT inhibitor PKF118-310 was tested *in vivo* in this model, resulting in reduction of kidney mass, and the number of cystic and neoplastic lesions [94].

This model can be useful for mechanistic and therapeutic studies on TFEB-fusion associated RCC. This subgroup of RCC includes both clear cell and papillary histology, but in this animal model no analysis to distinguish the histological type was performed. It is worth stressing that kidney function in both models was severely impaired – animals had highly increased blood urea levels and presented with albuminuria [94], what hardly ever occurs in humans with RCC. This complication shortened the animals' survival limiting the utility of this model in studies on long term effects of potential treatments.

Wt1^{-f/l}H19^{+/-m}Cre^{-ERTM} Mice

Nephroblastoma, or Wilms tumor, is the most frequent kidney tumor in children. At the molecular level it is characterized by various genetic alterations with most commonly loss of heterozygosity or loss of imprinting at the chromosomal region 11p15 resulting in biallelic expression of IGF2 observed in 70% of cases [116]. Moreover, approx. 20% of tumors harbor inactivating mutations of the *WT1* gene [117]. The first attempts to create a Wilms tumor model were based on the homo- and heterozygous knock-down of the *Wt1* gene, however, they were unsuccessful. Homozygotes lacked kidneys and died pre- or perinatally while heterozygotes did not develop kidney tumors [118,119]. Based on this, Hu et al. [120] have created an GEM model with conditional ablation of the *Wt1* gene and constitutive IGF2 upregulation in the metanephric mesenchyme in mice. *Wt1^{-fl}* mice received the H19⁻ allele that results in expression of the normally silenced maternal copy of IGF2 and *Cre-ERTM*, a tamoxifen-inducible *Cre*-expressing transgene. Embryos were treated in utero at E11.5 with a tamoxifen dose of 1 mg/40 g body weight, which resulted in *Cre*-mediated recombination in approximately 5%–10% of kidney cells and no decreased viability of mutant embryos. With this approach animals (*Wt1^{-f/l}H19^{+/-m}Cre^{-ERTM}*) developed tumors at an early age, with palpable tumors observed at 9 weeks of age [120]. At 19 weeks of age 64% animals presented with tumors [120]. Significant neoangiogenesis was observed in tumors, as evidenced by a dense network of CD34+ microvasculature [121]. Moreover, significant impairment of renal excretory function of the affected kidneys was observed in all animals at later stages of tumor development with an almost complete destruction of kidney anatomy and the formation of large heterogeneous tumor masses with multiple urine-filled hemorrhagic cysts [121]. Histologically and molecularly mouse nephroblastomas recapitulate human histology with typical, triphasic tumors, with predominant blastemal and epithelial cells along with stromal elements as well as similar gene expression patterns [120]. Moreover, *Wt1* ablation and *Igf2*

upregulation in tumors results in up-regulation of glucose utilization during initial stages of tumor development, followed by a gradual decrease in tumor glycolytic activity, consistent with the development of large areas of hemorrhagic necrosis [121]. The same authors have tried to develop this model further by additional stabilizing *Ctnnb1* mutation under both the *Cited1-Cre* and the *Six2-Cre* recombinase that target nephron progenitors [122]. It resulted in the development of tumors with a predominantly epithelial histology, contrary to typical triphasic morphology with aberrations only in WT1 and IGF2.

To sum up, *Wt1^{-f/l}H19^{+/-m}Cre^{-ERTM}* mice are the only available GEM model of nephroblastoma with a high resemblance to human neoplasms. Moreover, some therapeutic strategies, like MEK inhibitors, have already been tested in this model [121].

Chemically-Induced Models

Before the era of genetic modifications most of the diseases were modeled *in vivo* by chemical compounds. When several compounds were tested for different applications in small animals, some of them developed renal tumors [123]. These observations led to trials to identify chemically-induced orthotopic models of RCC. There is a large range of chemically induced models of RCC, however, they have several limitations (Table 2). They are usually induced by single administration of a chemical carcinogen that does not resemble exposure in humans, which is usually persistent and observed at much lower doses. Moreover, chemical substances do not act in a tissue or organ specific fashion and besides renal tumors they may also cause a variety of other lesions, including other malignancies what significantly limits the utility of such models in preclinical tests. On the other hand, these models allow us to study sequential stages in the carcinogenic process that lead to formation of heterogeneous tumors presenting with different genetic aberrations between animals or even between tumors in the same animal. Moreover, in chemically induced models, tumors occur in immunocompetent animals which is crucial in studies on therapies targeting the immune system [124]. Below we summarize data about available chemically-induced models of RCC but we want to underline that most of them are rather historical and not used in RCC research nowadays. We also mention several examples where tumors produced in chemically-induced models can be a source of cancer cells for subsequent implantation in animals.

Streptozotocin-induced RCC

In 1977 Horton et al. [125] reported the incidental finding of renal tumors in Wistar rats with diabetes induced by a single injection of 25 mg/kg of streptozotocin, an antibiotic and diabetogenic agent produced by a strain of *Streptomyces achromogenes*. 45% (36/80) of animals developed renal tumors. Epithelial tumors, ranging in size from 0.5 to 22 cm, composed of large polygonal clear or granular eosinophilic cells, forming solid sheets or papillary glandular structures, were observed in 13/36 rats. Larger tumors presented with hemorrhage, necrosis and increased mitotic activity thus could be considered as equivalent to human adenocarcinomas. Moreover, 32 mesenchymal tumors, uniformly pale and mostly solid in appearance but with some cystic areas, arose in Wistar rats. 25% of them were clearly mesenchymal, while the remaining 75% had both mesenchymal and epithelial cells, mostly present in the form of tubules [125]. Microscopically, the mixed tumors resembled the nephroblastomas found in man [125]. Animals in this model did not form any distant metastases [125].

Kidney tumors resembling nephroblastoma were also found in spontaneously hypertensive (SHR) rats and Wistar rats treated neonatally with 37.5 to 70 mg/kg or 100 to 150 mg/kg of streptozotocin, respectively [126]. Incidence of renal tumors ranged from 10 to 40% but the study was performed on a small number of animals [126].

Later, Hard [127] created the first mouse model of streptozotocin-induced renal carcinoma. CBA/H/T6J inbred mice were treated with a single dose of 250 mg/kg i.v. streptozotocin at the age of 6 weeks. Tumors,

usually multiple, occurred in 97% of female mice and 73% of the males at death, however, mean survival times were significantly shorter in males than females, 42.2 and 58.4 weeks, respectively. The authors suggest that lower incidence of renal tumors in males is associated with early mortality due to pyelonephritis rather than a difference in effectiveness of streptozotocin [127].

Based on the size and histology, only 60% of tumors in female mice and 31% in males were classified as carcinoma. Carcinomas were characterized by a diameter of over 2 mm, basophilic cells with cellular pleomorphism, prominent mitotic activity, hemorrhage, necrosis, local invasion. Smaller lesions (0.5 to 1 mm) were classified as papillary or solid adenomas. Adenomas of intermediate size (1 to 2 mm) appeared to be transitional stages between the papillary/cystopapillary adenomas and the more rapidly expansive carcinomas [127]. While streptozotocin-induced renal tumor cells have some ultrastructural features in common with human chRCC, the overall ultrastructural morphology differs significantly from various histological types of human RCC [128]. 22% of carcinoma-bearing females developed distant metastases, mainly to lungs, while no distant metastases were observed in males [127].

In another study, a similar approach was used in BALB/c and C57BL/6 mice [129]. When tumors were induced by single i.v. injection of 200 mg/kg streptozotocin, 33/180 (18%) of BALB/c and only 1/180 (<1%) C57BL/6 mice developed renal carcinoma. To minimize the diabetogenic effect of streptozotocin, in further experiments mice received i.v. injections of streptozotocin 160 mg/kg on day 0 and 110 mg/kg on day 75, or 160 mg/kg streptozotocin on day 0. Histologically confirmed RCCs were observed in 10% of BALB/c after two i.v. injections and in 3% after a single injection of streptozotocin. Tumors from both groups were successfully repassaged, adapted to orthotopic transplantation and further underwent comprehensive histological and molecular characterization as SIRCC-1 and SIRCC-2 isolates, respectively. SIRCC-1 cells implanted orthotopically at a dose of 10^5 cells presented slow progression *in vivo* with a mean survival time of 3 months. SIRCC-1 tumors had high heterogeneity and high potential to form lung metastases depending on the aggressiveness of the subclone. Tumor metastases were usually observed in animals by days 17 to 19, while some subclones had a significantly lower ability to form metastases. SIRCC-1 tumors developed extensive tumor-associated neovasculation and showed expression of proangiogenic genes, such as vascular endothelial growth factor, fibroblast growth factor 2, transforming growth factor β 1 and β 2, vascular endothelial growth factor receptors Flt1 and Flt4 and the angiopoietin R Tiel [129]. In contrast to human ccRCC, no *Vhl* or *Ras* mutations were found in SIRCC-1 tumors [129]. Intratumoral heterogeneity observed in SIRCC-1 tumors provides a setting in which experimental therapies can be tested against a backdrop of widely varying tumor cell phenotypes to discover the mechanisms of susceptibility or resistance to various anticancer drugs. Aggressiveness of tumors from BALB/c mice gives the possibility to utilize this model in the studies on regulation of metastasis formation.

Due to resistance of C57BL/6 mice to streptozotocin, higher doses of the drug (250 mg/kg i.r. on day 0 or 375 mg/kg i.v. on days 0 and 75) were tested [129]. Since only one RCC, not adaptable to serial transplantation, was found in the i.v. group of C57BL/6 mice, the ability of streptozotocin to induce renal tumors in this mouse strain is very limited [129].

It seems that induction of RCC by streptozotocin is not dependent on the *Vhl* or the *Ras* gene. Some authors suggest that hyperglycemia, resulting from specific destruction of the insulin-producing β -cells of the islets of Langerhans by streptozotocin, is the main trigger of the carcinogenesis in this model [130] but the reduction of glucose concentration by insulin injections or peritoneal implantation of porcine islets in diabetic Wistar-Furth rats did not protect the animals from development of renal carcinomas [131]. Similarly neither insulin treatment nor low-carbohydrate diet reduced the effects of streptozotocin in Wistar rats [125]. Because of the diabetogenic effect of streptozotocin, high mortality of animals can occur [129].

Typically, as carcinogenesis induced by chemicals is not completely specific to one organ or type of cells, tumors other than renal carcinomas were found in the streptozotocin-induced model. The most common

alveogenic lung neoplasm was found in 87% of female and 35% of male CBA/H/T6J mice. Other concomitant tumors included liver, uterine and pancreatic tumors [127]. In BALB/c mice lung tumors were found in 20% of animals [129]. Even as low a dose of streptozotocin as 30 mg/kg can induce adenomas of pancreatic islets in up to 89% of rats [126,132]. Also liver tumors, resembling hepatomas were observed in Wistar or SHR rats after streptozotocin injection [126].

An interesting observation was made by Reddi et al. [133] who reported potentiation of the tumorigenic potential of streptozotocin by cyclosporine A (CyA). In Wistar rats which after i.p. injection of 60 mg/kg streptozotocin received 10 mg/kg of CyA every 3 days for 20 weeks, renal tumors were found in 53.8% of animals while in the group not treated with CyA only in 12.5% [133]. The increased incidence of renal tumors in diabetic rats may be due to synergistic action of streptozotocin and CyA. Moreover, CyA impairs the production of interleukin-2 and thus suppresses the generation of T-cells [134], what can promote tumor growth by silencing the immune response of the host animal. It is not known whether CyA could potentiate renal tumorigenicity in nonchemically-induced animal models. Despite interesting observation, no further studies have been performed on combined use of streptozotocin and CyA in generation of RCC animal models.

Streptozotocin can be also combined with nicotinamide to induce renal tumors. Kato et al. [135] treated 6-week-old Crl:CD(SD) rats with i.v. injection of streptozotocin (50 or 75 mg/kg) and intraperitoneally co-administrated nicotinamide (350 mg/kg) twice, 10 min before and 3 h after the streptozotocin treatment. Over 60% of renal tumors were classified as renal cell adenomas, and many of them were of the basophilic type. The incidence of eosinophilic or clear cell type of tumors was lower than 10% [135]. Over 50% of animals develop concomitant tumors of liver, adrenal glands and pancreatic islets [135]. In contrast, Rakieten et al. [136] reported that nicotinamide can reverse the effect of streptozotocin – the incidence of tumors was reduced from 77% observed after streptozotocin injection to 18% when nicotinamide was injected before and after streptozotocin, as described above. This discrepancy in the results is hard to explain because nicotinamide is a well known carcinogen and should rather increase tumor incidence.

Summarizing, wide discrepancies in the incidence of renal carcinomas, ranging from 0% to 77%, in streptozotocin-induced tumors should be underlined. These inconsistencies may be caused by different induction protocols, streptozotocin doses, animal strains and time of evaluation. However, significant changes are observed also even if the same dosing scheme and same strain is used, suggesting the heterogeneity of this model and non-specific molecular mechanisms leading to RCC development induced by streptozotocin. Moreover, a broad histological spectrum of renal tumors, from clear cell and chRCC to mesenchymal tumors, is observed. Those issues should be considered as limiting factors in the use of streptozotocin-induced tumor animal models in studies on RCC pathogenesis or therapy.

2-Acetylaminofluorene-Induced RCC in BALB/c Mice

2-Acetylaminofluorene (2-AAF) has been proposed as another carcinogen useful in establishing a chemically-induced RCC model, however, only 108 of 25916 (0.42 %) Balb/c female mice treated with several dose levels of 2-AAF developed renal tumors, with 27% of them diagnosed as carcinomas and 63% as adenomas. The carcinomas were often bilateral or multifocal, varying from a diameter of 3 or 4 to 12 mm [137]. RCCs were composed of epithelial cells with granular eosinophilic- or basophilic-staining cytoplasm, small and round nuclei with mitotic figures. The arrangement of tumor cells showed a basic tubular pattern, but careful histologic studies revealed that they could be subdivided into the following three morphologic patterns: tubule-solid, tubule-papillary, and tubule-pleomorphic. Mouse RCC appeared to grow by expansion and sometimes replaced almost all of the renal parenchyma. The tumors were not encapsulated, but infiltration of the tumor into adjacent renal parenchyma was unclear [137].

Due to very low incidence of renal tumors 2-AAF cannot be used to induce RCC tumors in animals to create a reliable and reproducible model of this disease. However, this study proves the carcinogenic potential of 2-AAF.

Nitrosamine-Induced Renal Tumors

Magee and Barnes [138] observed that dimethylnitrosamine (DMN) can induce kidney tumors in rats in 1962. This observation was extended by Swann and McLean [139] who demonstrated that a no-protein high-carbohydrate diet enhances the capacity of renal tumor induction, due to the decrease of microsomal enzyme activity in the liver and the increased amount of DMN reaching the kidney. A single i.p. injection of 50 to 60 mg/kg of DMN to immature female Wistar rats or 5-week-old male Porton rats, pre-conditioned for 3 to 5 days with a no-protein, sugar-only diet, has been used for induction of mesenchymal renal tumor with near 80% to 90% incidence [139,140]. Moreover, up to 40% of animals developed concomitant epithelial tumors [140].

Renal mesenchymal tumors consist mainly of fibroblastic spindle cells which can be organized as fibrosarcoma, but other neoplastic features invariably present are stellate cells, often arranged in a reticular pattern as primitive mesenchyme, and smooth muscle fibers which can be sporadic or form areas of leiomyosarcoma. Other elements encountered less commonly are rhabdomyoblasts, striated muscle, cartilage, osteoid and extensive deposition of collagen. Characteristically, the tumors have poorly cellular myxoid areas as well as densely cellular areas [124,141,142]. These tumors partially resemble a small proportion of Wilms' tumors with similarity between rat tumor and the human connective tissue component by virtue of the range of neoplastic cell types which includes spindle cells, smooth muscle, and striated muscle fibers in both species [124]. Many similarities are also observed with congenital mesoblastic nephroma of infancy [124], a solely mesenchymal tumor with heterogeneous composition, including fibroblastic spindle cells, smooth muscle, and sequestered remnants of pre-existing tubules. Moreover, sheets of mesenchymal cells supported by a rich vascular network, heavy collagen deposition, liquefaction, and inclusion of tubular and cystic profiles resemble human clear cell sarcoma of the kidney [124].

Susceptibility to DMN induction of mesenchymal renal tumors is age-dependent with a peak of predisposition at 3 to 4 weeks, but declining rapidly after 6 weeks of age with no mesenchymal tumors formed in 5-month-old animals [143]. Older, more mature animals, exposed to DMN predominantly develop RCC [143]. It is necessary to reduce the dose of DMN to 20 mg/kg in neonatal animals in order to achieve approximately equivalent numbers of survivors [143].

The DMN model has been sequentially used to trace the pathogenesis of renal mesenchymal tumors [141,142]. This model enables cell transfer to cell culture, which is particularly useful in studying chemical carcinogenesis and the evolution of cell transformation in kidney [144].

RCC can be induced by single i.p. injection of DMN at a dose of 30 mg/kg body in 9- to 10-week-old female Wistar rats following a 5-day schedule of high-sugar no-protein diet. This method resulted in about 90% incidence of cortical epithelial tumors with a 70% frequency of lesions classified as adenocarcinomas or carcinomas [145]. Those tumors consist of clear or granular cells arranged in acinar, papillary, or solid carcinomatous patterns and can be identified as originating from the proximal tubule [146]. Adenocarcinomas are usually preceded by microscopic foci of solid epithelial proliferations [147]. This model presented a 15% rate of distant metastases, mainly in lungs. However, almost 50% of animals with large tumors (2.9 cm in diameters or more) develop distant lesions [145].

When DMN-induced epithelial tumors in Wistar rats were screened, only tumors showing prominent swollen clear cell cytology with a signet-ring appearance had *Vhl* mutations that are characteristic for human ccRCC [148]. This observation suggests a closer correlation between RCC in man and clear cell tumors in animals treated with DMN but no further studies confirming this or presenting further genetic and molecular similarities have been published.

Another compound belonging to nitrosamines—N-ethyl-N-hydroxyethylnitrosamine (EHEN) is also an inducer of renal and liver tumors. It was first described by Druckrey et al. in 1964 [149]. Most studies were performed on the Wistar strain because it has higher incidences of renal lesions and neoplasms compared to the Fischer strain, moreover, males are more sensitive than females [150]. EHEN is metabolized to water-soluble products and excreted in the urine. Its metabolites do not induce any lesions in rats but induce lesions in the lungs of mice [151]. EHEN can be given in small doses with food or water for a short period of time. It results in a high degree of tumor induction, but with longer developing time and without frequent metastasis. In most studies EHEN was an initiator of renal tumors, and then other compounds were used to check their impact on the development of the initiated tumors. Some of them increased the number and size of renal tumors (like β -cyclodextrin) [152], others were used to observe their antitumor properties (like green tea catechin) [153].

EHEN induces renal tumors with a rather high incidence. In two studies on male Wistar rats EHEN was given with the diet for 2 weeks in concentrations 0.1% (30 week experiment) or 0.1% and 0.2% (40 week experiment), which resulted in 45% and 60% and 78% incidence of tumors, respectively. [154,155]. In a longer 60-week experiment where young Wistar rats received EHEN in drinking water at dose 0.1% during one week, incidence of renal cancer and adenomas amounted to 47% [156]. In the same experimental lesions that were noted besides tubular hyperplasia were basophilic or eosinophilic cell adenomas, one case was eosinophilic cell adenoma with clear cells, renal tumors were basophilic cell carcinomas [156]. In the 40-week experiment lesions were not distinguished as precancerous or cancerous types. Observed atypical cells in kidneys were similar to the renal tubular cell tumors and possessed abundant clear or slightly basophilic cytoplasm, and a slightly enlarged nucleus. In renal tumors there were 3 types of cells: cells containing large clear cytoplasm with a large nucleus, cells with large cytoplasm and a small nucleus and cells with a papillary or trabecular pattern [155].

However, the mechanism of EHEN action is not fully understood but it was shown that oxidative DNA damage can play an important role. Treatment with EHEN results in formation of the DNA damage product 8-hydroxydeoxyguanosine (8-OHdG). Immunohistochemical staining confirms its presence in the nucleus of tubular epithelium in the renal cortex [150,157]. PCR-SSCP analysis and direct sequencing show that similarly to Eker rats, in EHEN induced animals point mutations occur in *Tsc2*, but not in the *Vhl* gene [158]. Alterations in large parts of the genome were checked only by 2-dimensional gel electrophoresis of genomic DNA and they were not more specifically characterized [137]. Renal tumors induced by EHEN can be a source of tumor cells. The obtained tumor cell lines were injected by the s.c. route into nude mice and, as a result, gave poorly differentiated adenocarcinomas [159]. In another study tumors were induced in male Wistar rats fed a diet containing 0.1% of EHEN for 2 weeks, and followed by a s.c. injection of β -cyclodextrin at a dose of 45 mg/100g body weight once a day for a week. Tumors removed from these animals were transplanted three times in newborn Wistar rats, followed by either i.p. or s.c. injection into young Wistar rats (4-weeks old). S.c. injection resulted in tumors at inoculation sites. The i.p. route of inoculation led to faster growing tumors than s.c., in half of the inoculated animals there was invasion to the spleen, liver, stomach, peritoneum, intestine and lungs. Metastasis to the lung was observed only in two cases out of 12 i.p. inoculated rats. The transplantable tumor cells give alveolar or papillary patterns [160].

Ferric Nitrotriacetate-Induced RCC model

In 1986 Ebina et al. reported that the use of ferric nitrotriacetate (Fe-NTA) in Wistar rats leads to high incidence of RCC [161]. Fe-NTA is an iron chelate that was found to cause oxidative modification in the kidney, including DNA base modifications such as 8-oxoguanine, thymine-tyrosine cross-links, thiobarbituric acid-reactive substances, saturated and unsaturated mutagenic aldehydes such as 4-hydroxy-2-nonenal (HNE) and malondialdehyde (MDA), and HNE- or MDA-modified proteins [162].

When Fe-NTA was tested for nephrotoxicity and carcinogenicity in Wistar rats, 14 of 18 animals, that survived 1 year after sublethal doses of Fe-NTA (5 to 7 mg Fe/kg for 3 weeks), developed primary RCC. In further studies Fe-NTA was injected i.p. according to the protocol: 5 mg iron/kg for 3 days, 10 mg iron/kg for the next 2 days and then 5 days a week for 11 weeks [163,164]. RCC induction rate was approximately 50% - 68% [163,165]. The histological subtype of tumors in this model is unclear. Li et al. [163] reported that tumors resemble human non-clear cell RCCs, Athar et al. [166] described acinar and papillary tumors, while Vargas-Olvera et al. [165] published a report where all tumors had typical clear-cell histology. Different morphological patterns reported in these studies may be due to the use of different experimental animal strains, differences in schemes of treatment to induce RCC, and changes in histological classifications of RCCs. Up to 50% animals with RCC developed metastases to the liver, lungs or peritoneum [161,163]. Metastatic potential has been positively correlated with tumor grade [167]. Besides RCC a few cases of mesotheliomas [163] and renal lymphoma [168] induced by Fe-NTA were found in animals.

Reactive oxygen species (ROS) and the Fenton reaction are proposed as the main mechanisms underlying Fe-NTA-induced RCC. Considering the non-specific nature of ROS reactions, it is crucial to determine whether certain genes are selectively damaged by ROS or the whole genome is randomly damaged. Genetic alterations leading to RCC in this model are not fully known and present some significant differences in comparison to human RCC. Low or no incidence of genetic alterations in the coding region of *H-*, *K-* and *N-Ras* oncogenes, *p53*, *VHL* and *Tsc2* tumor suppressor genes have been recorded [163, 167]. Array-based CGH profiling showed that genomes of the Fe-NTA-induced rat RCCs are often complex and have many extensive chromosomal alterations [169]. The most common alterations were losses of chromosome regions, especially for chromosomes 3, 5, 6, 8, 9, 14, 15, 17 and 20, or frequent amplification over a long pericentromeric region in chromosome 4 [169]. High frequency of loss of heterozygosity (>40%) was found on rat chromosome 5, syntenic to human chromosome 1 and 9, that contains p15^{INK4B} (p15) and p16^{INK4A} (p16) tumor suppressor genes [164]. This observation was confirmed by aCGH where deletions in the *Cdkn2a/2b* locus, containing p15, p16 and p19 genes, were frequently observed [169]. The second copy of these genes can be inactivated by somatic mutations or 5' CpG island methylation; this has been observed in 33.3% of cases in the p16 gene [164]. The *Met* oncogene resides in the most common overlapping genomic section of chromosome 4 what results in a greater than 5-fold increase in *Met* mRNA expression in 66.6% of analyzed Fe-NTA induced RCCs [169]. The pattern of alterations in Fe-NTA-induced rat RCC is most similar to human RCCs, followed by human malignant mesothelioma [169]. In this renal carcinogenesis model, preferred alterations were *Cdkn2A/2B* deletion and *Met* amplification.

Chemical induction of RCC by Fe-NTA was also used to develop cancer cells that underwent implantation in the syngeneic model. Kobayashi et al. [170] described a model in which rat renal cancer cells were established from immunocompetent ACI rats exposed to Fe-NTA. Additionally, a part of these cells was transformed to produce luciferase for further bioluminescence *in vivo* imaging. 1x10⁶ tumor cells were injected into the abdominal subcutaneous space. About one week later the formed tumors exhibited moderately differentiated carcinoma of the basophilic cell type. In an orthotopic injection (in the same concentration) into the left renal subcapsular space metastatic spread to the lung was observed about 2 weeks after inoculation. Modified cells with expression of luciferase also formed metastasis in lungs in a similar time after implantation [170].

Due to not fully understood genetic mechanisms of the non-specific action of Fe-NTA and ROS, long time to tumor induction, no consistent data about histological subtype of tumor and co-occurrence of mesothelioma, use of this RCC model in cancer research is very limited. However, it could potentially be useful in studies on the role of oxidative stress in carcinogenesis or be a source of cancer cells for transplantation.

20-Methylcholanthrene-Induced Renal Tumors

Stevenson et al. [171] induced a variety of renal tumors by implantation of cotton strings impregnated with 20-methylcholanthrene in the kidney of C57BL6 mice. During 5 to 7 months of experiments, 53% of animals developed renal tumors, half of them being renal carcinomas and half spindle-cell sarcomas. Despite the well-known potential to induce experimental sarcomas by 20-methylcholanthrene, it has not been successful in creation of renal sarcoma models, mostly due to lack of specificity and possible development of renal carcinomas [171,172].

Other Compounds Inducing Renal Tumors

There are studies of several dozen compounds that can cause renal tumors [173]. Although lesions caused by these compounds are similar to those found in humans or in animal models, for example potassium bromate (KBrO₃) induces clear cell renal tumors in male Fisher rats [174], consumption of mycotoxins like ochratoxin induces lesions similar to the ones found in Eker rats [175] or Fumosisin B1 results in tumors with high anaplasia and metastasis to lungs [176], these studies do not establish new distinct animal models for renal tumor research.

Models in Immunodeficient Animals

Immunodeficient animals are organisms that have an impaired capacity for fighting infections and generate immune response against tumor cells. Wide application of this approach in oncology studies was an effect of discovery of two groups of immunodeficient animals: firstly, nude mice [177] and later severe combined immunodeficient (SCID) mice [178]. Athymic nude mice are hairless, which is an effect of a Forkhead box protein N1 mutation (*Foxn1^{nu}*). They also lack a thymus and are T-cell deficient but produce functional B-cells at the same time [179]. SCID mice have a single nucleotide polymorphism in the DNA-dependent protein kinase of catalytic polypeptide *Prkdc* gene (*Prkdc^{scid}*). This mutation affects both T and B lymphocytes [178]. SCID rodents display less pronounced immunoreactivity than athymic nude mice to the implanted cancer cells what results in greater receptivity to tumor xenotransplantation [180]. Recently, several promising transgenic models have become available, including humanized NOD/scid/IL-2γ-receptor null (NSG) mice [181]. NSG mice not only have the SIRP1α polymorphism of the SCID mouse, which enables SIRP1α-CD47 interactions and prevents phagocytosis of human cells by murine monocytes, but also lack the common gamma chain (IL-2Rγc), resulting in NK cell deficiency and a lack of IL-2, IL-4, IL-7, IL-9, IL-15, and IL-21 signaling [182]. All immunodeficient animals allow transplantation of cells originating from all of the tissues from other species, most importantly humans, without rejection. Based on this, xenografts formed by implantation of human cell lines and various kinds of patient derived cells can be formed with immunodeficient animals.

Xenograft Models

Xenograft models are based on the implantation of tumor cells or tissue samples into immunocompromised animals, mostly mice. Xenografting into mice has advanced pre-clinical cancer research significantly by permitting a complete and accurate study of tumor growth and evaluating the therapeutic efficacy of novel anti-cancer drugs. Specimens of RCC tumors usually originate from biopsy/surgery samples of human primary or metastatic tumors and such model are called "patient derived xenografts" (PDX) and are described further in this article. Conventional xenograft RCC models are constructed by implantation of tumor cells from commercially available cell lines. Cells can be implanted orthotopically under the kidney capsule or ectopically, usually subcutaneously. Other routes of ectopic implantation of tumor cells include i.p., intravenous or intramuscular.

The main advantage of orthotopic models is the fact that the tumor is formed exactly in the tissue where it originated and thus allows taking advantage of the circulatory system, local cytokines and surrounding stromal

cells along with the extracellular matrix components of the tissue to study metastasis for human subjects [183,184]. On the other hand, the procedure of cell implantation under the renal capsule requires surgery under anesthesia, is more stressful for the animal, can be associated with additional inflammation caused by surgical cuts or sutures and can lead to higher mortality and morbidity [185]. Moreover, when working with orthotopic models, more advanced imaging techniques like bioluminescence, ultrasound, computed tomography or magnetic resonance imaging, are necessary to monitor tumor development since it is not visible with the naked eye.

Ectopic, subcutaneous models are much easier to develop – they do not require anesthesia and the injection takes a few seconds. Tumors are easily visible under the skin and can be measured with simple calipers. However, the microenvironment does not completely resemble the one observed in the kidney. On the other hand, we should be aware that in RCC most of the patients undergo nephrectomy and systemic therapies are used for treatment of metastases, that can be localized in any organ, thus the tumor niche identical as in the kidney could not be necessary for studies on new therapies.

The key issue in xenograft models is the selection of an appropriate cell type and number of cells. For the pRCC the most commonly used cell lines are ACHN [186] and Caki-2 [187,188], while for ccRCC Caki-1 [189–192] and 786-O [189,192–195] [196]. Other lines that have been used less often include among others 769-P [197], RCC4 [198], SMKT-R [199], SKR-RC [200], SN12K-1 [201], RC29-MK [202] and SKRC-17 [203]. Cell lines for other tumors, e.g. the G401 cell line that enables xenograft studies on rhabdoid kidney tumor [204] or UOK262 – a cell line of hereditary leiomyomatous renal cell carcinoma [205, 206] are also available.

Some RCC cell lines have not been proved to be tumorigenic in nude mice: 769-P, SK-RC-7, TK 10, TK 164 UM-RC-6, or UOK108 [189,196, 200,207–209]. Moreover, some cell lines are tumorigenic but the tumor histology does not resemble human neoplasms as for example with nephroblastoma cell lines WIT49 an 17.94 that when inoculated under the renal capsule do not produce blastema-containing triphase Wilms tumors [210]. There were also serial studies using the SK-NEP-1 cell line to create nephroblastoma xenografts [211–213], however, recent studies showed that this cell line is related to Ewing sarcoma, not nephroblastoma, and should not be used for such purposes [214].

The number of injected cells varies significantly between authors from 2×10^4 [197] up to 2×10^7 [198] with the majority using approximately 1.5×10^6 [190,192,195,199]. Cancer stem cell-like side population cells might have higher tumorigenic potential than non-stem cells, as it was shown for stem cells derived from the 769-P cell line, which were tumorigenic when only 200 cells were implanted s.c., while non-stem cells required at least 20000 cells [197]. The cell number required to form a tumor can depend on the cell line, passage, animal strain, route of injection, individual conditions and requirements of the investigator. Cells from highly tumorigenic lines can form a tumor even when injected in low numbers but they will require a longer period to develop a visible lesion. For drug testing usually a volume of approx. 100 mm^3 or more is required before administration of the tested compounds – depending on the cell line and the number of cells, tumors of such volume develop after around 2 to 4 weeks. Cells can be suspended in neutral buffer or culture medium with or without solubilized tissue basement membrane matrix rich in extracellular matrix proteins that can facilitate the establishment of xenografts [215].

Some modifications of orthotopic implantation methods were proposed by different authors. Chapman et al. [190] in their study first created a tumor in a BALB/c nude mouse by injecting approximately 1×10^5 Caki-1 tumor cells s.c. and once the tumors reached a size of 400 to 500 mm^3 they were fragmented into roughly equal size $2 \times 2\text{-mm}$ tissue chunks and implanted into the flanks of the experimental BALB/c nude mice. When the secondary tumors reached an appropriate size, the animals were randomized for further experiments [190].

Even though immunocompromised mice are the most commonly used for xenograft formation, there are single observations for rat models. An example of human ccRCC xenograft in the athymic nude rat was described by

Buvall et al. [203]. In these animals after suppression of B cell-mediated immune response by irradiation, 1×10^7 SKRC-17 human derived tumor cells were implanted s.c. in the rat shoulder region. Tumors arose during the period of several days. This model was developed to test the anti-cancer potential of orellanine and has not yet found wide application.

Metastases in Xenograft Models

One of the most challenging issues in xenograft models is the simulation of metastatic disease. Already in 1986 Naito et al. [216] published a study in which they showed that transplantation of a human RCC tissue sample under the skin or under the renal capsule is tumorigenic and subcapsular inoculation leads to metastatic spread into the liver and peritoneum. Different cell lines derived from primary tumors or metastases were metastatic when injected subcutaneously, intravenously, into the spleen or under the renal capsule, however, their effectiveness in formation of metastases varied between different cell lines and routes of administration. The subcapsular route seems to give the highest rate of successful development of metastases and resulted in extensive metastasis to the lungs and in all peritoneal organs. The potential of orthotopic models to develop distant metastases has been confirmed in later studies [217] [184].

An et al. [184] compared two approaches of subcapsular xenografting: surgical orthotopic implantation (SOI) of histologically intact tumor tissue obtained from a previous subcutaneous tumor from SN12C cells, and cellular orthotopic injection of SN12C cell suspensions (COI). The SOI method resulted in 2 to 3 times higher metastatic rate when pieces of tumor tissues were used. Moreover, primary renal tumors were also of higher grade and had richer vasculature in the SOI model than in COI. This study can be considered an ancestor of PDX.

Additionally, Kozłowski et al. [193] showed that use of 786-O cells can lead to formation of lung metastases when given i.v. (1×10^6), subcutaneously (0.5×10^6) or into the spleen (5×10^5), with the frequency of 73%, 20% and 60%, respectively. Moreover, when cells were injected into the spleen, metastases in liver and regional lymph nodes could be found.

Bone Metastases Models

Models of bone metastases of RCC have gained attention in different tested approaches. 786-O cells form osteoclastic bone metastases when inoculated in the left heart ventricle (5×10^5 or 1×10^6 cells) of an athymic nude mouse with 100% frequency within 50 to 80 days [218,219]. Interestingly, no metastases in other organs were found in one study [218] while in another lesions in liver and lymph nodes were present [219]. ACHN cells have the same properties when injected intracardially (3×10^6) [220] or i.v. (5×10^5) [221] in nude mice which develop bone metastases within at least 3 weeks. Sunitinib was tested in this model and showed significant activity against bone metastases [220].

Bone metastases can also be obtained by inoculation of 786-O or RBM1 cells in the bone, e.g. tibia, however, this method is characterized by approx. 50% engraftment success and development of the lesion only in the inoculation site [194,222]. In another study a piece ($\sim 0.3 \text{ mm} \times 0.3 \text{ mm}$) of the previously harvested subcutaneous tumor of ACHN origin was placed onto the decorticated spinous process and lamina in NOD/SCID mice to form spinal metastases that were present at 12 weeks after surgery [223].

D'Amico et al. [224] described the “human-in-mice” model of bone metastases. First, they transplanted a small fragment of human bone into the flank of NOD/SCID mice and later injected human RCC stem cells, isolated from the primary tumor, subcutaneously in Matrigel in the proximity of the bone graft or intracardially. 53% of animals developed metastases in the engrafted bone and 25% also had lung metastases. Because stem cells were c-MET positive, c-MET inhibitor JNJ-38877605 was tested with this model resulting in a complete blockade of bone metastasis development.

Currently, more effort is put into the development of patient derived models of bone metastases. Valta et al. [225] constructed the first human RCC bone metastasis model using a patient-derived tissue slice graft (TSG) technique. $300\text{-}\mu\text{m}$ thick slices of fresh RCC tissue obtained during nephrectomy were implanted under the renal capsules of immunodeficient

RAG2^{-/-}γC^{-/-} mice. Most of the animals developed bone metastases while some also presented with soft tissue metastases. Importantly, similar engraftment rates were observed when cryopreserved TSGs were used allowing the use of bio-banked RCC tissues, e.g. at the moment of disease progression to test possible therapeutic options. The frequency of metastasis development was different for each patient sample but correlated with the further course of the disease in the human. This indicates that TSGs can be predictive of metastatic disease and may provide prognostic information for RCC management.

Patient-Derived Xenograft (PDX)

PDX are cancer models where the patients' tumor tissues or cells are implanted into immunodeficient or humanized mice. The orthotopic xenograft model of RCC formed by subcapsular injection may preserve histological, immunophenotypic and genetic features of tumors in patients [226,227]. In large study with RCC, PDX models achieved an engraftment rate into NOD-SCID IL2Rg^{-/-} mice of 45% [228]. Importantly there were no significant differences in engraftment between samples obtained from biopsy and surgically resected tumors (58% vs 41%; p = 0.3) or between metastatic and primary tumors (54% vs 34%; p = 0.091). Lang et al. also observed that the engraftment rate increases with the Fuhrman grade, from 0% success rate for grade 1 to 36.1% for grade 4 [229]. A similar observation was made for tumor stage and sarcomatoid differentiation [229]. As observed in previous studies, histology, genetic alterations and therapy responses were preserved in PDXs [228,229]. Sanz et al. reported that RCC PDXs can maintain human endothelial cells 35 days after implantation [230]. There are also single studies with PDX models for kidney tumors other than RCC, e.g. nephroblastoma tumor samples or cell suspensions xenografted subcutaneously or under the renal capsule [211,231,232]. Ascites fluid can also be used as the source of the tumor cells for the formation of PDXs, however, it resembles more cell line-derived xenografts than PDX methodology [228]. A detailed, validated protocol for RCC PDX formation is available [233]. Shibasaki et al. have established two primary PDX models of Grade 2 >3 and Grade 3 ccRCC named KURC1 and KURC2, respectively [234]. Both of these PDX were able to recapture the histopathological features and architecture of the original tumors [228,234]. Sivanand et al. developed and validated large scale PDX models for the evaluation of molecularly targeted therapies for RCC [235]. Samples from 94 patients with kidney cancer were implanted for establishing PDX models. More than 90% of PDX were from RCC and 75% were of the ccRCC subtype (87% have the *VHL* mutation). Detailed analysis of these orthotopic PDX models revealed that most of them retained not only histological features of the corresponding RCC patient tumors but also gene expression patterns, DNA copy number alterations, point mutations and indels from the same RCC patient [235].

The success rate of preclinical research for oncological compounds tested in clinical trials from first-in-man studies to compound registration

is less than 5%. The major causes of this failure rate in clinics were lack of efficacy (30%) and safety (toxicology and clinical safety amounting to as high as 30%) [236]. The root causes of the compound attrition in clinics were poor understanding of the human cancer complexity and limited predictive value of preclinical models used to test new cancer compounds [237,238]. Use of above-mentioned conventional cell-line derived xenograft models has improved our understanding of cancer development and the mechanisms of drug actions. However, they have major limitations like inappropriate tumor microenvironment and lack of tumor heterogeneity. As a consequence, the idea of PDX models, which can produce clinical outcomes that can be observed in the individual patient donors, arose. In comparison to conventional xenografts, immunocompromised mice bearing subcutaneous surgically-derived patient tumor samples (PDX models) are better aligned with human cancer pathophysiology [10]. PDX models enable to better preserve tumor architecture than conventional xenograft models which are compromised by *in vitro* cell adaptation before injection (Figure 2). To date PDX models most accurately represent the tumor heterogeneity and reflect tumor-stroma interactions of the original tumor [239,240]. These models are now becoming an important tool to recapitulate the clinical situation of RCC patients, particularly in drug development and studying the mechanisms of metastasis and drug resistance [225,241–244]. In fact, PDX models were used for testing novel targeted therapies, such as multi-targeted tyrosine kinase inhibitors (TKI) sunitinib [229,234,245], mTOR inhibitor everolimus [229], MET inhibitor savitinib [242,245] and dovitinib (CHIR-258) [235]. Tumor progression was observed in KURC1 after 4 weeks of sunitinib treatment, while KURC2 retained its sensitivity to sunitinib for more than 6 months. The sunitinib resistant profile was successfully reproduced when KURC1 tumors that acquired resistance were transferred to other xenografts. These KURC1 transferred xenografts were found to be completely resistant to sunitinib and maintained the ccRCC histotype [234]. Furthermore, upregulation of IL-13 receptor, alpha 2 (IL13RA2) was found as a candidate molecule responsible for the acquired resistance to sunitinib in ccRCC in this PDX model. Diaz-Montero et al. used the PDX model to circumvent the sunitinib acquired resistance by combining sunitinib with MEK inhibitor [245]. The Ren-02 PDX model established from a metastatic ccRCC patient retained the ccRCC phenotype and acquired sunitinib resistance after 30 days (approx. 4 weeks) of treatment. Development of the acquired sunitinib resistance was similar to that observed clinically in metastatic ccRCC patients [246]. Two other PDX models of pRCC, RCC-43b from metastatic pRCC and RCC-47 from a primary lesion, were also used for studies with MEK inhibitors [242]. Another important aspect of Simvad study was that the PDX models were able to reproduce drug responsiveness as observed in clinical responses of the RCC patients. In addition, dovitinib, a multi-targeted TKI, was able to inhibit tumor graft growth in these PDX models [235].

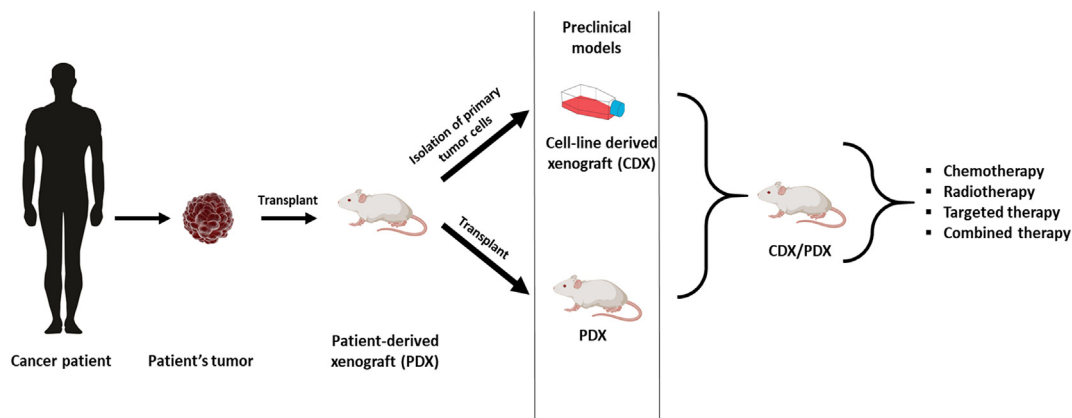


Figure 2. Development of patient-derived xenograft (PDX) and cell-derived xenograft (CDX) models in clinical oncology. A sample of tumor tissue is obtained from patient and transplanted into immunodeficient mice to form PDX. Further, tumor from the PDX can be transplanted to another animal to create PDX or primary tumor cells can be isolated and transplanted into mice to create CDX. Both approaches allow testing different therapeutic strategies, e.g. chemotherapy, radiotherapy or targeted therapy.

Despite many advantages of PDXs, one must be aware of their limitations. Tumors that successfully engraft in mice are usually more aggressive, and thus less aggressive ones are underrepresented in the studies. Moreover, tumors derived from metastatic sites tend to engraft at higher frequencies than from the primary site [235]. However, this can be considered as a prognostic factor and tumors that fail to engraft are the tumors of lower aggressiveness and a lower risk of developing distant metastases in the human. The engraftment success rate may vary depending on the tissue sample, e.g. necrotic samples or those with few tumor cells may not engraft at all, and it is challenging to predict the timing of growth [233,247]. Moreover, NOD/SCID mice may develop thymic lymphomas and malignant lymphocytes can infiltrate the tumor, thus a sample should be closely monitored between each serial passage [233].

Avatar Models

Personalised medicine, also called precision medicine, aims to reach beyond the “one size fits all” approach to treatment and promotes the use of “tailored therapy” for each patient. In this approach, based on pharmacogenomics and gene expression profiling, physicians should be able to personalise the treatment to achieve the highest safety and efficacy in a particular patient. Avatar model is a personalized PDX that is derived from a patient tumor sample and used to test different active compounds for the particular patient. Development of avatar models is a new tool for personalized medicine which entails implantation (either subcutaneous or orthotopic) of patient tumor cells into immunodeficient mice for drug efficacy studies (Figure 3). Avatar models allow physicians to culture a patient’s tumor in an *in vivo* system. This system can also be used to identify a personalised therapeutic regimen which can be superior to non-targeted therapies in terms of costs and toxicities, i.e. radio/chemotherapy [248].

In RCC, avatar models were used to predict response/resistance to anti-angiogenic drugs (sunitinib) in first and second line therapy [249]. A

unique panel of 12 patient-derived avatar models was developed by orthotopic implantation of primary and metastatic tumor biopsies from RCC patients. In this study, avatar models were treated with first-line drugs and at the moment of resistance development treatment was switched to different second-line drugs. Such avatar models successfully reproduced each patient’s histological type, metastatic capacity and the time to tumor growth significantly correlated with the clinical outcome in each original patient [249]. Moret et al. [250] used another approach with sub-capsular injection of luciferase-tagged cell lines derived from 2 RCC patients. They compared different combinations of two antineoplastic drugs (out of three possible: sunitinib, everolimus, pazopanib) proving a different response for each patient.

Recently, avatar models have been proposed as a promising approach for prediction of immunotherapy response in RCC. In a pioneer study, pieces of tumors were engrafted into the chorioallantoic membrane of avian embryos and later programmed cell death 1 (PD-1) and programmed death-ligand 1 (PD-L1) checkpoint inhibitors were injected intravenously [251]. High frequency ultrasound enabled quantification of changes in tumor volume, vascularity and tumor infiltrating lymphocyte (TIL) expansion in the tumor. The authors have observed different responses to immunotherapy over a short period of treatment (8 days). Avatar models possess the advantage of preserving the natural tumor microenvironment with TILs and no need for humanized models. They can become a useful tool to predict personalised response to checkpoint inhibitors and molecularly targeted therapies, however, larger studies and verification are required since the first study included specimens from only three patients.

Humanized Mouse Models

After decades of failed conventional therapies, the focus is now on “proof of concept” pre-clinical and clinical trials of cancer immunotherapy. Remarkable progress has been made in clinical application of

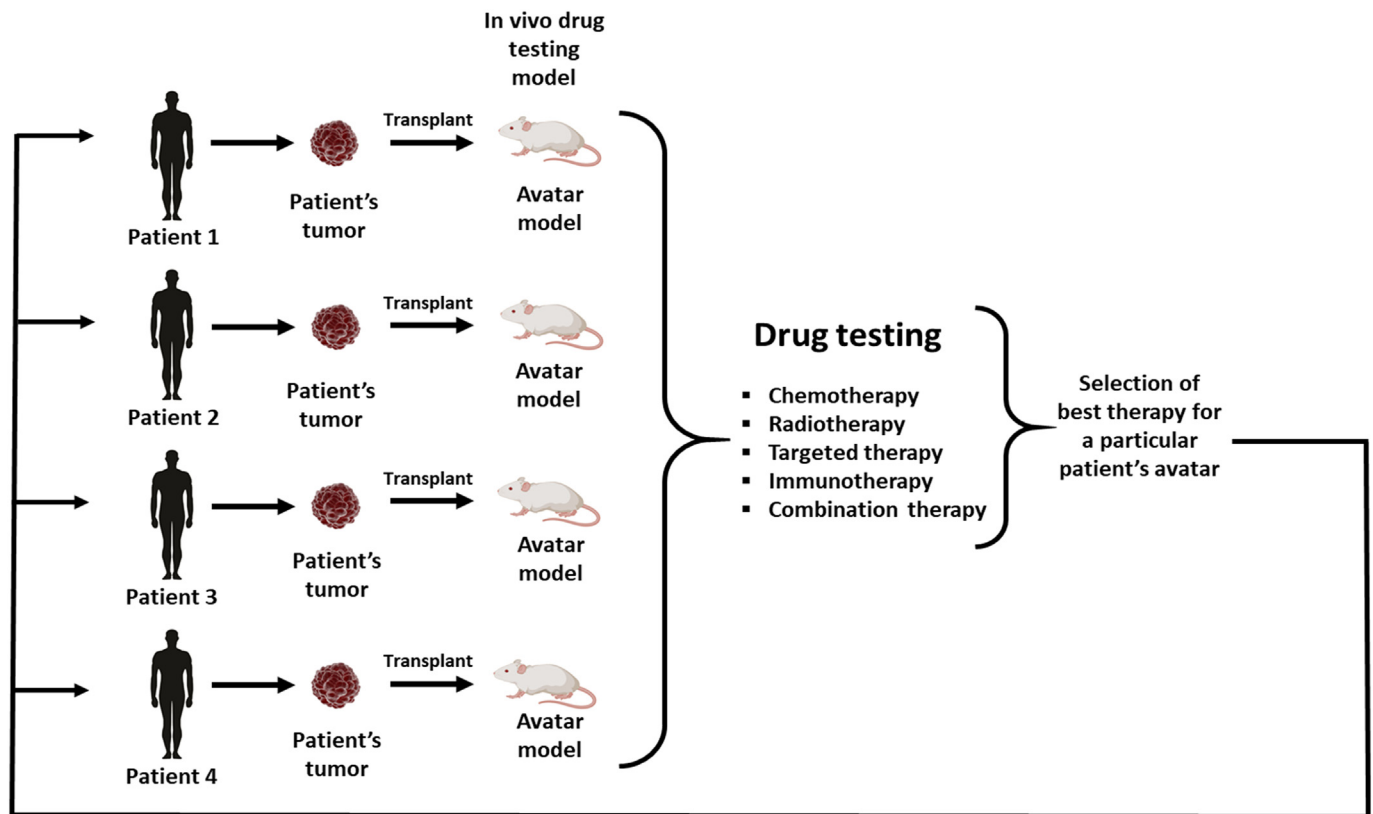


Figure 3. The general approach of avatar models in clinical oncology. Samples of tumor tissue are obtained from different patients and implanted into immunodeficient animals to create avatar models that resemble individual patients. This allows testing different therapeutic strategies, e.g. chemotherapy, radiotherapy, targeted therapy or immunotherapy and selecting the best therapy for a particular patient.

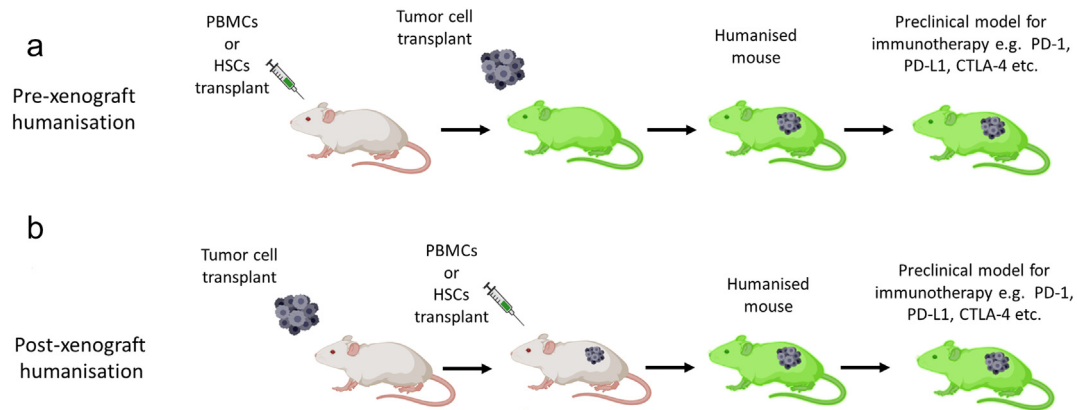


Figure 4. Generating a humanised mouse model for onco-immunology research. (a) Human PBMCs or HSCs were injected before the tumor cell transplantation and later these mice were used as a model for immunotherapy. (b) Tumor cells were transplanted first and later mice were humanised with the human PBMCs or HSCs for immunotherapy. In both approaches the human immune environment has to be confirmed by collecting peripheral blood before and after humanization of mice and by analyzing human immune cells using flow cytometry.

immunotherapies in a variety of cancers including RCC. The most notable targets are immune checkpoint proteins such as cytotoxic T lymphocyte antigen 4 (CTLA-4 or CD152), PD-1 or CD279 [252]. Furthermore, there is a great interest in the innate immune cells such as natural killer (NK), tumor associated macrophages and dendritic cells in the cancer context including recognition and followed by antigen presentation and adaptive immunity [253]. However, the development of these novel immunotherapies is often challenged by discrepancies observed between *in vitro* and *in vivo* study and actual clinical trial outcomes. These discrepancies may be attributed to the lack of clinically relevant models for human immunotherapy drug testing in the human immune environment. Undoubtedly, there is a great need for establishing PDXs and avatar models with the human immune microenvironment - “humanized mice” for basic and translational research. The functional immune system can be developed in NSG (NOD-*scid* *IL2rg*^{-/-}) and NCG (NOD-*Prkdc*^{em26Cd52} *IL2rg*^{em26Cd22}/NjuCrl) by transplanting human hematopoietic stem cells (HSCs) or peripheral blood mononuclear cells (PBMCs) that further differentiate into functional immune T cells, NK cells and monocytes (Figure 4) [254]. In a recent study, an orthotopic RCC tumor model was established by injecting 5×10^4 engineered CAIX expressing SKRC-59 cells into NSG mice [255]. After 4 days of tumor engraftment the mice were humanised by i.v. injection of 1×10^7 PBMCs from a healthy human donor. The results showed that CAIX antibody was able to mediate human immune response by priming T-cell activity and tumor infiltration by NK cells in inhibition of RCC growth in humanised NSG mice. However, humanized mice can be an ideal model to study onco-immunology based therapies in *in vivo* settings but still require further improvement. For example, the most likely risk associated with humanization is the development of graft versus host disease (GvHD) if the NCG mice engrafted with human PBMCs or HSCs and cancer cells would develop GvHD before the endpoint of the study [256]. Weight loss of more than 15% of original starting mouse weight is a sign of GvHD development and that might require euthanasia. However, to overcome this issue, use of HLA matched PBMCs and cancer cells from same the patient can be employed for mouse engraftment [257].

Other Models

Apart from the conventional mouse and rat models, other vertebrates such as zebrafish (*Danio rerio*) and dogs (*Canis familiaris*) are emerging as powerful model organisms to improve understanding of human pathophysiology of renal diseases. Zebrafish has gained much attention in studies recapitulating human renal genetic abnormalities as the larval zebrafish pronephrons share remarkable similarity with human nephrons in terms of pathology [258].

Alterations of the tumor suppressor *VHL* gene are frequently reported in pathogenesis of ccRCC. Noonan et al. described *vhl*^{-/-} zebrafish embryos and assessed pronephric epithelial cells for the features of ccRCC. Examination of the *vhl*^{-/-} proximal pronephric tubules revealed structural abnormalities, abundant cytoplasmic vesicles, increased glycogen accumulation, higher cellular proliferation and significantly higher cell death as compared to the wt siblings. The features markedly recapitulate the characteristics of human ccRCC indicating *vhl*^{-/-} zebrafish embryos as a promising model organism to study early stage RCC [259].

In recent years, great attention was given to using the domestic dog, *Canis familiaris* as a model organism to study human malignancies. With the advancements in comparative oncology and genome sequencing approaches canine tumors were observed to be similar to human neoplasms and can be used as representative models to explore new therapeutic interventions [260]. Canine models are already being utilized to study osteosarcoma [261], leukemia [262–264], breast cancer [265] and soft tissue sarcomas [266,267]. Clinical trials for various pharmacological molecules including liposomes encapsulating drugs [268,269] and several inhibitors of tyrosine kinases, including VEGF, PDGF, KIT, and FLT3 inhibitors, were tested in dogs [270,271]. New immunotherapy approaches utilizing interleukins IL-12 and IL-2 are also being evaluated in dogs [272].

Maekawa et al. describe the role of the PD-1/PD-L1 pathway as an immunotherapeutic target against RCC utilizing a canine tumor model. PD-1, an immunoinhibitory receptor, is involved in the immune evasion of tumor cells. Canine melanoma, mastocytoma and RCC, expressed PD-L1. Human RCC patients with tumor PD-L1 also show significant increase in tumor progression and high mortality suggesting that PD-L1 is associated with poor prognosis in patients with tumors. Thus inhibiting the PD-1/PD-L1 pathway using inhibitory molecules or PD-1 antibody may help reverse the symptoms and may inhibit cancer progression [273].

In 1985, Liem and Moe [274] noticed hereditary renal cystadenocarcinomas and nodular dermatofibrosis (RCND) in German shepherd dogs. Bilateral and multifocal cysts of various sizes were found in each kidney. In areas of the renal cortex several types of lesions (hyperplastic and dysplastic proliferations, neoplastic transformations) of renal tubular epithelial cells were present. The observed metastatic sites were situated in the sternal lymph nodes, liver, lung, renal and other abdominal lymph nodes, pleura, peritoneum, spleen and bones [274, 275]. Some of the features described above of renal cystadenocarcinomas in dogs were similar to these found in Eker rats. However, later studies showed that lesions in dogs occurred with a mutation in the *Flcn* gene and not in the *Tsc2* gene [276]. Mutations in the *Flcn* gene in humans are connected with the BHD syndrome, which predisposes to a wide spectrum of renal tumors (hybrid oncocytic tumors, chromophobe and clear cell carcinomas, renal oncocytosis) [277].

Table 5

A summary of the major features of imaging modalities in preclinical RCC research

Imaging modality	Means of detection	Tracers/contrast agents	Typical special resolution, depth limit	Target	Time of acquisition	Cost	References – applications in preclinical RCC research
US	Acoustic waves	Microbubbles	50 μ m, up to 3 cm	Anatomical, physiological	Short	Low	[281,332]
Optical imaging	Light	Fluorochromes, fluorescent proteins	1-5 mm, typically under 1 cm	Physiological, metabolic, molecular	Short	Low/moderate	[333,334]
CT	X-rays	Iodinated compounds	50 μ m, no limit	Anatomical, physiological	Moderate	Moderate	[281,335]
PET	γ -rays	Radioactive compounds (^{18}F -, ^{64}Cu -, ^{68}Ga -, ^{11}C -, ^{89}Zr -labelled)	1-2 mm, no limit	Metabolic, molecular	Long/moderate	High	[190,335–339]
SPECT	γ -rays	Radioactive compounds ($^{99\text{m}}\text{Tc}$ -, ^{111}In - or ^{67}Ga -labelled)	0.3-1 mm, no limit	Metabolic, molecular	Long/moderate	High (lower than PET)	[333,334]
MRI	Electromagnetism	Paramagnetic compounds (chelated gadolinium, ferrite oxide nanoparticles); hyperpolarized tracers (e.g. hyperpolarized pyruvate)	70-100 μ m, no limit	Anatomical, physiological, metabolic, molecular (with functionalized contrast agents)	Long	High	[281,297,317,340,341]

CT, computed tomography; MRI, magnetic resonance imaging; PET, positron emission tomography; RCC, renal cell carcinoma; SPECT, single-photon emission computed tomography; US, ultrasound.

In Vivo Imaging Techniques in Preclinical RCC Research

Involvement of non-invasive or low-invasive high resolution imaging techniques in preclinical RCC research provides a unique opportunity for ‘real time’ *in vivo* tracking of tumor development. These techniques may provide a variety of valuable information at morphological, physiological and molecular levels. They allow substantial reduction of animal numbers, e.g. because of the ability to monitor disease/therapeutic effect in the same animals, provide high quality results with minimal invasiveness and allow precise determination of humane endpoints in oncology research. Therefore these techniques fully comply with the 3R rules (Replacement, Reduction and Refinement) [278].

The applicable preclinical imaging techniques (modalities) are ultrasound (US) imaging, optical imaging, computed tomography (CT), positron emission tomography (PET) and magnetic resonance imaging (MRI). All these methods have their strengths and weaknesses, in particular in terms of costs, time of acquisition, spatial and temporal resolution and kind of information acquired. A short summary of these techniques and examples of application in RCC research are provided in Table 5, for more information see some recent reviews, e.g. [279,280]. A selection of the most relevant imaging strategy (that is currently often a combination of multiple imaging techniques: ‘multimodal imaging’) must be chosen individually and closely linked to the specific aims of the study. Here, we shortly review imaging/quantification of various aspects of RCC tumors in preclinical models: monitoring RCC tumor growth, detection of metastases, vascularization, imaging/quantification of metabolic status of the tumors and molecular imaging.

Measurement of Tumor Volume

Evaluation of tumor volume with calipers is still relatively widely used in preclinical RCC research. However, this approach has several limitations. First of all, it provides very inaccurate quantification of tumor volume, since typically it takes into account only two dimensions of the tumor. Moreover, this approach cannot be used for *in vivo* measurements of tumors that are not located subcutaneously.

More accurate *in vivo* evaluation of tumor volume can be performed with several imaging techniques. Recently, Linxweiler, Körbel [281] conducted a comparative study between high-resolution 3D ultrasonography, contrast-enhanced *in vivo* micro-CT and 9.4T small animal MRI for monitoring of RCC orthotopic xenografts in mice. Mean examination time in this study was around 5 minutes for high resolution US, 13 minutes for micro-CT and 38 minutes for MRI. It was shown that tumor volumes obtained with all these methods were in good correlation with each other and with

results obtained *ex vivo*. One important issue is proper identification of the tumors and processing of the image data to quantify volumes. In the case of tumors that appear homogenous in tomographic images like CT or MRI and could be easily distinguished from surrounding tissues, application of automated/semi-automated volumetric evaluation (e.g. region growth algorithm) may be possible and it increases the efficiency of data processing.

Detection of Metastases

In vivo detection of metastases in animal RCC models is much more challenging than monitoring of primary tumors of known localization. Notably, the limitations that apply to imaging of metastases also apply to chemically induced RCC models and other models that develop tumors in localizations that are not precisely defined. The imaging strategy must provide enough spatial resolution and contrast to differentiate the metastases from healthy tissues. However, the need for seeking the lesions within the animal body implies usage of a large field of view and may affect spatial resolution and in consequence efficiency of metastasis detection. The efficiency may be also limited in the case of metastatic tumors that are localized in deeper regions of the body or close to tissues/organs or cavities that produce imaging modality-specific artifacts.

US enables fast and efficient examination of potential metastases with high spatial resolution. However, detection using this modality suffers from limited penetration of acoustic waves. Another important limitation is localization of metastases: visualization of metastases to lungs and bones seems not to be feasible [281]. However, visualization of metastases to lymph nodes or visceral organs like liver seems to be feasible with US [282,283]. On the other hand, both micro-CT and MRI were shown to effectively visualize pulmonary metastases in the animal model of metastatic RCC [281].

Another attractive approach for metastasis detection is bioluminescence. However, it requires transfection of tumor cells with plasmids encoding luciferase and therefore is limited to animal models based on inoculation of immortalized cell lines. Additionally, bioluminescence/optical imaging provides only two-dimensional information on the luminescence intensity and therefore information on exact localization of the metastasis or its morphology is limited [284,285].

PET is also a potentially attractive approach for detection of metastasis in RCC and RCC models. While clinical use of PET imaging is not currently recommended for routine diagnostic application in RCC [286–288], a meta-analysis by Wang et al. [289] indicates that PET could be useful for detection of metastasis in RCC patients. In preclinical application uptake of certain PET tracers in RCC tumors seems to depend on the model. The

most commonly used PET tracer [18F]-fluorodeoxyglucose (FDG, [18F] FDG) failed to visualize SK-RC-52 tumors [290] but an increased FDG uptake was noted for 786-O xenografts ($SUV_{max} > 10$) [291].

Microstructure

Diffusion-weighted imaging (DWI) provides information on the water molecule diffusivity in the tissue. This quantitative technique allows measurement of several parameters that describe diffusivity, in particular the apparent diffusion coefficient (ADC, expressed in mm^2/s), a widely-used measure of tissue diffusivity. In the case of tumor imaging, low diffusivity (low ADC) may indicate increased cellular density and low water content in the extracellular space [292,293]. ADC values in healthy renal parenchyma in humans were in a range of 2.5 to $3.4 \times 10^{-3} mm^2/s$ [294–296]. In all types of RCC, ADC values were lower in tumors than in healthy renal tissue, in a range of 1.4 to $1.8 \times 10^{-3} mm^2/s$ [294]. Moreover, some recent studies demonstrated that ADC measurement allowed differentiation between benign lesions, malignant tumors and histological subtypes of RCC suggesting ADC as an important biomarker in RCC [296]. It seems that monitoring of ADC may be used for tracking the response to therapy in animal studies, e.g. Jeon et al. [297] noted a significant increase of ADC 7 days after sorafenib treatment of xenograft RCC tumors (induced by injection of ACHN cells).

Another approach for assessment of changes in tumor microstructure is MR relaxometry, a technique that provides quantitative data on magnetic properties of the tissue. In contrast to standard imaging techniques (T1-weighted, T2-weighted, T2*-weighted that are susceptible to various not fully controlled factors besides the 'real' relaxation time values) they actually measure the relaxation times and allow creation of relaxation time 'maps' (i.e. parametric images). Importantly, T1 or T2 time values can be directly compared and used for longitudinal evaluation of tumor growth or efficacy of therapeutic approach. T1 shortening in tumors is thought to indicate necrosis because of release of complexed paramagnetic ions from necrotic cells [298], in particular in response to chemotherapy [299]. On the other hand, T1 elongation may be a result of increased water content in the extracellular space and possibly correlate with elevated tumor interstitial pressure [300].

Metabolic Imaging

Magnetic resonance spectroscopy allows assessment of the metabolic fingerprints of tumors *in vivo*. This is not in fact an imaging technique, although repeating the MRS experiment allows generation of maps of major metabolites. The number of RCC animal studies involving MRS techniques is limited. One reason for this is that acquiring high quality spectra in experimental animals of the tumors located in the abdomen is challenging, mostly because of motion artifacts and difficulties in shimming (i.e. maximizing of B0 magnetic field homogeneity that is crucial for obtaining of good MR spectra). The main expected peaks include:

- Choline (also referred to as total choline, tCho, peak at 3.20 ppm) is in fact a sum of signals from trimethylamine groups in glycerylphosphocholine (GPC), phosphocholine (PC) and free choline (Cho). Choline compounds are present in healthy renal tissue since kidneys are involved in choline metabolism [301]. High tCho signal is regarded as a biomarker of elevated lipid membrane turnover and proliferation [302]. Furthermore, tCho is an established biomarker of malignancy, especially in breast cancer [303] and it was proposed as a biomarker of malignancy in RCC [304]. In human RCCs the tCho signal measured by MRS *in vivo* was shown to be elevated and correlated with aggressiveness of the tumors [305]. At higher field strengths these signals can be separated and quantified allowing calculation of GPC/PC ratio.
- Lipids mostly form two peaks: Lip09 (at 0.9 ppm) and Lip13 (at 1.3 ppm). Presence of lipid droplets was demonstrated in RCC cells [306] and high MRS lipid signals were shown for RCC tumors [304].

- Taurine. Taurine levels are low in healthy renal tissue [301]. Moreover, taurine quantification may be challenging due to partial overlap of the taurine peaks with signals of choline compounds, myo-inositol and glucose [307]. It was proposed that taurine could be a biomarker of apoptosis in gliomas and it was proposed as a biomarker for anti-cancer treatment efficiency [308]. However, its potential was not exploited in RCC. Importantly, taurine levels were found to be elevated in pRCC [301].

An emerging new technique for evaluation of tumor metabolism and metabolism in general is imaging based on hyperpolarized ^{13}C -tracers. Advanced techniques based on dynamic nuclear polarization allow a substantial enhancement of the carbon signal in MRI and detection of the injected tracer. $[1-^{13}C_1]$ pyruvate is currently the most promising metabolic tracer for this method. $[1-^{13}C_1]$ pyruvate is avidly taken up by cells of most organs including brain and heart, where it is converted to $[1-^{13}C_1]$ lactate, $[1-^{13}C_1]$ alanine, and $H^{13}CO_3^-$. Metabolic imaging with this approach has been performed in a variety of applications, including cancer diagnosis and monitoring of the therapeutic response, and cardiovascular pathologies [309–314], including animal models of malignancies [315]. Recently, this approach was introduced into the RCC field. Sriram et al. [316] demonstrated on cultured slices of tumors derived from RCC patients (slices were cultured in MR-compatible bioreactors) that ccRCC tumors have significantly increased lactate production and elevated rapid lactate efflux compared to benign lesions. The same group demonstrated the feasibility of this approach in orthotopic xenograft models of RCC. They have shown that A498 xenografts had a higher ^{13}C pyruvate-to-lactate conversion rate than 786-O and UOK262 tumors [317].

Humane Endpoints

In this section, we focus on humane endpoints in animal models of cancer, but the majority of the following indications have a general application. The Canadian Council on Animal Care (CCAC) guideline describes an endpoint as a point of time "that reduces animal pain and/or distress, while still satisfying the experimental design requirements for objective evaluation when animals are used in biomedical research, teaching and testing" [318]. Selection of the endpoint should relate to scientific outcomes and take animal welfare into account. Setting humane endpoints, monitoring and criteria of intervention should be determined before studies on animals, when researchers plan experiments [319,320]. An endpoint matrix can be helpful in assessment of endpoints. This tool divides humane endpoints into three groups: scientific, justifiable and unpredicted. A scientific endpoint is a moment when scientific goals are achieved, all experimental data is collected, so the experiment can be finished. There is no need to develop the next stages of disease, especially if this is connected with animal suffering. A justifiable endpoint refers to the end of an experiment which could be reached when possible benefits are larger than the permissible maximum level of animal suffering. An unpredicted endpoint applies to the appearance of unexpected animal suffering. It needs intervention without looking at scientific or justified endpoints. Animals should not to be exposed to additional unexpected suffering, except justified suffering assumed in the experimental procedure [321]. There are several clinical signs which need immediate intervention (i.e. termination of animal life): when animals stop drinking or eating during 24 to 48 hours, persistent hypothermia, hind-limb paralysis, rapid loss of body weight, bloodstained discharge, labored respiration, significant abdominal distension, incontinence and diarrhea longer than 48h, skin breakdown or exudation longer than 48 h, large necrosis, inability to move and maintain an upright position, unconsciousness [319,322].

Assessment of pain, distress and discomfort of animals could be based on evaluation of several factors, such as: bodyweight, physical appearance, measurable clinical signs (e.g. heart or respiratory rate), behavioral reactions. They were precisely described by Morton and Griffiths [323]. Observation and evaluation of the animal condition can be supported by appropriate checklists. They contain a set of factors and the scale of

Table 6
Classification of animal models of RCC based on the histology of the renal tumor

	ccRCC	pRCC	chRCC	Other/unclassified
Syngeneic model	Nihon rat	ND	ND	- RENCA model - Eker rat
GEM models	- Vhl ^{Δ/Δ} Pbrm1 ^{Δ/Δ} mice - Vhl ^{Δ/Δ} Bap1 ^{Δ/Δ} mice - Vhl ^{Δ/Δ} Trp53 ^{Δ/Δ} Rb1 ^{Δ/Δ} mice - Myc overexpression with Vhl and Ink/Arf (CDKN2A) knock-out (VIM model)	- Myc overexpression - FLCN gene knock-out	- FLCN gene knock-out	- FLCN gene knock-out - TFEB overexpression - TRACK model
Chemically-induced models	ND	ND	ND	All models
CDX	- Caki-1 - 786-O - 769-P - RCC4	- ACHN - Caki-2 - SKRC39	ND	- A498
PDX	Depending on the donor			

ccRCC, clear cell renal cell carcinoma; CDX, cell-derived xenograft; chRCC, chromophobe renal cell carcinoma; GEM, genetically engineered mice; ND, no data; PDX, patient-derived xenograft; pRCC, papillary renal cell carcinoma.

assessment assigned to these factors, depending on their severity and size. The use of checklists helps set endpoints and track changes that occur in the appearance and behavior of animals. Examples of factors to be considered may be found in CCAC [318]. Checklists were also used in studies on breast and bladder cancer models. The authors evaluated using a scale the biological parameters of each animal, such as: body weight and condition, food and water intake, mental status, coat and grooming, eyes, ears, whiskers, skin and mucosa, posture, response to manipulation or external stimuli, breathing, heart rate, hydration status, body temperature, urine color and volume, hematocrit, tumor location and burden, ulceration [324,325].

Development of tumors in sites like the eye, brain, muscle, footpad or tail may require special monitoring and probably establishing an early endpoint, because these sites could be painful and distressing to animals [319,320]. Early endpoints could be used in therapeutic studies when results are statistically significant and there is no need to maintain the tumor in the animal [326]. Early endpoints could also be adopted in studies when developed tumors are the source of cells for further research (*in vitro* cell line establishment, molecular characterization and transplantation) [319].

Endpoints for animals developing cachexia (MAC 16 mouse colonic adenocarcinoma or Leydig cell rat tumor) are connected with emaciation and loss of weight (maximum 20% to 25% weight loss compared to the beginning of the experiment) [320,327,328].

Cancer in the hematopoietic or lymphatic system gives anemia, enlargement of the spleen or lymph nodes. To identify endpoints in these types of cancer, researchers should pay attention to symptoms such as steady weight loss, behavioral changes or use diagnostic techniques such as imaging or simple palpation [320].

If a tumor develops s.c., it is important to measure tumor size systematically. This helps in determining the endpoints and can be easily done by caliper. The mean diameter of a tumor should not be wider than 1.2 cm (1.5 cm for therapeutic studies) in mice and 2.5 (2.8) cm in rats, respectively. Measuring tumors could be better than only weighing animals (they could lose weight during tumorigenesis). Some tumor models result in quick unpredictable death, so systematically collecting data of tumor behavior could be better than simple assessment at the end of the experiment.

Ulceration may occur in several cases in tumors developed s.c. or inoculated into the dermis, when tumors develop on the ventral surface, when the injected tumor cell line predisposes to ulceration, and in some tumor types (e.g. papillomas). If this happens, termination of the experiment can be considered. Although ulceration compromises the well-being of animals, it has an influence on the reliability of the experiment. It alters tumor growth, may result in continuous loss of body fluid or increase the risk of infection. When ulceration is necessary and unavoidable, animal condition should be assessed daily [320].

Induction of internal tumors due to growth and metastasis may be difficult to monitor. However, it could be done by application of magnetic resonance or bioluminescence imaging. Bioluminescent imaging facilitated

monitoring of tumor growth and metastatic spread in an orthotopic kidney tumor model in immunocompetent ACI rats [170]. Circulation of cancer cells could be evaluated by molecular identification of tumor biomarkers or the presence of viral or human DNA [320].

The death of an animal should not be defined as an endpoint, but surgical excision and weighing of tumors are made at the end of the study [319, 320]. Pilot studies with necropsy will be helpful to assess endpoints. This solution could give a wider knowledge of a particular type of tumor, especially with unknown pathogenesis [319].

Conclusions

As discussed above, a variety of animal cancer models is now available (Table 6), each of them has certain strengths and weaknesses (Table 2). When planning a study, it is of utmost importance to consider the characteristics of available animal models, the type of conducted research (Figure 1) and the mechanisms of action of the studied drug to ensure that the chosen model is fit-for-purpose (Table 7).

Historically, the first group of drugs tested in animal models of RCC were chemotherapeutic agents, used either as monotherapies or adjunctive treatments. Firstly chemotherapeutics were tested in the 1970s in RENCA and Wistar–Lewis rat renal adenocarcinoma syngeneic models [38]. Owing to RCC resistance to chemotherapeutic drugs and development of novel targeted therapies, preclinical research of chemotherapeutics has lost its importance. However, all of the above-mentioned types of mouse models seem to be good choices for testing this group of drugs. Cytotoxic drugs that act through cell mitosis and division inhibition act independently of immune status, microenvironment context or the tumor implantation method.

Table 7
Possible animal models to study different drug types

Tested drug type	Animal model of choice
Cytotoxic chemotherapy	Syngeneic model PDX CDX GEM Chemically-induced model
Molecular-targeted agents	Syngeneic model PDX CDX GEM Chemically-induced model
Immunotherapy (cancer vaccines, check-point inhibitors, adoptive cell therapies)	Syngeneic model GEM (possibly incorporating human MHC) Humanized tumor model In immunodeficient mice

CDX, cell-derived xenograft; GEM, genetically engineered mice; PDX, patient-derived xenograft.

Later on, in the 1980s, IFN and IL-2 chemoimmunotherapy was tested in the RENCA syngeneic model [14]. Before the era of antiangiogenic drugs, cytokines (IL-2 and IFN) were used for the treatment of RCC as immunomodulating drugs. With the introduction of targeted therapies, IFNs have lost their importance in RCC treatment, however, novel immune-related drugs i.e. checkpoint inhibitors are currently being introduced into clinical practice. Immunotherapy drugs act through modulation of the immune system of the host. Therefore, models that require immunodeficiency in order to induce tumorigenesis (cell line-derived xenografts, patient-derived xenografts) are not suitable for this type of research. In the era of immunotherapy in oncology, syngeneic models, one of the oldest and most commonly used animal models, have been reintroduced to preclinical research. Thanks to their ease of use, reproducibility and immunocompetence they serve as an adequate model for study of the immune response. However, due to their lack of tumor heterogeneity and lack of native tumor microenvironment, other models have to be considered when studying the immune response. Humanized animal models and GEMs, that more accurately reflect the tumor microenvironment may serve as valuable tools for preclinical research of immunotherapies. Therefore, models which enable testing of this type of drugs include: syngeneic models, GEM models and humanized models (Table 7) [329,330].

The discovery of the role of VEGF and its receptor (VEGFR) in RCC and establishment of anti-VEGFR targeted therapy have radically changed the landscape of therapeutic options and improved prognosis for patients with RCC. Moreover, discovery of dysregulation of the mammalian target of rapamycin (mTOR) signaling pathway and development of mTOR inhibitors was another step towards effective treatment of RCC. Generally, all the mouse models described above can be used for testing this group of drugs, however, the choice of a particular animal model depends on the characteristics of the study. When studying the impact of a targeted drug in a syngeneic or GEM model it must be remembered that the molecular pathways involved in animal carcinogenesis may differ from those observed in humans, which may influence study results and applicability to human cancer pathophysiology. Cell line-derived xenografts do not have this limitation, however, they have failed to predict efficacy for most targeted drugs in humans [331], with a low approval rate by the FDA [10]. On the other hand, no other animal model offers better results in terms of drug development.

PDX models develop tumors with more resemblance to human cancers, which has contributed to the increase in their application in preclinical research in the last years, especially for molecular-targeted drugs. Tumors in PDX models preserve the stromal composition as well as histological and molecular heterogeneity characteristic of those in patients. Therefore, PDX models allow direct evaluation of the activities of human-specific drugs, such as antibodies or molecular-targeted drugs and identification of accurate personalized therapy regimens for cancer patients [235]. However, it must be remembered that human stromal elements are present for only 2–3 passages, since mouse stromal components become dominant later on.

As mentioned above, PDX models can be a useful tool for preclinical research, however, due to immunodeficiency they are not suitable for testing of immunotherapeutics. The use of syngeneic mouse models with a murine immune system is also limiting, since they fail to accurately resemble the human immune system. The so-called humanized PDX are mouse models with a fully competent human immune system. They are created by engraftment of various types of human cells i.e. leukocytes or human CD34+ hematopoietic stem cells followed by implantation of fresh human tumor cells [255]. Therefore, humanized PDX models are one of the best approaches to immunotherapeutic drug testing and represent a promising tool in RCC research.

In the last few years, unconventional animal models such as zebrafish or canine models gained recognition in the scientific community. Due to shared characteristics and similarities with human carcinomas, they seem to be a promising tool in cancer research but for the moment their utility in RCC research is limited by shortage of high-quality evidence.

Due to histological diversity of renal tumors, certain subtypes are under-represented in preclinical research and lack an adequate animal model (Tables 1, 6). Most research on animal models concentrates on ccRCC with only single studies related to papillary, chromophobe or rarer subtypes. This is the key challenge for future research. Establishing of adequate models resembling distinct subtypes of renal tumors may lead to better understanding of its pathophysiology and development of therapies that will revolutionize cancer treatment in the future.

Acknowledgments

This work was supported by Polish National Science Centre grant No. DEC-2014/13/B/NZ1/04010.

All authors have read the journal's authorship agreement and policy on disclosure of potential conflicts of interest. The authors declare that they have no conflict of interest.

References

- Capitaino U, Bensalah K, Bex A, Boorjian SA, Bray F, Coleman J, Gore JL, Sun M, Wood C, and Russo P (2019). Epidemiology of renal cell carcinoma. *Eur Urol* **75**, 74–84.
- Motzer RJ, Bander NH, and Nanus DM (1996). Renal-cell carcinoma. *N Engl J Med* **335**, 865–875.
- Rini BI, Hutson TE, Figlin RA, Lechuga MJ, Valota O, and Serfass L, et al (2018). Sunitinib in patients with metastatic renal cell carcinoma: clinical outcome according to International Metastatic Renal Cell Carcinoma Database Consortium Risk Group. *Clin Genitourin Cancer* **16**, 298–304.
- Brodaczewska KK, Szczylik C, Fiedorowicz M, Porta C, and Czarnicka AM (2016). Choosing the right cell line for renal cell cancer research. *Mol Cancer* **15**, 83.
- Anglard P, Trahan E, Liu S, Latif F, Merino MJ, and Lerman MI, et al (1992). Molecular and cellular characterization of human renal cell carcinoma cell lines. *Cancer Res* **52**, 348–356.
- Kaminska K, Szczylik C, Bielecka ZF, Bartnik E, Porta C, and Lian F, et al (2015). The role of the cell-cell interactions in cancer progression. *J Cell Mol Med* **19**, 283–296.
- Maliszewska-Olejniczak K, Brodaczewska KK, Bielecka ZF, and Czarnicka AM (2018). Three-dimensional cell culture model utilization in renal carcinoma cancer stem cell research. *Methods Mol Biol* **1817**, 47–66.
- Batchelder CA, Martínez ML, Duru N, Meyers FJ, and Tarantall AF (2015). Three dimensional culture of human renal cell carcinoma organoids. *PLoS One* **10**, e0136758.
- Talmadge JE, Singh RK, Fidler IJ, Raz A. Murine models to evaluate novel and conventional therapeutic strategies for cancer. *Am J Pathol*. 2007;170:793-804.
- Day CP, Merlino G, and Van Dyke T (2015). Preclinical mouse cancer models: a maze of opportunities and challenges. *Cell* **163**, 39–53.
- Hrushesky WJ and Murphy GP (1973). Investigation of a new renal tumor model. *J Surg Res* **15**, 327–336.
- Hillman GG (2002). Experimental animal models for renal cell carcinoma. In: Teicher BA, editor. *Tumor Models in Cancer Research*. Totowa, NJ: Humana Press; 2002. p. 493–505.
- Chakrabarty A, Hillman GG, Maughan RL, Visscher DW, Ali E, and Pontes JE, et al (1994). Influence of tumor site on the therapy of murine kidney cancer. *Anticancer Res* **14**, 373–378.
- Salup RR and Wiltrout RH (1986). Adjuvant immunotherapy of established murine renal cancer by interleukin 2-stimulated cytotoxic lymphocytes. *Cancer Res* **46**, 3358–3363.
- Salup RR (1987). Back TC, Wiltrout RH. Successful treatment of advanced murine renal cell cancer by biocompartmental adoptive chemoimmunotherapy. *J Immunol* **138**, 641–647.
- de Souza Braga M, Chaves KB, Chammas R, Schor N, and Bellini MH (2012). Endostatin neo-adjuvant gene therapy extends survival in an orthotopic metastatic mouse model of renal cell carcinoma. *Biomed Pharmacother* **66**, 237–241.
- Rayman P, Diaz-Montero CM, Yang Y, Rini B, Elson P, and Finke J (2015). Modulation of immune cell infiltrate with sunitinib to improve anti-PD1 therapy in preclinical tumor model. *Journal for immunotherapy of cancer* **3**, P310.
- Verheul HM, Hammers H, van Erp K, Wei Y, Sanni T, and Salumbides B, et al (2007). Vascular endothelial growth factor trap blocks tumor growth, metastasis formation, and vascular leakage in an orthotopic murine renal cell cancer model. *Clinical cancer research : an official journal of the American Association for Cancer Research*. **13**, 4201–4208.
- Hillman GG, Younes E, Visscher D, Hamzavi F, Kim S, and Lam JS, et al (1997). Inhibition of murine renal carcinoma pulmonary metastases by systemic administration of interferon gamma: mechanism of action and potential for combination with interleukin 4. *Clin Cancer Res* **3**, 1799–1806.
- Larkin J, Esser N, Calvo E, Tsuchihashi Z, Fiedler U, and Graeser R, et al (2012). Efficacy of sequential treatment with sunitinib-everolimus in an orthotopic mouse model of renal cell carcinoma. *Anticancer Res* **32**, 2399–2406.
- Zhang X, Shi X, Li J, Hu Z, Gao J, and Wu S, et al (2019). Combination immunotherapy with interleukin-2 surface-modified tumor cell vaccine and programmed death receptor-1 blockade against renal cell carcinoma. *Cancer Sci* **110**, 31–39.
- Nogawa M, Yuasa T, Kimura S, Kuroda J, Sato K, and Segawa H, et al (2005). Monitoring luciferase-labeled cancer cell growth and metastasis in different *in vivo* models. *Cancer Lett* **217**, 243–253.
- Bibby MC (2004). Orthotopic models of cancer for preclinical drug evaluation. *advantages and disadvantages Eur J Cancer* **40**, 852–857.
- Devaud C, Westwood JA, John LB, Flynn JK, Paquet-Fifield S, and Duong CP, et al (2014). Tissues in different anatomical sites can sculpt and vary the tumor microenvironment to affect responses to therapy. *Mol Ther* **22**, 18–27.

- [25] Matin SF, Sharma P, Gill IS, Tannenbaum C, Hobart MG, and Novick AC, et al (2010). Immunological response to renal cryoablation in an *in vivo* orthotopic renal cell carcinoma murine model. *J Urol* **183**, 333–338.
- [26] Murphy KA, James BR, Wilber A, and Griffith TS (2017). A syngeneic mouse model of metastatic renal cell carcinoma for quantitative and longitudinal assessment of preclinical therapies. *J Vis Exp* **122** 55080.
- [27] Kausch I, Jiang H, Brocks C, Bruderek K, Kruger S, Szczakiel G, et al. Ki-67-directed antisense therapy in an orthotopic renal cell carcinoma model. *Eur Urol*. 2004;46:118-24; discussion 24-5.
- [28] Tracz A, Mastrri M, Lee CR, Pili R, and Ebos JM (2014). Modeling spontaneous metastatic renal cell carcinoma (mRCC) in mice following nephrectomy. *J Vis Exp* **86** 51485.
- [29] Ding J, Wang C, and Chang X (2018). Establishment of a bioluminescent Renca cell line for renal carcinoma research. *Int Urol Nephrol* **50**, 55–61.
- [30] Dybal EJ, Haas GP, Maughan RL, Sud S, Pontes JE, and Hillman GG (1992). Synergy of radiation therapy and immunotherapy in murine renal cell carcinoma. *J Urol* **148**, 1331–1337.
- [31] Salup RR, Herberman RB, and Wiltrout RH (1985). Role of natural killer activity in development of spontaneous metastases in murine renal cancer. *J Urol* **134**, 1236–1241.
- [32] Norian LA, Kresovik TP, Rosevear HM, James BR, Rosean TR, and Lightfoot AJ, et al (2012). Eradication of metastatic renal cell carcinoma after adenovirus-encoded TNF-related apoptosis-inducing ligand (TRAIL)/CpG immunotherapy. *PLoS One* **7**:e31085.
- [33] Younes E, Haas GP, Dezzo B, Ali E, Maughan RL, and Kukuru MA, et al (1995). Local tumor irradiation augments the response to IL-2 therapy in a murine renal adenocarcinoma. *Cell Immunol* **165**, 243–251.
- [34] Chakrabarty A, Hillman GG, Maughan RL, Ali E, Pontes JE, and Haas GP (1994). Radiation therapy enhances the therapeutic effect of immunotherapy on pulmonary metastases in a murine renal adenocarcinoma model. *In Vivo* **8**, 25–31.
- [35] Hu J, Schokpur S, Archang M, Herrmann K, Sharrow AC, and Khanna P, et al (2018). A non-integrating lentiviral approach overcomes Cas9-induced immune rejection to establish an immunocompetent metastatic renal cancer model. *Mol Ther Methods Clin Dev* **9**, 203–210.
- [36] White RV and Olsson DA (1980). Renal adenocarcinoma in the rat: a new tumor model. *Investig Urol* **17**, 405–412.
- [37] Clayman RV, Bilhartz LE, Buja LM, Spady DK, and Dietsch JM (1986). Renal cell carcinoma in the Wistar-Lewis rat: a model for studying the mechanisms of cholesterol acquisition by a tumor *in vivo*. *Cancer Res* **46**, 2958–2963.
- [38] Hillman GG, Droz JP, and Haas GP (1994). Experimental animal models for the study of therapeutic approaches in renal cell carcinoma. *In Vivo*. **8**, 77–80.
- [39] Eker R (1954). Familial renal adenomas in Wistar rats; a preliminary report. *Acta Pathol Microbiol Scand* **34**, 554–562.
- [40] Eker R and Mossige J (1961). A dominant gene for renal adenomas in the rat. *Nature* **189**, 858–859.
- [41] Hino O, Klein-Szanto AJ, Freed JJ, Testa JR, Brown DQ, and Vilenky M, et al (1993). Spontaneous and radiation-induced renal tumors in the Eker rat model of dominantly inherited cancer. *Proc Natl Acad Sci U S A* **90**, 327–331.
- [42] Hino O, Mitani H, and Knudson AG (1993). Genetic predisposition to transplacentally induced renal cell carcinomas in the Eker rat. *Cancer Res* **53**, 5856–5858.
- [43] Hino O and Kobayashi T (2017). Mourning Dr. Alfred G. Knudson: the two-hit hypothesis, tumor suppressor genes, and the tuberous sclerosis complex. *Cancer Sci* **108**, 5–11.
- [44] Hino O, Kobayashi T, Tsuchiya H, Kikuchi Y, Kobayashi E, and Mitani H, et al (1994). The predisposing gene of the Eker rat inherited cancer syndrome is tightly linked to the tuberous sclerosis (TSC2) gene. *Biochem Biophys Res Commun* **203**, 1302–1308.
- [45] Yeung RS, Xiao GH, Jin F, Lee WC, Testa JR, and Knudson AG (1994). Predisposition to renal carcinoma in the Eker rat is determined by germ-line mutation of the tuberous sclerosis 2 (TSC2) gene. *Proc Natl Acad Sci U S A* **91**, 11413–11416.
- [46] Kobayashi T, Hirayama Y, Kobayashi E, Kubo Y, and Hino O (1995). A germline insertion in the tuberous sclerosis (Tsc2) gene gives rise to the Eker rat model of dominantly inherited cancer. *Nat Genet* **9**, 70–74.
- [47] Yeung RS, Buetow KH, Testa JR, and Knudson Jr AG (1993). Susceptibility to renal carcinoma in the Eker rat involves a tumor suppressor gene on chromosome 10. *Proc Natl Acad Sci U S A* **90**, 8038–8042.
- [48] Everitt JI, Goldsworthy TL, Wolf DC, and Walker CL (1995). Hereditary renal cell carcinoma in the Eker rat: a unique animal model for the study of cancer susceptibility. *Toxicol Lett* **82-83**, 621–625.
- [49] Kubo Y, Klimek F, Kikuchi Y, Bannasch P, and Hino O (1995). Early detection of Knudson's two-hits in preneoplastic renal cells of the Eker rat model by the laser microdissection procedure. *Cancer Res* **55**, 989–990.
- [50] Kobayashi T, Urakami S, Hirayama Y, Yamamoto T, Nishizawa M, and Takahara T, et al (1997). Intragenic Tsc2 somatic mutations as Knudson's second hit in spontaneous and chemically induced renal carcinomas in the Eker rat model. *Jpn J Cancer Res* **88**, 254–261.
- [51] Kokubo T, Kakinuma S, Kobayashi T, Watanabe F, Iritani R, and Tateno K, et al (2010). Age dependence of radiation-induced renal cell carcinomas in an Eker rat model. *Cancer Sci* **101**, 616–623.
- [52] Everitt JI, Goldsworthy TL, Wolf DC, and Walker CL (1992). Hereditary renal cell carcinoma in the Eker rat: a rodent familial cancer syndrome. *J Urol* **148**, 1932–1936.
- [53] Everitt JI, Walker CL, Goldsworthy TW, and Wolf DC (1997). Altered expression of transforming growth factor- α : an early event in renal cell carcinoma development. *Mol Carcinog* **19**, 213–219.
- [54] Liu MY, Poellinger L, and Walker CL (2003). Up-regulation of hypoxia-inducible factor 2 α in renal cell carcinoma associated with loss of Tsc-2 tumor suppressor gene. *Cancer Res* **63**, 2675–2680.
- [55] Turner KJ, Moore JW, Jones A, Taylor CF, Cuthbert-Heavens D, and Han C, et al (2002). Expression of hypoxia-inducible factors in human renal cancer: relationship to angiogenesis and to the von Hippel-Lindau gene mutation. *Cancer Res* **62**, 2957–2961.
- [56] Horesovsky G, Recio L, Everitt J, Goldsworthy T, Wolf DC, and Walker C (1995). p53 status in spontaneous and dimethylnitrosamine-induced renal cell tumors from rats. *Mol Carcinog* **12**, 236–240.
- [57] Uchida T, Wada C, Shitara T, Egawa S, Mashimo S, and Koshiba K (1993). Infrequent involvement of p53 mutations and loss of heterozygosity of 17p in the tumorigenesis of renal cell carcinoma. *J Urol* **150**, 1298–1301.
- [58] Tomasino RM, Morello V, Tralongo V, Nagar C, Nuara R, Daniele E, et al. p53 expression in human renal cell carcinoma: an immunohistochemical study and a literature outline of the cytogenetic characterization. *Pathologica* 1994;86:227-33.
- [59] Noon AP, Vlatkovic N, Polanski R, Maguire M, Shawki H, and Parsons K, et al (2010). p53 and MDM2 in renal cell carcinoma: biomarkers for disease progression and future therapeutic targets? *Cancer* **116**, 780–790.
- [60] van den Berg A and Buys CH (1997). Involvement of multiple loci on chromosome 3 in renal cell carcinoma development. *Genes Chromosomes Cancer* **19**, 59–76.
- [61] Kikuchi Y, Kobayashi E, Nishizawa M, Hamazaki S, Okada S, and Hino O (1995). Cloning of the rat homologue of the von Hippel-Lindau tumor suppressor gene and its non-somatic mutation in rat renal cell carcinomas. *Jpn J Cancer Res* **86**, 905–909.
- [62] Aizawa Y, Shirai T, Kobayashi T, Hino O, Tsujii Y, and Inoue H, et al (2016). Metabolic abnormalities induced by mitochondrial dysfunction in skeletal muscle of the renal carcinoma Eker (TSC2^{-/-}) rat model. *Biosci Biotechnol Biochem* **80**, 1513–1519.
- [63] Aizawa Y, Shirai T, Kobayashi T, Hino O, Tsujii Y, and Inoue H, et al (2016). The tuberous sclerosis complex model Eker (TSC2^{-/-}) rat exhibits hyperglycemia and hyperketonemia due to decreased glycolysis in the liver. *Arch Biochem Biophys* **590**, 48–55.
- [64] Rennebeck G, Kleymenova EV, Anderson R, Yeung RS, Artzt K, and Walker CL (1998). Loss of function of the tuberous sclerosis 2 tumor suppressor gene results in embryonic lethality characterized by disrupted neuroepithelial growth and development. *Proc Natl Acad Sci U S A* **95**, 15629–15634.
- [65] Kenerson H, Dundon TA, and Yeung RS (2005). Effects of rapamycin in the Eker rat model of tuberous sclerosis complex. *Pediatr Res* **57**, 67–75.
- [66] Chi OZ, Wu CC, Liu X, Rah KH, Jacinto E, and Weiss HR (2015). Restoration of normal cerebral oxygen consumption with rapamycin treatment in a rat model of autism-tuberous sclerosis. *Neuromolecular Med* **17**, 305–313.
- [67] Okimoto K, Kouchi M, Kikawa E, Toyosawa K, Koujitani T, and Tanaka K, et al (2000). A novel "Nihon" rat model of a Mendelian dominantly inherited renal cell carcinoma. *Jpn J Cancer Res* **91**, 1096–1099.
- [68] Okimoto K, Sakurai J, Kobayashi T, Mitani H, Hirayama Y, and Nickerson ML, et al (2004). A germ-line insertion in the Birt-Hogg-Dube (BHD) gene gives rise to the Nihon rat model of inherited renal cancer. *Proc Natl Acad Sci U S A* **101**, 2023–2027.
- [69] Kouchi M, Okimoto K, Matsumoto I, Tanaka K, Yasuda M, and Hino O (2006). Natural history of the Nihon (Bhd gene mutant) rat, a novel model for human Birt-Hogg-Dube syndrome. *Virchows Arch* **448**, 463–471.
- [70] Richmond A and Su Y (2008). Mouse xenograft models vs GEM models for human cancer therapeutics. *Dis Model Mech* **1**, 78–82.
- [71] Kohan DE (2008). Progress in gene targeting: using mutant mice to study renal function and disease. *Kidney Int* **74**, 427–437.
- [72] Espana-Agusti J, Warren A, Chew SK, Adams DJ, and Matakidou A (2017). Loss of PBRM1 rescues VHL dependent replication stress to promote renal carcinogenesis. *Nat Commun* **8**:2026.
- [73] Gu YF, Cohn S, Christie A, McKenzie T, Wolff N, and Do QN, et al (2017). Modeling renal cell carcinoma in mice: Bap1 and Pbm1 inactivation drive tumor grade. *Cancer discovery* **7**, 900–917.
- [74] Nargund AM, Pham CG, Dong Y, Wang PI, Osmangoyoglu HU, and Xie Y, et al (2017). The SWI/SNF protein PBRM1 restrains VHL-loss-driven clear cell renal cell carcinoma. *Cell Rep* **18**, 2893–2906.
- [75] Harlander S, Schonenberger D, Toussaint NC, Prummer M, Catalano A, and Brandt L, et al (2017). Combined mutation in Vhl, Trp53 and Rb1 causes clear cell renal cell carcinoma in mice. *Nat Med* **23**, 869–877.
- [76] Baba M, Furihata M, Hong SB, Tassarollo L, Haines DC, and Southon E, et al (2008). Kidney-targeted Birt-Hogg-Dube gene inactivation in a mouse model: Erk1/2 and Akt-mTOR activation, cell hyperproliferation, and polycystic kidneys. *J Natl Cancer Inst* **100**, 140–154.
- [77] Chen J, Futami K, Petillo D, Peng J, Wang P, and Knol J, et al (2008). Deficiency of FLCN in mouse kidney led to development of polycystic kidneys and renal neoplasia. *PLoS One* **3**:e3581.
- [78] Bailey ST, Smith AM, Kardos J, Wobker SE, Wilson HL, and Krishnan B, et al (2017). MYC activation cooperates with Vhl and Ink4a/Arf loss to induce clear cell renal cell carcinoma. *Nat Commun* **8**:15770.
- [79] Fu L, Wang G, Shevchuk MM, Nanus DM, and Gudas LJ (2011). Generation of a mouse model of Von Hippel-Lindau kidney disease leading to renal cancers by expression of a constitutively active mutant of HIF1 α . *Cancer Res* **71**, 6848–6856.
- [80] Shroff EH, Eberlin LS, Dang VM, Gouw AM, Gabay M, and Adam SJ, et al (2015). MYC oncogene overexpression drives renal cell carcinoma in a mouse model through glutamine metabolism. *Proc Natl Acad Sci U S A* **112**, 6539–6544.
- [81] Gopinathan A and Tuveson DA (2008). The use of GEM models for experimental cancer therapeutics. *Dis Model Mech* **1**, 83–86.
- [82] Nickerson ML, Jaeger E, Shi Y, Durocher JA, Mahurkar S, and Zaridze D, et al (2008). Improved identification of von Hippel-Lindau gene alterations in clear cell renal tumors. *Clin Cancer Res* **14**, 4726–4734.
- [83] Sato Y, Yoshizato T, Shiraishi Y, Maekawa S, Okuno Y, and Kamura T, et al (2013). Integrated molecular analysis of clear-cell renal cell carcinoma. *Nat Genet* **45**, 860–867.
- [84] Haase VH, Glickman JN, Socolovsky M, and Jaenisch R (2001). Vascular tumors in livers with targeted inactivation of the von Hippel-Lindau tumor suppressor. *Proc Natl Acad Sci U S A* **98**, 1583–1588.
- [85] Ma W, Tassarollo L, Hong SB, Baba M, and Southon E (2003). Back TC, et al. Hepatic vascular tumors, angiectasis in multiple organs, and impaired spermatogenesis in mice with conditional inactivation of the VHL gene. *Cancer Res* **63**, 5320–5328.
- [86] Kleymenova E, Everitt JI, Pluta L, Portis M, Gnarr JR, and Walker CL (2004). Susceptibility to vascular neoplasms but no increased susceptibility to renal carcinogenesis in Vhl knockout mice. *Carcinogenesis* **25**, 309–315.
- [87] Rankin EB, Tomaszewski JE, and Haase VH (2006). Renal cyst development in mice with conditional inactivation of the von Hippel-Lindau tumor suppressor. *Cancer Res* **66**, 2576–2583.
- [88] Frew IJ, Thoma CR, Georgiev S, Minola A, Hitz M, and Montani M, et al (2008). pVHL and PTEN tumor suppressor proteins cooperatively suppress kidney cyst formation. *EMBO J* **27**, 1747–1757.
- [89] Pritchett TL, Bader HL, Henderson J, and Hsu T (2015). Conditional inactivation of the mouse von Hippel-Lindau tumor suppressor gene results in wide-spread hyperplastic, inflammatory and fibrotic lesions in the kidney. *Oncogene* **34**, 2631–2639.

- [90] Schietke RE, Hackenbeck T, Tran M, Gunther R, Klanke B, and Warnecke CL, et al (2012). Renal tubular HIF-2 α expression requires VHL inactivation and causes fibrosis and cysts. *PLoS One* **7**:e31034.
- [91] Lehmann H, Vicari D, Wild PJ, and Frew IJ (2015). Combined deletion of Vhl and Kif3a accelerates renal cyst formation. *Journal of the American Society of Nephrology : JASN* **26**, 2778–2788.
- [92] Nargund AM, Osmanbeyoglu HU, Cheng EH, and Hsieh JJ (2017). SWI/SNF tumor suppressor gene PBRM1/BAF180 in human clear cell kidney cancer. *Mol Cell Oncol* **4**:1342747.
- [93] Wang SS, Gu YF, Wolff N, Stefanis K, Christie A, and Dey A, et al (2014). Bap1 is essential for kidney function and cooperates with Vhl in renal tumorigenesis. *Proc Natl Acad Sci U S A* **111**, 16538–16543.
- [94] Calcagni A, Kors L, Verschuren E, De Cegli R, Zampelli N, and Nusco E, et al (2016). Modelling TFE renal cell carcinoma in mice reveals a critical role of WNT signaling. *elife* **5**.
- [95] Johansson E, Rono B, Johansson M, Lindgren D, Moller C, and Axelson H, et al (2016). Simultaneous targeted activation of Notch1 and Vhl-disruption in the kidney proximal epithelial tubular cells in mice. *Sci Rep* **6**:30739.
- [96] Cancer Genome Atlas Research N (2013). Comprehensive molecular characterization of clear cell renal cell carcinoma. *Nature* **499**, 43–49.
- [97] Cancer Genome Atlas Research (2016). N, Linehan WM, Spellman PT, Ricketts CJ, Creighton CJ, Fei SS, et al. Comprehensive molecular characterization of papillary renal-cell carcinoma. *N Engl J Med* **374**, 135–145.
- [98] Davis CF, Ricketts CJ, Wang M, Yang L, Cherniack AD, and Shen H, et al (2014). The somatic genomic landscape of chromophobe renal cell carcinoma. *Cancer Cell* **26**, 319–330.
- [99] Ricketts CJ, De Cubas AA, Fan H, Smith CC, Lang M, Reznik E, et al. The Cancer Genome Atlas Comprehensive Molecular Characterization of Renal Cell Carcinoma. Cell reports. 2018;23:313-26 e5.
- [100] Varela I, Tarpey P, Raine K, Huang D, Ong CK, and Stephens P, et al (2011). Exome sequencing identifies frequent mutation of the SWI/SNF complex gene PBRM1 in renal carcinoma. *Nature* **469**, 539–542.
- [101] Pena-Llopis S (2012). Vega-Rubin-de-Celis S, Liao A, Leng N, Pavia-Jimenez A, Wang S, et al. BAP1 loss defines a new class of renal cell carcinoma. *Nat Genet* **44**, 751–759.
- [102] Zhang L, Jiao M, Wu K, Li L, Zhu G, and Wang X, et al (2014). TNF- α induced epithelial mesenchymal transition increases stemness properties in renal cell carcinoma cells. *Int J Clin Exp Med* **7**, 4951–4958.
- [103] Kapur P, Peña-Llopis S, Christie A, Zhebker L, Pavia-Jiménez A, and Rathmell WK, et al (2013). Effects on survival of BAP1 and PBRM1 mutations in sporadic clear-cell renal-cell carcinoma: a retrospective analysis with independent validation. *The Lancet Oncology* **14**, 159–167.
- [104] Ellisen LW, Bird J, West DC, Soreng AL, Reynolds TC, and Smith SD, et al (1991). TAN-1, the human homolog of the Drosophila notch gene, is broken by chromosomal translocations in T lymphoblastic neoplasms. *Cell* **66**, 649–661.
- [105] Chen Y, De Marco MA, Graziani I, Gazdar AF, Strack PR, and Miele L, et al (2007). Oxygen concentration determines the biological effects of NOTCH-1 signaling in adenocarcinoma of the lung. *Cancer Res* **67**, 7954–7959.
- [106] Balint K, Xiao M, Pinnix CC, Soma A, Veres I, and Juhasz I, et al (2005). Activation of Notch1 signaling is required for beta-catenin-mediated human primary melanoma progression. *J Clin Invest* **115**, 3166–3176.
- [107] Sjolund J, Johansson M, Manna S, Norin C, Pietras A, and Beckman S, et al (2008). Suppression of renal cell carcinoma growth by inhibition of Notch signaling *in vitro* and *in vivo*. *J Clin Invest* **118**, 217–228.
- [108] Sjolund J, Bostrom AK, Lindgren D, Manna S, Moustakas A, and Ljungberg B, et al (2011). The notch and TGF- β signaling pathways contribute to the aggressiveness of clear cell renal cell carcinoma. *PLoS One* **6**:e23057.
- [109] Hudon V, Sabourin S, Dydensborg AB, Kottis V, Ghazi A, and Paquet M, et al (2010). Renal tumour suppressor function of the Birt-Hogg-Dube syndrome gene product folliculin. *J Med Genet* **47**, 182–189.
- [110] Hasumi Y, Baba M, Ajima R, Hasumi H, Valera VA, and Klein ME, et al (2009). Homozygous loss of BHD causes early embryonic lethality and kidney tumor development with activation of mTORC1 and mTORC2. *Proc Natl Acad Sci U S A* **106**, 18722–18727.
- [111] Hartman TR, Nicolas E, Klein-Szanto A, Al-Saleem T, Cash TP, and Simon MC, et al (2009). The role of the Birt-Hogg-Dube protein in mTOR activation and renal tumorigenesis. *Oncogene* **28**, 1594–1604.
- [112] Chen J, Huang D, Rubera I, Futami K, Wang P, and Zickert P, et al (2015). Disruption of tubular Fln expression as a mouse model for renal tumor induction. *Kidney Int* **88**, 1057–1069.
- [113] Fu L, Minton DR, Zhang T, Nanus DM, and Gudas LJ (2015). Genome-wide profiling of TRACK kidneys shows similarity to the human ccRCC transcriptome. *Mol Cancer Res* **13**, 870–878.
- [114] Tang SW, Chang WH, Su YC, Chen YC, Lai YH, and Wu PT, et al (2009). MYC pathway is activated in clear cell renal cell carcinoma and essential for proliferation of clear cell renal cell carcinoma cells. *Cancer Lett* **273**, 35–43.
- [115] Komai Y, Fujiwara M, Fujii Y, Mukai H, Yonese J, and Kawakami S, et al (2009). Adult Xp11 translocation renal cell carcinoma diagnosed by cytogenetics and immunohistochemistry. *Clin Cancer Res* **15**, 1170–1176.
- [116] Steenman MJ, Rainier S, Dobry CJ, Grundy P, Horon IL, and Feinberg AP (1994). Loss of imprinting of IGF2 is linked to reduced expression and abnormal methylation of H19 in Wilms' tumour. *Nat Genet* **7**, 433–439.
- [117] Huff V (1998). Wilms tumor genetics. *Am J Med Genet* **79**, 260–267.
- [118] Kreidberg JA, Sariola H, Loring JM, Maeda M, Pelletier J, and Housman D, et al (1993). WT-1 is required for early kidney development. *Cell* **74**, 679–691.
- [119] Herzer U, Crocoll A, Barton D, Howells N, and Englert C (1999). The Wilms tumor suppressor gene wt1 is required for development of the spleen. *Current biology : CB* **9**, 837–840.
- [120] Hu Q, Gao F, Tian W, Ruteshouser EC, Wang Y, and Lazar A, et al (2011). Wt1 ablation and Igf2 upregulation in mice result in Wilms tumors with elevated ERK1/2 phosphorylation. *J Clin Invest* **121**, 174–183.
- [121] Flores 2nd LG, Yeh HH, Soghomonyan S, Young D, Bankson J, and Hu Q, et al (2013). Monitoring therapy with MEK inhibitor U0126 in a novel Wilms tumor model in Wt1 knockout Igf2 transgenic mice using 18F-FDG PET with dual-contrast enhanced CT and MRI: early metabolic response without inhibition of tumor growth. *Mol Imaging Biol* **15**, 175–185.
- [122] Huang L, Mokkapat S, Hu Q, Ruteshouser EC, Hicks MJ, Huff V. nephron progenitor but not stromal progenitor cells give rise to wilms tumors in mouse models with beta-catenin activation or Wt1 ablation and Igf2 upregulation. *Neoplasia* (New York, NY) **2016**:18:71-81.
- [123] Mandel TE, Hoffman L, and Carter WM (1981). Long-term isografts of cultured fetal mouse pancreatic islets. The oncogenic effects of streptozotocin and the prevention of diabetic renal complications. *Am J Pathol* **104**, 227–236.
- [124] Hard GC (1986). Experimental models for the sequential analysis of chemically-induced renal carcinogenesis. *Toxicol Pathol* **14**, 112–122.
- [125] Horton L, Fox C, Corrin B, and Sonksen PH (1977). Streptozotocin-induced renal tumours in rats. *Br J Cancer* **36**, 692–699.
- [126] Iwase M, Nunoi K, Sadoshima S, Kikuchi M, and Fujishima M (1989). Liver, kidney and islet cell tumors in spontaneously hypertensive and normotensive rats treated neonatally with streptozotocin. *Tohoku J Exp Med* **159**, 83–90.
- [127] Hard GC (1985). Identification of a high-frequency model for renal carcinoma by the induction of renal tumors in the mouse with a single dose of streptozotocin. *Cancer Res* **45**, 703–708.
- [128] Delahunt B and Wakefield JS (1997). Ultrastructure of streptozotocin-induced renal tumours in mice. *Virchows Archiv : an international journal of pathology* **430**, 173–180.
- [129] Gruys ME (2001). Back TC, Subleski J, Wiltrout TA, Lee JK, Schmidt L, et al. Induction of transplantable mouse renal cell cancers by streptozotocin: *in vivo* growth, metastases, and angiogenic phenotype. *Cancer Res* **61**, 6255–6263.
- [130] Dombrowski F, Klotz L, Bannasch P, and Evert M (2007). Renal carcinogenesis in models of diabetes in rats: metabolic changes are closely related to neoplastic development. *Diabetologia* **50**, 2580–2590.
- [131] Vinerean H, Gazda L, Hall R, and Smith B (2011). Streptozotocin is responsible for the induction and progression of renal tumorigenesis in diabetic Wistar-Furth rats treated with insulin or transplanted with agarose encapsulated porcine islets. *Islets* **3**, 196–203.
- [132] Kazumi T, Yoshino G, Fujii S, and Baba S (1978). Tumorigenic action of streptozotocin on the pancreas and kidney in male Wistar rats. *Cancer Res* **38**, 2144–2147.
- [133] Reddi AS, Jyothirmayi GN, Halka K, and Khan MY (1991). Potentiation of renal tumorigenicity by cyclosporine A in streptozotocin diabetic rats. *Cancer Lett* **56**, 109–115.
- [134] Randak C, Brabletz T, Hergenrother M, Sobotta I, and Seifling E (1990). Cyclosporin A suppresses the expression of the interleukin 2 gene by inhibiting the binding of lymphocyte-specific factors to the IL-2 enhancer. *EMBO J* **9**, 2529–2536.
- [135] Kato Y, Masuno K, Fujisawa K, Tsuchiya N, Torii M, and Hishikawa A, et al (2017). Characterization of pancreatic islet cell tumors and renal tumors induced by a combined treatment of streptozotocin and nicotinamide in male SD rats. *Exp Toxicol Pathol* **69**, 413–423.
- [136] Rakieten N, Gordon BS, Beaty A, Cooney DA, Schein PS, Dixon RL. Modification of renal tumorigenic effect of streptozotocin by nicotinamide: spontaneous reversibility of streptozotocin diabetes. *Proc Soc Exp Biol Med* **1976**:151:356-61.
- [137] Shinohara Y and Frith CH (1980). Morphologic characteristics of benign and malignant renal cell tumors in control and 2-acetylaminofluorene-treated BALB/c female mice. *Am J Pathol* **100**, 455–468.
- [138] Magee PN and Barnes JM (1962). Induction of kidney tumours in the rat with dimethylnitrosamine (N-nitrosodimethylamine). *The Journal of pathology and bacteriology* **84**, 19–31.
- [139] Swann PF and McLean AE (1971). Cellular injury and carcinogenesis. The effect of a protein-free high-carbohydrate diet on the metabolism of dimethylnitrosamine in the rat. *The Biochemical journal* **124**, 283–288.
- [140] Hard GC and Butler WH (1970). Cellular analysis of renal neoplasia: induction of renal tumors in dietary-conditioned rats by dimethylnitrosamine, with a reappraisal of morphological characteristics. *Cancer Res* **30**, 2796–2805.
- [141] Hard GC and Butler WH (1970). Cellular analysis of renal neoplasia: light microscope study of the development of interstitial lesions induced in the rat kidney by a single carcinogenic dose of dimethylnitrosamine. *Cancer Res* **30**, 2806–2815.
- [142] Hard GC and Butler WH (1971). Ultrastructural study of the development of interstitial lesions leading to mesenchymal neoplasia induced in the rat renal cortex by dimethylnitrosamine. *Cancer Res* **31**, 337–347.
- [143] Hard GC (1979). Effect of age at treatment on incidence and type of renal neoplasm induced in the rat by a single dose of dimethylnitrosamine. *Cancer Res* **39**, 4965–4970.
- [144] Hard GC and Borland R (1975). In vitro culture of cells isolate from dimethylnitrosamine-induced renal mesenchymal tumors of the rat. I. Qualitative morphology. *J Natl Cancer Inst* **54**, 1085–1095.
- [145] Hard GC (1984). High frequency, single-dose model of renal adenoma/carcinoma induction using dimethylnitrosamine in Crl:(W)BR rats. *Carcinogenesis* **5**, 1047–1050.
- [146] Hard GC and Butler WH (1971). Ultrastructural aspects of renal adenocarcinoma induced in the rat by dimethylnitrosamine. *Cancer Res* **31**, 366–372.
- [147] Hard GC and Butler WH (1971). Morphogenesis of epithelial neoplasms induced in the rat kidney by dimethylnitrosamine. *Cancer Res* **31**, 1496–1505.
- [148] Whaley JMNJ, Gelbert L, Hsia YE, Lamiell JM, Green JS, Collins D, Neumann HP, Laidlaw J, and Li FP (1994). Germ-line mutations in the von Hippel-Lindau tumor-suppressor gene are similar to somatic von Hippel-Lindau aberrations in sporadic renal cell carcinoma. *Am J Hum Genet* **55**, 1092–1102.
- [149] Druckrey HSD, Preussmann R, and Ivankovic S (1964). Erzeugung von Krebs durch eine einmalige Dosis von Methylnitroso-Harnstoff und verschiedenen Dialkylnitrosaminen an Ratten. *Zeitschrift für Krebsforschung* **66**, 1–10.
- [150] Takashima K, Ozono S, Nakanou I, Ota M, Tanaka M, and Tani M, et al (2001). Strain variation in renal carcinogenesis by N-ethyl-N-hydroxyethylnitrosamine in F1 (Wistar-Fischer) rats. *Cancer Lett* **170**, 125–130.
- [151] Hiasa Y, Paul M, Hayashi I, Mochizuki M, Tsutsumi H, and Kuwashima S, et al (1999). Carcinogenic effects of N-ethyl-N-hydroxyethylnitrosamine and its metabolites in rats and mice. *Cancer Lett* **145**, 143–149.
- [152] Hiasa Y, Ohshima M, Kitahori Y, Konishi N, and Fujita T (1982). Yuasa T. beta-Cyclodextrin: promoting effect on the development of renal tubular cell tumors in rats treated with N-ethyl-N-hydroxyethylnitrosamine. *J Natl Cancer Inst* **69**, 963–967.
- [153] Yoshioka N, Hiasa Y, Cho M, Kitahori Y, Hirao K, and Konishi N, et al (1999). Effect of polyphenon-60 on the development of renal cell tumors in rats treated with N-ethyl-N-hydroxyethylnitrosamine. *Cancer Lett* **136**, 79–82.

- [154] Konishi N, Nakamura M, Ishida E, Kawada Y, Nishimine M, and Nagai H, et al (2001). Specific genomic alterations in rat renal cell carcinomas induced by N-ethyl-N-hydroxyethylnitrosamine. *Toxicol Pathol* **29**, 232–236.
- [155] Hiasa Y, Ohshima M, Iwata C, and Tanikake T (1979). Histopathological studies on renal tubular cell tumors in rats treated with N-ethyl-N-hydroxyethylnitrosamine. *Gann* **70**, 817–820.
- [156] Satake N, Miyagawa M, Sakurai J, Mitani H, Kobayashi T, and Tamura H, et al (2002). N-ethyl-N-hydroxyethylnitrosamine (EHEN)-induced renal and hepatocarcinogenesis in the tumor suppressor Tsc2 transgenic rat. *Cancer Lett* **184**, 157–163.
- [157] Sato M, Kitahori Y, Nakagawa Y, Konishi N, Cho M, and Hiasa Y (1998). Formation of 8-hydroxydeoxyguanosine in rat kidney DNA after administration of N-ethyl-N-hydroxyethylnitrosamine. *Cancer Lett* **124**, 111–118.
- [158] Satake N, Urakami S, Hirayama Y, Izumi K, and Hino O (1998). Biallelic mutations of the Tsc2 gene in chemically induced rat renal cell carcinoma. *International journal of cancer Journal international du cancer* **77**, 895–900.
- [159] Tokuzen R, Iwahori Y, Asamoto M, Iigo M, Hasegawa F, and Satoh T, et al (2001). Establishment and characterization of three new rat renal cell carcinoma cell lines from N-ethyl-N-hydroxyethylnitrosamine-induced basophilic cell tumors. *Pathol Int* **51**, 65–71.
- [160] Hiasa Y, Lin JC, Konishi N, Kitahori Y, Enoki N, and Shimoyama T (1984). Histopathological and biochemical analyses of transplantable renal adenocarcinoma in rats induced by N-ethyl-N-hydroxyethylnitrosamine. *Cancer Res* **44**, 1664–1670.
- [161] Ebina Y, Okada S, Hamazaki S, Ogino F, Li JL, and Midorikawa O (1986). Nephrotoxicity and renal cell carcinoma after use of iron- and aluminum-nitritriacetate complexes in rats. *J Natl Cancer Inst* **76**, 107–113.
- [162] Toyokuni S (1999). Reactive oxygen species-induced molecular damage and its application in pathology. *Pathol Int* **49**, 91–102.
- [163] Nishiyama Y, Suwa H, Okamoto K, Fukumoto M, Hiai H, and Toyokuni S (1995). Low incidence of point mutations in H-, K- and N-ras oncogenes and p53 tumor suppressor gene in renal cell carcinoma and peritoneal mesothelioma of Wistar rats induced by ferric nitrilotriacetate. *Japanese journal of cancer research : Gann* **86**, 1150–1158.
- [164] Tanaka T, Iwasa Y, Kondo S, Hiai H, and Toyokuni S (1999). High incidence of allelic loss on chromosome 5 and inactivation of p15INK4B and p16INK4A tumor suppressor genes in oxystyrene-induced renal cell carcinoma of rats. *Oncogene* **18**, 3793–3797.
- [165] Vargas-Olvera CY, Sanchez-Gonzalez DJ, Solano JD, Aguilar-Alonso FA, Montalvo-Munoz F, and Martinez-Martinez CM, et al (2012). Characterization of N-diethylnitrosamine-initiated and ferric nitrilotriacetate-promoted renal cell carcinoma experimental model and effect of a tamarind seed extract against acute nephrotoxicity and carcinogenesis. *Mol Cell Biochem* **369**, 105–117.
- [166] Athar M and Iqbal M (1998). Ferric nitrilotriacetate promotes N-diethylnitrosamine-induced renal tumorigenesis in the rat: implications for the involvement of oxidative stress. *Carcinogenesis* **19**, 1133–1139.
- [167] Toyokuni S, Okada K, Kondo S, Nishioka H, Tanaka T, and Nishiyama Y, et al (1998). Development of high-grade renal cell carcinomas in rats independently of somatic mutations in the Tsc2 and VHL tumor suppressor genes. *Japanese journal of cancer research : Gann* **89**, 814–820.
- [168] Li GH, Akatsuka S, Chew SH, Jiang L, Nishiyama T, and Sakamoto A, et al (2017). Fenton reaction-induced renal carcinogenesis in Mutyh-deficient mice exhibits less chromosomal aberrations than the rat model. *Pathol Int* **67**, 564–574.
- [169] Akatsuka S, Yamashita Y, Ohara H, Liu YT, Izumiya M, and Abe K, et al (2012). Fenton reaction induced cancer in wild type rats recapitulates genomic alterations observed in human cancer. *PLoS One* **7**, e43403.
- [170] Kobayashi M, Murakami T, Uchibori R, Chun NA, Kobayashi E, and Morita T, et al (2010). Establishment and characterization of transplantable, luminescence labeled rat renal cell carcinoma cell lines. *J Urol* **183**, 2029–2035.
- [171] Stevenson JL and von Haam E (1962). Induction of Kidney Tumors in Mice by the Use of 20-Methylcholanthrene-impregnated Strings. *Cancer Res* **22**, 1177–1179.
- [172] Hirtzler R (1958). V-reactions to implantation of methylcholanthrene soaked silk thread into kidneys and adrenals of experimental animals. *J R Microsc Soc* **78**, 67–73.
- [173] Lock EA and Hard GC (2004). Chemically induced renal tubule tumors in the laboratory rat and mouse: review of the NCI/NTP database and categorization of renal carcinogens based on mechanistic information. *Crit Rev Toxicol* **34**, 211–299.
- [174] Wolf DC, Crosby LM, George MH, Kilburn SR, Moore TM, and Miller RT, et al (1998). Time- and dose-dependent development of potassium bromate-induced tumors in male Fischer 344 rats. *Toxicol Pathol* **26**, 724–729.
- [175] Gazinska P, Herman D, Gillett C, Pinder S, and Mantle P (2012). Comparative immunohistochemical analysis of ochratoxin A tumorigenesis in rats and urinary tract carcinoma in humans; mechanistic significance of p-S6 ribosomal protein expression. *Toxins (Basel)* **4**, 643–662.
- [176] Hard GC, Howard PC, Kovatch RM, and Bucci TJ (2001). Rat kidney pathology induced by chronic exposure to fumonisin B1 includes rare variants of renal tubule tumor. *Toxicol Pathol* **29**, 379–386.
- [177] Flanagan SP (1966). 'Nude', a new hairless gene with pleiotropic effects in the mouse. *Genet Res* **8**, 295–309.
- [178] Bosma MJ and Carroll AM (1991). The SCID mouse mutant: definition, characterization, and potential uses. *Annu Rev Immunol* **9**, 323–350.
- [179] Morton CL and Houghton PJ (2007). Establishment of human tumor xenografts in immunodeficient mice. *Nat Protoc* **2**, 247–250.
- [180] Taghian A, Budach W, Zietman A, Freeman J, Gioioso D, and Ruka W, et al (1993). Quantitative comparison between the transplantability of human and murine tumors into the subcutaneous tissue of NCr/Sed-nu/nu nude and severe combined immunodeficient mice. *Cancer Res* **53**, 5012–5017.
- [181] Budhu S, Wolchok J, and Merghoub T (2014). The importance of animal models in tumor immunity and immunotherapy. *Curr Opin Genet Dev* **24**, 46–51.
- [182] Decker WK, da Silva RF, Sanabria MH, Angelo LS, Guimaraes F, and Burt BM, et al (2017). Cancer immunotherapy: historical perspective of a clinical revolution and emerging preclinical animal models. *Front Immunol* **8**, 829.
- [183] Varna M, Bertheau P, and Legrès L (2014). Tumor microenvironment in human tumor xenografted mouse models. *Journal of Analytical Oncology* **3**, 159–166.
- [184] An Z, Jiang P, Wang X, Moossa AR, and Hoffman RM (1999). Development of a high metastatic orthotopic model of human renal cell carcinoma in nude mice: benefits of fragment implantation compared to cell-suspension injection. *Clin Exp Metastasis* **17**, 265–270.
- [185] Ruggeri BA, Camp F, and Miknyoczki S (2014). Animal models of disease: pre-clinical animal models of cancer and their applications and utility in drug discovery. *Biochem Pharmacol* **87**, 150–161.
- [186] Korhonen M, Sariola H, Gould VE, Kangas L, and Virtanen I (1994). Integrins and laminins in human renal carcinoma cells and tumors grown in nude mice. *Cancer Res* **54**, 4532–4538.
- [187] Pulkkanen KJ, Parkkinen JJ, Kettunen MI, Kauppinen RA, Lappalainen M, and Ala-Opas MY, et al (2000). Characterization of a new animal model for human renal cell carcinoma. *In vivo (Athens, Greece)* **14**, 393–400.
- [188] Pulkkanen KJ, Parkkinen JJ, Laukkanen JM, Kettunen MI, Tyynele K, and Kauppinen RA, et al (2001). HSV-tk gene therapy for human renal cell carcinoma in nude mice. *Cancer Gene Ther* **8**, 529–536.
- [189] Miyake M, Goodison S, Lawton A, Zhang G, Gomes-Giacoa E, and Rosser CJ (2013). Erythropoietin is a JAK2 and ERK1/2 effector that can promote renal tumor cell proliferation under hypoxic conditions. *J Hematol Oncol* **6**, 65.
- [190] Chapman DW, Jans HS, Ma I, Mercer JR, Wiebe LI, and Wuest M, et al (2014). Detecting functional changes with [(18)F]FAZA in a renal cell carcinoma mouse model following sunitinib therapy. *EJNMMI Res* **4**, 27.
- [191] Dos Santos C, Tijeras-Raballand A, Serova M, Sebbagh S, Slimane K, and Faivre S, et al (2015). Effects of preset sequential administrations of sunitinib and everolimus on tumour differentiation in Caki-1 renal cell carcinoma. *Br J Cancer* **112**, 86–94.
- [192] Joshi S, Singh AR, and Durden DL (2015). Pan-PI-3 kinase inhibitor SF1126 shows antitumor and antiangiogenic activity in renal cell carcinoma. *Cancer Chemother Pharmacol* **75**, 595–608.
- [193] Kozlowski JM, Fidler IJ, Campbell D, Xu ZL, Kaighn ME, and Hart IR (1984). Metastatic behavior of human tumor cell lines grown in the nude mouse. *Cancer Res* **44**, 3522–3529.
- [194] Xie C, Schwarz EM, Sampson ER, Dhillon RS, Li D, and O'Keefe RJ, et al (2012). Unique angiogenic and vasculogenic properties of renal cell carcinoma in a xenograft model of bone metastasis are associated with high levels of vegf-a and decreased ang-1 expression. *J Orthop Res* **30**, 325–333.
- [195] Raval RR, Lau KW, Tran MG, Sowter HM, Mandriota SJ, and Li JL, et al (2005). Contrasting properties of hypoxia-inducible factor 1 (HIF-1) and HIF-2 in von Hippel-Lindau-associated renal cell carcinoma. *Mol Cell Biol* **25**, 5675–5686.
- [196] Wu P, Zhang N, Wang X, Zhang C, Li T, and Ning X, et al (2012). The erythropoietin/erythropoietin receptor signaling pathway promotes growth and invasion abilities in human renal carcinoma cells. *PLoS One* **7**, e45122.
- [197] Huang B, Huang YJ, Yao ZJ, Chen X, Guo SJ, and Mao XP, et al (2013). Cancer stem cell-like side population cells in clear cell renal cell carcinoma cell line 769P. *PLoS One* **8**, e68293.
- [198] Harada H, Itasaka S, Zhu Y, Zeng L, Xie X, and Morinibu A, et al (2009). Treatment regimen determines whether an HIF-1 inhibitor enhances or inhibits the effect of radiation therapy. *Br J Cancer* **100**, 747–757.
- [199] Miyao N, Tsukamoto T, and Kumamoto Y (1989). Establishment of three human renal cell carcinoma cell lines (SMKT-R-1, SMKT-R-2, and SMKT-R-3) and their characters. *Urol Res* **17**.
- [200] Ebert T, Bander NH, Finstad CL, Ramsawak RD, and Establishment Old LJ (1990). Characterization of human renal cancer and normal kidney cell lines. *Cancer Res* **50**, 5531.
- [201] Hii SI, Nicol DL, Godey DC, Thompson LC, Green MK, and Jonsson JR (1998). Captopril inhibits tumour growth in a xenograft model of human renal cell carcinoma. *Br J Cancer* **77**, 880–883.
- [202] Prewett M, Rothman M, Waksal H, Feldman M, Bander NH, and Hicklin DJ (1998). Mouse-human chimeric anti-epidermal growth factor receptor antibody C225 inhibits the growth of human renal cell carcinoma xenografts in nude mice. *Clin Cancer Res* **4**, 2957–2966.
- [203] Buvall L, Hedman H, Khranova A, Najar D, Bergvall L, and Ebefor K, et al (2017). Orellanine specifically targets renal clear cell carcinoma. *Oncotarget* **8**, 91085–91098.
- [204] Garvin AJ, Re CG, Tarnowski BI, Hazen-Martin DJ, and Sens DA (1993). The G401 cell line, utilized for studies of chromosomal changes in Wilms' tumor, is derived from a rhabdoid tumor of the kidney. *Am J Pathol* **142**, 375–380.
- [205] Sourbier C, Valera-Romero V, Giubellino A, Yang Y, Sudarshan S, and Neckers L, et al (2010). Increasing reactive oxygen species as a therapeutic approach to treat hereditary leiomyomatosis and renal cell carcinoma. *Cell Cycle* **9**, 4183–4189.
- [206] Yang Y, Valera VA, Padilla-Nash HM, Sourbier C, Vocke CD, and Vira MA, et al (2010). UOK 262 cell line, fumarate hydratase deficient (FH-/FH-) hereditary leiomyomatosis renal cell carcinoma: *in vitro* and *in vivo* model of an aberrant energy metabolic pathway in human cancer. *Cancer Gene Cytogenet* **196**, 45–55.
- [207] Reiter RE, Anglard P, Liu S, Gnarr JR, and Linehan WM (1993). Chromosome 17p deletions and p53 mutations in renal cell carcinoma. *Cancer Res* **53**, 3092–3097.
- [208] Bear A, Clayman RV, Elbers J, Limas C, Wang N, and Stone K, et al (1987). Characterization of two human cell lines (TK-10, TK-164) of renal cell cancer. *Cancer Res* **47**, 3856–3862.
- [209] Grossman HB, Wedemeyer G, and Ren LQ (1985). Human renal carcinoma: characterization of five new cell lines. *J Surg Oncol* **28**, 237–244.
- [210] Brown KW, Charles A, Dallosso A, White G, Charlet J, and Standen GR, et al (2012). Characterization of 17.94, a novel anaplastic Wilms' tumor cell line. *Cancer genetics* **205**, 319–326.
- [211] Lunavat TR, Cheng L, Einarsdottir BO, Olofsson Bagge R, Veppil Muralidharan S, and Sharples RA, et al (2017). BRAF(V600) inhibition alters the microRNA cargo in the vesicular secretome of malignant melanoma cells. *Proc Natl Acad Sci U S A* **114**, E5930-9.
- [212] Fatore L, Sacconi A, Mancini R, and Ciliberto G (2017). MicroRNA-driven deregulation of cytokine expression helps development of drug resistance in metastatic melanoma. *Cytokine Growth Factor Rev* **36**, 39–48.
- [213] Abramson LP, Stellmach V, Doll JA, Cornwell M, Arensman RM, Crawford SE. Wilms' tumor growth is suppressed by antiangiogenic pigment epithelium-derived factor in a xenograft model. *Journal of pediatric surgery*. 2003;38:336-42; discussion 42.
- [214] Smith MA, Morton CL, Phelps D, Girtman K, Neale G, and Houghton PJ (2008). SK-NEP-1 and Rh1 are Ewing family tumor lines. *Pediatr Blood Cancer* **50**, 703–706.
- [215] Mullen P (2004). The use of matrigel to facilitate the establishment of human cancer cell lines as xenografts. In: Langdon SP, editor. *Cancer Cell Culture: Methods and Protocols*. Totowa, NJ: Humana Press; 2004. p. 287–292.
- [216] Naito S, von Eschenbach AC, Giavazzi R, and Growth Fidler IJ (1986). Metastasis of tumor cells isolated from a human renal cell carcinoma implanted into different organs of nude mice. *Cancer Res* **46**, 4109.
- [217] Hillman GG, Wang Y, Che M, Raffoul JJ, Yudelev M, and Kucuk O, et al (2007). Progression of renal cell carcinoma is inhibited by genistein and radiation in an orthotopic model. *BMC Cancer* **7**, 4.

- [218] Strube A, Stepina E, Mumberg D, Scholz A, Hauff P, and Kakonen SM (2010). Characterization of a new renal cell carcinoma bone metastasis mouse model. *Clin Exp Metastasis* **27**, 319–330.
- [219] Satcher RL, Pan T, Cheng CJ, Lee YC, Lin SC, and Yu G, et al (2014). Cadherin-11 in renal cell carcinoma bone metastasis. *PLoS One* **9**:e89880.
- [220] Maitra S, Yuasa T, Tsuchiya N, Mitobe Y, Narita S, and Horikawa Y, et al (2012). Antitumor effect of sunitinib against skeletal metastatic renal cell carcinoma through inhibition of osteoclast function. *Int J Cancer* **130**, 677–684.
- [221] Wang J, Chen A, Yang C, Zeng H, Qi J, and Guo FJ (2012). A bone-seeking clone exhibits different biological properties from the ACHN parental human renal cell carcinoma *in vivo* and *in vitro*. *Oncol Rep* **27**, 1104–1110.
- [222] Weber KL, Pathak S, Multani AS, and Price JE (2002). Characterization of a renal cell carcinoma cell line derived from a human bone metastasis and establishment of an experimental nude mouse model. *J Urol* **168**, 774–779.
- [223] Wang L, Rahman S, Lin CY, and Valdivia J (2012). Than K, La Marca F, et al. A novel murine model of human renal cell carcinoma spinal metastasis. *Journal of clinical neuroscience : official journal of the Neurosurgical Society of Australasia* **19**, 881–883.
- [224] D'Amico L, Belisario D, Migliardi G, Grange C, Bussolati B, and D'Amelio P, et al (2016). C-met inhibition blocks bone metastasis development induced by renal cancer stem cells. *Oncotarget* **7**.
- [225] Valta MP, Zhao H, Ingels A, Thong AE, Nolley R, and Saar M, et al (2014). Development of a realistic *in vivo* bone metastasis model of human renal cell carcinoma. *Clin Exp Metastasis* **31**, 573–584.
- [226] Grisanzio C, Seeley A, Chang M, Collins M, Di Napoli A, and Cheng SC, et al (2011). Orthotopic xenografts of RCC retain histological, immunophenotypic and genetic features of tumours in patients. *J Pathol* **225**, 212–221.
- [227] Thong AE, Zhao H, Ingels A, Valta MP, Nolley R, and Santos J, et al (2014). Tissue slice grafts of human renal cell carcinoma: an authentic preclinical model with high engraftment rate and metastatic potential. *Urol Oncol* **32**:e23–30.
- [228] Dong Y, Manley BJ, Becerra MF, Redzematovic A, Casuscelli J, and Tennenbaum DM, et al (2017). Tumor xenografts of human clear cell renal cell carcinoma but not corresponding cell lines recapitulate clinical response to sunitinib: feasibility of using biopsy samples. *Eur Urol Focus* **3**, 590–598.
- [229] Lang H, Beraud C, Bethry A, Danilin S, Lindner V, and Coquard C, et al (2016). Establishment of a large panel of patient-derived preclinical models of human renal cell carcinoma. *Oncotarget* **7**, 59336–59359.
- [230] Sanz L, Cuesta AM, Salas C, Corbacho C, Bellas C, and Alvarez-Vallina L (2009). Differential transplantability of human endothelial cells in colorectal cancer and renal cell carcinoma primary xenografts. *Laboratory investigation; a journal of technical methods and pathology* **89**, 91–97.
- [231] Kim JH, Ahn JH, and Lee M (2017). Upregulation of MicroRNA-1246 is associated with BRAF inhibitor resistance in melanoma cells with mutant BRAF. *Cancer research and treatment : official journal of Korean Cancer Association* **49**, 947–959.
- [232] Mohseni MJ, Amanpour S, Muhammadnejad S, Sabetkish S, Muhammadnejad A, and Heidari R, et al (2014). Establishment of a patient-derived 'Wilms' tumor xenograft model: a promising tool for individualized cancer therapy. *J Pediatr Urol* **10**, 123–129.
- [233] Pavia-Jimenez A, Tcheyuy VT, and Brugarolas J (2014). Establishing a human renal cell carcinoma tumorigraft platform for preclinical drug testing. *Nat Protoc* **9**, 1848–1859.
- [234] Shibasaki N, Yamasaki T, Kanno T, Arakaki R, Sakamoto H, and Utsunomiya N, et al (2015). Role of IL13RA2 in sunitinib resistance in clear cell renal cell carcinoma. *PLoS One* **10**:e0130980.
- [235] Sivanand S, Pena-Llopis S, Zhao H, Kucejova B, Spence P, and Pavia-Jimenez A, et al (2012). A validated tumorigraft model reveals activity of dovitinib against renal cell carcinoma. *Sci Transl Med* **4**, 137ra75.
- [236] Kola I and Landis J (2004). Can the pharmaceutical industry reduce attrition rates? *Nat Rev Drug Discov* **3**, 711–715.
- [237] Inoue T, Terada N, Kobayashi T, and Ogawa O (2017). Patient-derived xenografts as *in vivo* models for research in urological malignancies. *Nat Rev Urol* **14**, 267–283.
- [238] DiMasi JA, Reichert JM, Feldman L, and Malins A (2013). Clinical approval success rates for investigational cancer drugs. *Clin Pharmacol Ther* **94**, 329–335.
- [239] Hidalgo M, Amant F, Biankin AV, Budinska E, Byrne AT, and Caldas C, et al (2014). Patient-derived xenograft models: an emerging platform for translational cancer research. *Cancer Discov* **4**, 998–1013.
- [240] Tentler JJ, Tan AC, Weekes CD, Jimeno A, Leong S, and Pitts TM, et al (2012). Patient-derived tumour xenografts as models for oncology drug development. *Nat Rev Clin Oncol* **9**, 338–350.
- [241] Karam JA, Zhang XY, Tamboli P, Margulis V, Wang H, and Abel EJ, et al (2011). Development and characterization of clinically relevant tumor models from patients with renal cell carcinoma. *Eur Urol* **59**, 619–628.
- [242] Schuller AG, Barry ER, Jones RD, Henry RE, Frigault MM, and Beran G, et al (2015). The MET Inhibitor AZD6094 (Savitinib, HMPD-504) Induces Regression in Papillary Renal Cell Carcinoma Patient-Derived Xenograft Models. *Clin Cancer Res* **21**, 2811–2819.
- [243] Hammers HJ, Verheul HM, Salumbides B, Sharma R, Rudek M, and Jaspers J, et al (2010). Reversible epithelial to mesenchymal transition and acquired resistance to sunitinib in patients with renal cell carcinoma: evidence from a xenograft study. *Mol Cancer Ther* **9**, 1525–1535.
- [244] Miles KM, Seshadri M, Ciamporcero E, Adelajiyi R, Gillard B, and Sotomayor P, et al (2014). Dll4 blockade potentiates the anti-tumor effects of VEGF inhibition in renal cell carcinoma patient-derived xenografts. *PLoS One* **9**:e112371.
- [245] Diaz-Montero CM, Mao FJ, Barnard J, Parker Y, Zamanian-Daryoush M, and Pink JJ, et al (2016). MEK inhibition abrogates sunitinib resistance in a renal cell carcinoma patient-derived xenograft model. *Br J Cancer* **115**, 920–928.
- [246] Vasudev NS, Goh V, Jurtka JK, Thompson VL, Larkin JM, and Gore M, et al (2013). Changes in tumour vessel density upon treatment with anti-angiogenic agents: relationship with response and resistance to therapy. *Br J Cancer* **109**, 1230–1242.
- [247] Angevin E, Glukhova L, Pavon C, Chassevent A, Terrier-Lacombe MJ, and Goguel AF, et al (1999). Human renal cell carcinoma xenografts in SCID mice: tumorigenicity correlates with a poor clinical prognosis. *Laboratory investigation; a journal of technical methods and pathology* **79**, 879–888.
- [248] Malaney P, Nicosia SV, and Dave V (2014). One mouse, one patient paradigm: New avatars of personalized cancer therapy. *Cancer Lett* **344**, 1–12.
- [249] Suarez C, Martinez M, Trilla E, Jimenez-Valerio G, de Torres I, and Morales R, et al (2016). Patient-derived AVATAR mouse models to predict prognosis in advanced renal cell carcinoma. *J Clin Oncol* **34**.
- [250] Moret R, Zhang X, Maresh G, Canter D, Matrana M, and Morais C, et al (2019). Mp25-11a mouse avator model for screening targeted sequential therapies for individual renal cell carcinoma patient. *J Urol* **201**:e346–e7.
- [251] Cepeda M, Lowerison M, Liu C, Fedysyn Y, Joshi V, Shah P, et al. Abstract LB-155: Rapid patient derived xenograft avatars that consider tumor heterogeneity for prediction of cancer immunotherapy responses in metastatic renal cell carcinoma patients. *Cancer Research*. 2018;78:LB-155-LB.
- [252] Motzer RJ, Escudier B, McDermott DF, George S, Hammers HJ, and Srinivas S, et al (2015). Nivolumab versus everolimus in advanced renal-cell carcinoma. *N Engl J Med* **373**, 1803–1813.
- [253] Woo SR, Corrales L, and Gajewski TF (2015). Innate immune recognition of cancer. *Annu Rev Immunol* **33**, 445–474.
- [254] Shultz LD, Brehm MA, Garcia-Martinez JV, and Greiner DL (2012). Humanized mice for immune system investigation: progress, promise and challenges. *Nat Rev Immunol* **12**, 786–798.
- [255] Chang DK, Moniz RJ, Xu Z, Sun J, Signoretti S, and Zhu Q, et al (2015). Human anti-CAIX antibodies mediate immune cell inhibition of renal cell carcinoma *in vitro* and in a humanized mouse model *in vivo*. *Mol Cancer* **14**:119.
- [256] Schroeder MA and DiPersio JF (2011). Mouse models of graft-versus-host disease: advances and limitations. *Dis Model Mech* **4**, 318–333.
- [257] Brehm MA, Shultz LD, Luban J, and Greiner DL (2013). Overcoming current limitations in humanized mouse research. *J Infect Dis* **208**(Suppl 2), S125–S130.
- [258] Elmonem MA, Berlingiero SP, van den Heuvel LP, de Witte PA, Lowe M, and Levchenko EN (2018). Genetic renal diseases: the emerging role of zebrafish models. *Cells* **7**, 130.
- [259] Noonan HR, Metelo AM, Kamei CN, Peterson RT, Drummond IA, and Iliopoulos O (2016). Loss of vhl in the zebrafish pronephros recapitulates early stages of human clear cell renal cell carcinoma. *Dis Model Mech* **9**, 873–884.
- [260] Gardner HL, Fenger JM, London CA. Dogs as a model for cancer. *Annual review of animal biosciences* **4**:199–222.
- [261] Scott MC, Sarver AL, Gavin KJ, Thyanithy V, Getzy DM, and Newman RA, et al (2011). Molecular subtypes of osteosarcoma identified by reducing tumor heterogeneity through an interspecies comparative approach. *Bone* **49**, 356–367.
- [262] Breen M and Modiano JF (2008). Evolutionarily conserved cytogenetic changes in hematological malignancies of dogs and humans—man and his best friend share more than companionship. *Chromosome research : an international journal on the molecular, supramolecular and evolutionary aspects of chromosome biology* **16**, 145–154.
- [263] Dohner H, Stilgenbauer S, Benner A, Leupolt E, Krober A, and Bullinger L, et al (2000). Genomic aberrations and survival in chronic lymphocytic leukemia. *N Engl J Med* **343**, 1910–1916.
- [264] Usher SG, Radford AD, Villiers EJ, and Blackwood L (2009). RAS, FLT3, and C-KIT mutations in immunophenotyped canine leukemias. *Exp Hematol* **37**, 65–77.
- [265] Uva P, Aurisicchio L, Watters J, Loboda A, Kulkarni A, and Castle J, et al (2009). Comparative expression pathway analysis of human and canine mammary tumors. *BMC Genomics* **10**, 135.
- [266] Clark MA, Fisher C, Judson I, and Thomas JM (2005). Soft-tissue sarcomas in adults. *N Engl J Med* **353**, 701–711.
- [267] Sargan DR, Milne BS, Hernandez JA, O'Brien PCM, Ferguson-Smith MA, and Hoather T, et al (2005). Chromosome rearrangements in canine fibrosarcomas. *J Hered* **96**, 766–773.
- [268] MacEwen EG, Kurzman ID, Rosenthal RC, Smith BW, Manley PA, and Roush JK, et al (1989). Therapy for osteosarcoma in dogs with intravenous injection of liposome-encapsulated muramyl tripeptide. *JNCI: Journal of the National Cancer Institute* **81**, 935–938.
- [269] Meyers PA, Schwartz CL, Krailo MD, Healey JH, Bernstein ML, and Betcher D, et al (2008). Osteosarcoma: the addition of muramyl tripeptide to chemotherapy improves overall survival—a report from the Children's Oncology Group. *Journal of clinical oncology : official journal of the American Society of Clinical Oncology* **26**, 633–638.
- [270] London CA, Hannah AL, Zadovskaya R, Chien MB, Kollias-Baker C, and Rosenberg M, et al (2003). Phase I dose-escalating study of SU11654, a small molecule receptor tyrosine kinase inhibitor, in dogs with spontaneous malignancies. *Clinical cancer research : an official journal of the American Association for Cancer Research* **9**, 2755–2768.
- [271] Mendel DB, Laird AD, Xin X, Louie SG, Christensen JG, and Li G, et al (2003). In vivo antitumor activity of SU11248, a novel tyrosine kinase inhibitor targeting vascular endothelial growth factor and platelet-derived growth factor receptors: determination of a pharmacokinetic/pharmacodynamic relationship. *Clinical cancer research : an official journal of the American Association for Cancer Research* **9**, 327–337.
- [272] Zhang J, Jiang H, and Zhang H (2018). In situ administration of cytokine combinations induces tumor regression in mice. *EBioMedicine* **37**, 38–46.
- [273] Maekawa N, Konnai S, Ikebuchi R, Okagawa T, Adachi M, Takagi S, et al. Expression of PD-L1 on canine tumor cells and enhancement of IFN- γ production from tumor-infiltrating cells by PD-L1 blockade. *PLoS one* **9**:e8415-e.
- [274] Lium B and Moe L (1985). Hereditary multifocal renal cystadenocarcinomas and nodular dermatofibrosis in the German shepherd dog: macroscopic and histopathologic changes. *Vet Pathol* **22**, 447–455.
- [275] Moe L and Lium B (1997). Hereditary multifocal renal cystadenocarcinomas and nodular dermatofibrosis in 51 German shepherd dogs. *J Small Anim Pract* **38**, 498–505.
- [276] Lingas F, Comstock KE, Kirkness EF, Sorensen A, Aarskaug T, and Hitte C, et al (2003). A mutation in the canine BHD gene is associated with hereditary multifocal renal cystadenocarcinoma and nodular dermatofibrosis in the German Shepherd dog. *Hum Mol Genet* **12**, 3043–3053.
- [277] Pavlovich CP, Walther MM, Eyley RA, Hewitt SM, Zbar B, and Linehan WM, et al (2002). Renal tumors in the Birt-Hogg-Dube syndrome. *Am J Surg Pathol* **26**, 1542–1552.
- [278] Lauber DT, Fulop A, Kovacs T, Szigeri K, Mathe D, and Szijarto A (2017). State of the art *in vivo* imaging techniques for laboratory animals. *Lab Anim* **51**, 465–478.
- [279] de Jong M, Essers J, and van Weerden WM (2014). Imaging preclinical tumour models: improving translational power. *Nat Rev Cancer* **14**, 481.
- [280] Hormuth DA, 2nd, Sorace AG, Virostko J, Abramson RG, Bhujwala ZM, Enriquez-Navas P, et al. Translating preclinical MRI methods to clinical oncology. *Journal of magnetic resonance imaging : JMIR*. 2019.
- [281] Linxweiler J, Körbel C, Müller A, Juengel E, Blaheta R, and Heinzelmann J, et al (2017). Experimental imaging in orthotopic renal cell carcinoma xenograft models: comparative evaluation of high-resolution 3D ultrasonography, in-vivo micro-CT and 9.4T MRI. *Sci Rep* **7**.
- [282] Li L, Mori S, Sakamoto M, Takahashi S, and Kodama T (2013). Mouse model of lymph node metastasis via afferent lymphatic vessels for development of imaging modalities. *PLoS One* **8**:e55797.

- [283] Sperling J, Brandhorst D, Schafer T, Ziemann C, Benz-Weisser A, and Scheuer C, et al (2013). Liver-directed chemotherapy of cetuximab and bevacizumab in combination with oxaliplatin is more effective to inhibit tumor growth of C531 colorectal rat liver metastases than systemic chemotherapy. *Clin Exp Metastasis* **30**, 447–455.
- [284] Tseng JC, Kung AL. Quantitative bioluminescence imaging of mouse tumor models. Cold Spring Harbor protocols. 2015;2015.pdb.prot078261.
- [285] O'Neill K, Lyons SK, Gallagher WM, Curran KM, and Byrne AT (2010). Bioluminescent imaging: a critical tool in pre-clinical oncology research. *J Pathol* **220**, 317–327.
- [286] Donat SM, Diaz M, Bishoff JT, Coleman JA, Dahm P, and Derweesh IH, et al (2013). Follow-up for clinically localized renal neoplasms: AUA Guideline. *J Urol* **190**, 407–416.
- [287] Escudier B, Porta C, Schmidinger M, Rioux-Leclercq N, Bex A, and Khoo V, et al (2016). Renal cell carcinoma: ESMO Clinical Practice Guidelines for diagnosis, treatment and follow-up. *Ann Oncol* **27**, v58–v68.
- [288] Ljungberg B, Albiges L, Abu-Ghanem Y, Bensalah K, Dabestani S, and Fernández-Pello S, et al (2019). European Association of Urology Guidelines on Renal Cell Carcinoma: The 2019 Update. *Eur Urol* **75**, 799–810.
- [289] Wang HY, Ding HJ, Chen JH, Chao CH, Lu YY, and Lin WY, et al (2012). Meta-analysis of the diagnostic performance of [18F]FDG-PET and PET/CT in renal cell carcinoma. *Cancer imaging: the official publication of the International Cancer Imaging Society* **12**, 464–474.
- [290] Brouwers A, Verel I, Van Eerd J, Visser G, Steffens M, and Oostervijk E, et al (2004). PET radioimmuno-scintigraphy of renal cell cancer using 89Zr-labeled cG250 monoclonal antibody in nude rats. *Cancer Biother Radiopharm* **19**, 155–163.
- [291] Ishibashi K, Haber T, Breuksch I, Gebhard S, Sugino T, and Kubo H, et al (2017). Overriding TKI resistance of renal cell carcinoma by combination therapy with IL-6 receptor blockade. *Oncotarget* **8**, 55230–55245.
- [292] Hamstra DA, Rehemtulla A, and Ross BD (2007). Diffusion magnetic resonance imaging: a biomarker for treatment response in oncology. *J Clin Oncol* **25**, 4104–4109.
- [293] Tang L and Zhou XJ (2019). Diffusion MRI of cancer: From low to high b-values. *J Magn Reson Imaging* **49**, 23–40.
- [294] Mytsyk Y, Borys Y, Komnatska I, Dutka I, and Shatynska-Mytsyk I (2014). Value of the diffusion-weighted MRI in the differential diagnostics of malignant and benign kidney neoplasms - our clinical experience. *Pol J Radiol* **79**, 290–295.
- [295] Mytsyk Y, Dutka I, Borys Y, Komnatska I, Shatynska-Mytsyk I, and Farooqi AA, et al (2017). Renal cell carcinoma: applicability of the apparent coefficient of the diffusion-weighted estimated by MRI for improving their differential diagnosis, histologic subtyping, and differentiation grade. *Int Urol Nephrol* **49**, 215–224.
- [296] Mytsyk Y, Dutka I, Yuriy B, Maksymovych I, Caprnda M, and Gazdikova K, et al (2018). Differential diagnosis of the small renal masses: role of the apparent diffusion coefficient of the diffusion-weighted MRI. *Int Urol Nephrol* **50**, 197–204.
- [297] Jeon TY, Kim CK, Kim JH, Im GH, Park BK, and Lee JH (2015). Assessment of early therapeutic response to sorafenib in renal cell carcinoma xenografts by dynamic contrast-enhanced and diffusion-weighted MR imaging. *Br J Radiol* **88**(2015)0163.
- [298] Jakobsen I, Kaalhus O, Lyng H, and Rofstad EK (1995). Detection of necrosis in human tumour xenografts by proton magnetic resonance imaging. *Br J Cancer* **71**, 456–461.
- [299] Weidensteiner C, Allegrini PR, Sticker-Jantschke M, Romanet V, Ferretti S, and McSheehy PM (2014). Tumour T1 changes *in vivo* are highly predictive of response to chemotherapy and reflect the number of viable tumour cells—a preclinical MR study in mice. *BMC Cancer* **14**(88).
- [300] Rofstad EK, Steinsland E, Kaalhus O, Chang YB, Hovik B, and Lyng H (1994). Magnetic resonance imaging of human melanoma xenografts *in vivo*: proton spin-lattice and spin-spin relaxation times versus fractional tumour water content and fraction of necrotic tumour tissue. *Int J Radiat Biol* **65**, 387–401.
- [301] Righi V, Mucci A, Schenetti L, Tosi MR, Grigioni WF, and Corti B, et al (2007). Ex vivo HR-MAS magnetic resonance spectroscopy of normal and malignant human renal tissues. *Anticancer Res* **27**, 3195–3204.
- [302] Sonkar K, Ayyappan V, Tressler CM, Adelaja O, Cai R, and Cheng M, et al (2019). Focus on the glycerophosphocholine pathway in choline phospholipid metabolism of cancer. *NMR Biomed* **32**, e4112.
- [303] Fardaneh R, Marino MA, Avendano D, Leithner D, Pinker K, and Thakur SB (2019). Proton MR spectroscopy in the breast: Technical innovations and clinical applications. *JMRI: Journal of magnetic resonance imaging* 2019.
- [304] Stüllentrop F, Hahn J, and Moka D (2012). In vitro and *in vivo* (1)H-MR spectroscopic examination of the renal cell carcinoma. *International journal of biomedical science: IJBS* **8**, 94–108.
- [305] Sevenco S, Krssak M, Javor D, Ponthold L, Kuehhas FE, and Fajkovic H, et al (2015). Diagnosis of renal tumors by *in vivo* proton magnetic resonance spectroscopy. *World J Urol* **33**, 17–23.
- [306] Kobayashi T, Honke K, Kamio K, Sakakibara N, Gasa S, and Miyao N, et al (1993). Sulfolipids and glycolipid sulfotransferase activities in human renal cell carcinoma cells. *Br J Cancer* **67**, 76–80.
- [307] Govindaraju V, Young K, and Maudsley AA (2000). Proton NMR chemical shifts and coupling constants for brain metabolites. *NMR Biomed* **13**, 129–153.
- [308] Opstad KS, Bell BA, Griffiths JR, and Howe FA (2009). Taurine: a potential marker of apoptosis in gliomas. *Br J Cancer* **100**, 789.
- [309] Khemtong C, Carpenter NR, Lumata LL, Merritt ME, Moreno KX, and Kovacs Z, et al (2015). Hyperpolarized 13C NMR detects rapid drug-induced changes in cardiac metabolism. *Magn Reson Med* **74**, 312–319.
- [310] Nelson SJ, Kurhanewicz J, Vigneron DB, Larson PE, Harzstark AL, Ferrone M, et al. Metabolic imaging of patients with prostate cancer using hyperpolarized [1-(1)(3)C]pyruvate. *Sci Transl Med*. 2013;5:198ra08.
- [311] Rodrigues TB, Serrao EM, Kennedy BW, Hu DE, Kettunen MI, and Brindle KM (2014). Magnetic resonance imaging of tumor glycolysis using hyperpolarized 13C-labeled glucose. *Nat Med* **20**, 93–97.
- [312] Saito K, Matsumoto S, Takakusagi Y, Matsuo M, Morris HD, Lizak MJ, et al. 13C-MR Spectroscopic Imaging with Hyperpolarized [1-13C]pyruvate Detects Early Response to Radiotherapy in SCC Tumors and HT-29 Tumors. *Clinical cancer research: an official journal of the American Association for Cancer Research*. 2015;21:5073-81.
- [313] Sogaard LV, Schilling F, Janich MA, Menzel MI, and Ardenkjaer-Larsen JH (2014). In vivo measurement of apparent diffusion coefficients of hyperpolarized (1)(3)C-labeled metabolites. *NMR Biomed* **27**, 561–569.
- [314] Wilson DM and Kurhanewicz J (2014). Hyperpolarized 13C MR for molecular imaging of prostate cancer. *Journal of nuclear medicine: official publication, Society of Nuclear Medicine* **55**, 1567–1572.
- [315] Park JM, Josan S, Jang T, Merchant M, Yen YF, and Hurd RE, et al (2012). Metabolite kinetics in C6 rat glioma model using magnetic resonance spectroscopic imaging of hyperpolarized [1-(13)C] pyruvate. *Magn Reson Med* **68**, 1886–1893.
- [316] Sriram R, Van Crielinge M, DeLos Santos J, Keshari KR, Wilson DM, and Peehl D, et al (2016). Non-invasive differentiation of benign renal tumors from clear cell renal cell carcinomas using clinically translatable hyperpolarized 13C pyruvate magnetic resonance. *Tomography: a journal for imaging research* **2**, 35–42.
- [317] Sriram R, Gordon J, Baligand C, Ahamed F, Delos Santos J, and Qin H, et al (2018). Non-invasive assessment of lactate production and compartmentalization in renal cell carcinomas using hyperpolarized (13)C pyruvate MRI. *Cancers* **10**.
- [318] Carel CCCoA. CCAC guidelines on (1998). Choosing an appropriate endpoint in experiments using animals for research, teaching, and testing. Canadian Council on Animal Care; 1998.
- [319] Workman P, Aboagye EO, Balkwill F, Balmain A, Bruder G, and Chaplin DJ, et al (2010). Guidelines for the welfare and use of animals in cancer research. *Br J Cancer* **102**, 1555–1577.
- [320] Wallace J (2000). Humane endpoints and cancer research. *ILAR J* **41**, 87–93.
- [321] Ashall V and Millar K (2014). Endpoint matrix: a conceptual tool to promote consideration of the multiple dimensions of humane endpoints. *ALTEX* **31**, 209–213.
- [322] United Kingdom Co-ordinating Committee on Cancer Research (1998). (UKCCCR) Guidelines for the Welfare of Animals in Experimental Neoplasia (Second Edition). *Br J Cancer* **77**, 1–10.
- [323] Morton DB and Griffiths PH (1985). Guidelines on the recognition of pain, distress and discomfort in experimental animals and an hypothesis for assessment. *The Veterinary record* **116**, 431–436.
- [324] Oliveira M, Nascimento-Goncalves E, Silva J, Oliveira PA, Ferreira R, and Antunes L, et al (2017). Implementation of humane endpoints in a urinary bladder carcinogenesis study in rats. *In Vivo*. **31**, 1073–1080.
- [325] Faustino-Rocha AI, Ginja M, Ferreira R, and Oliveira PA (2019). Studying humane endpoints in a rat model of mammary carcinogenesis. *Iran J Basic Med Sci* **22**, 643–649.
- [326] Kripke ML, Gruys E, and Fidler IJ (1978). Metastatic heterogeneity of cells from an ultraviolet light-induced murine fibrosarcoma of recent origin. *Cancer Res* **38**, 2962–2967.
- [327] Bibby MC, Double JA, Ali SA, Fearon KC, Brennan RA, and Tisdale MJ (1987). Characterization of a transplantable adenocarcinoma of the mouse colon producing cachexia in recipient animals. *J Natl Cancer Inst* **78**, 539–546.
- [328] Cooke BA, Lindh LM, Janszen FH, van Driel MJ, Bakker CP, and van der Plank MP, et al (1979). A Leydig cell tumour: a model for the study of lutropin action. *Biochim Biophys Acta* **583**, 320–331.
- [329] Olson B, Li Y, Lin Y, Liu ET, and Parnik A (2018). Mouse models for cancer immunotherapy research. *Cancer Discov*. **8**, 1358–1365.
- [330] Choi Y, Lee S, Kim K, Kim SH, Chung YJ, and Lee C (2018). Studying cancer immunotherapy using patient-derived xenografts (PDXs) in humanized mice. *Exp Mol Med* **50**(9).
- [331] Johnson JI, Decker S, Zaharevitz D, Rubinstein LV, Venditti JM, and Schepartz S, et al (2001). Relationships between drug activity in NCI preclinical *in vitro* and *in vivo* models and early clinical trials. *Br J Cancer* **84**, 1424–1431.
- [332] Wei S, Fu N, Sun Y, Yang Z, Lei L, and Huang P, et al (2014). Targeted contrast-enhanced ultrasound imaging of angiogenesis in an orthotopic mouse tumor model of renal carcinoma. *Ultrason Med Biol* **40**, 1250–1259.
- [333] Muselaers CH, Stillebroer AB, Rijpkema M, Franssen GM, Oostervijk E, and Mulders PF, et al (2014). Optical imaging of renal cell carcinoma with anti-carbonic anhydrase IX monoclonal antibody girentuximab. *Journal of nuclear medicine: official publication, Society of Nuclear Medicine*. **55**, 1035–1040.
- [334] Muselaers CH, Rijpkema M, Bos DL, Langenhuijsen JF, Oyen WJ, and Mulders PF, et al (2015). Radionuclide and fluorescence imaging of clear cell renal cell carcinoma using dual labeled anti-carbonic anhydrase IX antibody G250. *J Urol* **194**, 532–538.
- [335] Vento J, Mulgaonkar A, Woolford L, Nham K, Christie A, and Bagrodia A, et al (2019). PD-L1 detection using (89)Zr-atezolizumab immuno-PET in renal cell carcinoma tumorgrafts from a patient with favorable nivolumab response. *Journal for immunotherapy of cancer*. 7144.
- [336] Ukon N, Zhao S, Yu W, Shimizu Y, Nishijima KI, and Kubo N, et al (2016). Dynamic PET evaluation of elevated FLT level after sorafenib treatment in mice bearing human renal cell carcinoma xenograft. *EJNMMI Res* **6**(90).
- [337] Murakami M, Zhao S, Zhao Y, Yu W, Fatema CN, and Nishijima KI, et al (2013). Increased intratumoral fluorothymidine uptake levels following multikinase inhibitor sorafenib treatment in a human renal cell carcinoma xenograft model. *Oncol Lett* **6**, 667–672.
- [338] Murakami M, Zhao S, Zhao Y, Chowdhury NF, Yu W, and Nishijima K, et al (2012). Evaluation of changes in the tumor microenvironment after sorafenib therapy by sequential histology and 18F-fluoromisonidazole hypoxia imaging in renal cell carcinoma. *Int J Oncol* **41**, 1593–1600.
- [339] Lawrentschuk N, Lee FT, Jones G, Rigopoulos A, Mountain A, and O'Keefe G, et al (2011). Investigation of hypoxia and carbonic anhydrase IX expression in a renal cell carcinoma xenograft model with oxygen tension measurements and (1)(2)(4)I-cG250 PET/CT. *Urol Oncol* **29**, 411–420.
- [340] Hillman GG, Singh-Gupta V, Al-Bashir AK, Zhang H, Yunker CK, and Patel AD, et al (2010). Dynamic contrast-enhanced magnetic resonance imaging of sunitinib-induced vascular changes to schedule chemotherapy in renal cell carcinoma xenograft tumors. *Transl Oncol* **3**, 293–306.
- [341] Robinson SP, Boul JKR, Vasudev NS, and Reynolds AR (2017). Monitoring the vascular response and resistance to sunitinib in renal cell carcinoma *in vivo* with susceptibility contrast MRI. *Cancer Res* **77**, 4127–4134.